AMERICAN UNIVERSITY OF BEIRUT

MECHANISTIC DFT STUDIES ON CARBON DIOXIDE AND CARBONYL COMPOUNDS INSERTION INTO TRANSITION METAL-HYDRIDE COMPLEXES

by
MARIAM ALI BARAKAT

A thesis
submitted in partial fulfillment of the requirements
for the degree of Master of Science
to the Department of Chemistry
of the Faculty of Arts and Sciences
at the American University of Beirut

Beirut, Lebanon
January 2022

AMERICAN UNIVERSITY OF BEIRUT

MECHANISTIC DFT STUDIES ON CARBON DIOXIDE AND CARBONYL COMPOUNDS INSERTION INTO TRANSITION METAL-HYDRIDE COMPLEXES

by

MARIAM ALI BARAKAT

Approved by:

Dr. Faraj Hasanayn, Professor — Advisor

Chemistry

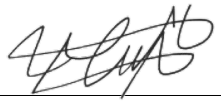

Dr. Mohamad Hmadeh, Professor — Member of Committee

Chemistry

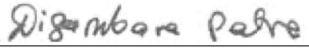

Dr. Digambara Patra, Professor — Member of Committee

Chemistry

Date of thesis defense: January 25, 2022

AMERICAN UNIVERSITY OF BEIRUT

THESIS, DISSERTATION, PROJECT RELEASE FORM

Student Name: Barakat (Last) Mariam (First) Ali (Middle)

☑ Master's Thesis ☐ Master's Project ☐ Doctoral Dissertation

☐ I authorize the American University of Beirut to: (a) reproduce hard or electronic copies of my thesis, dissertation, or project; (b) include such copies in the archives and digital repositories of the University; and (c) make freely available such copies to third parties for research or educational purposes.

☑ I authorize the American University of Beirut, to: (a) reproduce hard or electronic copies of it; (b) include such copies in the archives and digital repositories of the University; and (c) make freely available such copies to third parties for research or educational purposes after: **One ✓ year from the date of submission of my thesis, dissertation or project.**

Two _____ years from the date of submission of my thesis , dissertation or project.
Three _____ years from the date of submission of my thesis , dissertation or project.

Mariam 01/02/2022

Signature Date

This form is signed when submitting the thesis, dissertation, or project to the University Libraries

Acknowledgements

It is the support, care, motivation, and love of so many people around me that made this thesis work possibly done, to whom I wish to express my appreciation and gratitude. First, to my advisor, Dr. Faraj Hasanayn, thank you for your continuous support, patience, and good care during my time in your lab. Thank you for introducing me to research and letting me know how much I like it. Thank you for your kindness, for reminding me to value my work and be proud of it even when the situation in Lebanon has gone insane. I learned from you a lot and will be incredibly grateful for your guidance.

To my committee members, Dr. Mohamad Hmadeh and Dr. Digambara Patra, thank you for your time on my thesis and for being amazing instructors during my first semester at AUB.

To my mother, Hayat Makki, indeed my hayat, thank you for teaching me strength, for reminding me of what a true giver is, and to trust God's plan when life doesn't go our way. To my father, Ali Barakat, thank you for teaching me independency, for your guidance, and for always putting us first. I owe all this to both my parents' sacrifices and hard work. To my sisters, Fatima and Nour, thank you for being my role models, the shoulder to lean on during the darkest of my days, and for caring much more than I do. To Hussien, my brother, thank you for always being there. To my childhood friend, Rodaina Srour, thank you for standing in every memory, thick and thin, and being my first supporter. To my friend Nour Ismail, thank you for your shown care and love, thanks for being a beautiful source of art inspiration.

To my friends and colleagues at AUB who walked along side me on this journey; Justine Dagher, Patrick Damacet, Elissa Shehayeb, Lynn Yamout, and many others. Thank you for being a good part of it, your support and encouragement meant a lot to me. Thanks to my ex-lab mate Mohamad Ataya for helping me at the beginning of my research work. Deep gratitude goes to every person who taught me a letter, or had an impact on my simple life. To every child who smiled at me on a taught day back home, you gave me hope. Thank you.

Thank you AUB for giving me this opportunity two years ago, it has been rewarding, you had a lot to share and teach so that we may have life and have it more abundantly.

An Abstract of the Thesis of

Mariam Ali Barakat for Master of Science
Major: Chemistry

Title: Mechanistic DFT Studies on Carbon Dioxide and Carbonyl Compounds Insertion into Transition Metal-Hydride Complexes.

In this thesis, we utilize DFT calculations to investigate the mechanism of a fundamental chemical step that is widely implicated in homogenous catalysis, namely insertion of unsaturated molecules into a metal-hydride bond of octahedral saturated d^6-transition metal complexes. Our first investigation pertains to carbon dioxide insertion. For many complexes, the reaction has been experimentally determined to follow an associative mechanism. There have been, however, two views of the rate determining step (RDS) in such mechanism. A more prevailing view assumes a linear transition state (TS) leading to a C-H bound formate intermediate, the other assumes a cyclic TS. Herein, we conduct a detailed theoretical investigation of the associative PES of CO_2 insertion into the Re-H bond of *fac*-(bpy)Re$(CO)_3$H for which extensive experimental data are available. We calculate both these transition states and study how their barrier and KIE change as a function of the solvent and substitution at the 4,4' bpy positions. Surprisingly, results reveal that the initial stage of the reaction starts with a low energy linear TS (ts1) for formation of a bond between the carbon and the metal hydride bond leading to a bridged hydride species. A second stage of the reaction involves cleavage of the bridged metal hydride bond and rearrangement of the resulting ion-pair intermediate via a cyclic transition state (TS_{cyc}). To explore the generality of this finding we also calculated CO_2 insertion in the octahedral $(^{iPr}P^{H}NP)Ir(H)_3$. The amino functionality in on the ligand in this complex was proposed to assist insertion by hydrogen bonding. Again, our calculations show the PES to start with ts1 for bridge formation, followed by a RDS TS_{cyc}. We show that consideration of TS_{cyc} as RDS affords activation free energies, solvent effects, substituent effects and Kinetic Isotope Effects (KIE) that are all in excellent agreement with experimental data available for the two systems. In light of this finding, we initiated a second investigation aimed at understanding the mech-

anism of associative insertion of carbonyl compounds other than CO_2. For this purpose, we considered a series of eleven carbonyl compounds, including aldehydes, ketones, esters, carboxamides, carbamates and urea derivatives. We worked with Gusev's osmium (PNN)Os$(H)_2$(CO) catalyst. The insertion thermodynamics spanned a range of around 30 kcal/mol. Surprisingly, the substrates that disfavored insertion afforded equilibrium Isotope Effect (EIE) that were slightly more inverse than the more favored insertions. This implies that the less favored reactions result in formation of stronger C-H bonds. We rationalized this counterintuitive finding using thermodynamic cycles starting with distortion of the carbonyl moiety in the free substrates prior to formation of a C-H bond. Simply put, the different substrates have very different distortion energies, and the distorted substrates have comparable susceptibilities to reduction by formation of a C-hydride bond. Kinetically, the calculations predict associative insertion of all of the carbonyl compounds considered to follow initial bridge formation by a linear ts1 followed by rate limiting TS_{cyc}. Associative insertion provides a major shift from the more conventional insertion mechanism that requires initial coordination of the substrate to a metal. The results obtained in the present work provide new insights to understanding the associative mechanism for carbonyl group insertion into the M-H bond of octahedral complexes.

Contents

Acknowledgements **v**

Abstract **vi**

List of Figures **x**

List of Schemes **xii**

List of Tables **xiv**

1 Introduction **1**
1.1 Introduction to Insertion Reactions 1
1.2 Background of Isotope Effects 3
1.2.1 Discovery 3
1.2.2 Theoretical Basis of Kinetic Isotope effects 3
1.2.3 Classifications of Isotope Effects 7
1.3 Introduction to Computational Chemistry 7
1.3.1 Theories Behind Computing 7
1.3.2 Methods of Inquiry 9

2 Mechanistic DFT Study on CO_2 Insertion into Re-H Bond of (bpy)Re(CO)$_3$H **11**
2.1 Aim and Background of the Study 11
2.2 Results and Discussion 14
2.2.1 Energy Profile in THF 14
2.2.2 Computed Kinetic Isotope Effect 22
2.2.3 Computed Solvent and Substituent Effects 25
2.2.4 Conclusion 29

3 Effect of Hydrogen Bonding and *trans*-Hydride on CO_2 Insertion into Metal-Hydride Bond **31**
3.1 Introduction 31
3.2 Results and Discussion 32
3.2.1 Free Energy Profile 32

3.2.2 Computed Primary Kinetic Isotope Effect 35
3.2.3 Hydrogen Bonding Effect 38
3.2.4 Trans-Hydride Effect 40
3.2.5 Computed Solvent Effect 41
3.3 Conclusion 43

4 Structure - Activity Study of Insertion Reaction of a Series of Carbonyl Compounds 44
4.1 Introduction 44
4.2 Results and Discussion 46
4.2.1 Thermodynamics of Insertion 46
4.2.2 Mechanism of Insertion 51
4.3 Conclusion 55

5 Conclusion 57

A Abbreviations 59

B Job Script Samples 60
B.1 Optimization and Frequency Calculations 60
B.2 Single Point Calculations 65
B.3 Transition State and IRC Calculations 67
B.4 AIM Calculations 71

Bibliography 73

List of Figures

1.1 Potential Energy Curve of Bond to Hydrogen/Deuterium. 4
1.2 Potential Energy Profile based on TST.*(E is the activation Energy reaching TS)* 5
1.3 Milestones in quantum mechanics contributions to Computational Chemistry. 8

2.1 Calculated M06L-D3 (A):E_{Solv}+G and (B): Gibbs free energy profile for CO_2 insertion into 1-Re-H in THF; in kcal/mol at 298 K and 1 M. Some bond distances are given in Å. 15
2.2 Computed IRC plot for the Linear transition state "ts1" located on PES of CO_2 insertion into 1-Re-H in THF, bond length in Å. . 16
2.3 Computed IRC plot for the second Linear transition state "ts2" located on PES of CO_2 insertion into 1-Re-H in THF, bond length in Å. 17
2.4 Computed IRC plot for the Cyclic transition state "TS_{cyc}" located on PES of CO_2 insertion into 1-Re-H in THF, bond length in Å . 18
2.5 Energy and selected parameters on the gas phase IRC for CO_2 insertion in 1-Re-H. *The reference point for the energy is the combined reactants as converged from the IRC.* 19
2.6 Calculated ωB97XD Gibbs free energy profile for CO_2 insertion in 1-Re-H in THF; in kcal/mol at 298 K and 1 M. Some bond distances are given in Å. 20
2.7 Variation of the Energy Profile of the Reaction of CO_2 insertion into *fac*-(bpy)Re(CO)$_3$H at different levels of theory in THF . . . 21
2.8 Contribution of the Re-H and C-H stretching vibrations to the KIE of TS_{cyc}. 24
2.9 Calculated M06L-D3 Gibbs free energy profile for CO_2 insertion in 1-Re-H. (A) in THF, (B) in Acetone, and (C) in CH_3CN; in kcal/mol at 298 K and 1 M. Some bond distances are given in Å. 26
2.10 Calculated M06L-D3 Gibbs free energy profile for CO_2 insertion in Methoxy substituted analog of 1-Re-H in THF; in kcal/mol at 298 K and 1 M. Some bond distances are given in Å. 28

3.1 Calculated M06L-D3 (A):E_{Solv}+G and (B): Gibbs free energy profile for CO_2 insertion into 1-Ir-H in THF; in kcal/mol at 298 K and 1 M. Some bond distances are given in Å. 33
3.2 Computed IRC plot for the linear transition state "ts1" located on PES of CO_2 insertion into 1-Ir-H. Energy in kcal/mol. 33
3.3 Computed IRC plot for the Cyclic transition state "TS_{cyc}" located on PES of CO_2 insertion into 1-Ir-H. Energy in kcal/mol. 34
3.4 Contribution of the Ir-H and C-H stretching vibrations to the KIE of TS_{cyc}. ZPE in kcal/mol, Stretching vibrations in cm^{-1}. 36
3.5 Computed Gibbs Free Energy Profile for CO_2 insertion into 1-Re-H (red) and 1-Ir-H (blue). Energy in kcal/mol. 39
3.6 Calculated minima and TSs on the associative PES for CO_2 insertion in 1-Ir-H in THF(A and B) and CH_3CN (C). Bond distances are given in Å. Gibbs free energies are given in kcal/mol at 298 K and 1 M relative to the separated reactants. KIE values are kinetic isotope effects defined relative to the separated reactants. . 41
3.7 IRC originating from ts1 in the reaction between 2-Ir-H and CO_2 in acetonitrile. 42

4.1 Ketone hydrogenation mechanism involving carbonyl insertion into ruthenium-hydride bond. 45
4.2 Metal alkoxide mediated mechanism for hydrogenation of ester. Energies are given in kcal/mol 45
4.3 M06L-D3 Gibbs Free Energy profile for insertion of Formaldehyde (A), and Dimethylurea (B) in toluene. 51

B.1 Input sample job showing the commands needed for the optimization and frequency calculation of the Carbon dioxide in THF. . . 60
B.2 Output sample showing the completed optimization for CO_2 in THF. 61
B.3 Output Sample showing the frequency calculations of the CO_2 molecule in THF. 62
B.4 Output Sample showing the Thermodynamic section calculations of the CO_2 molecule in THF. 63
B.5 Input sample job showing the commands needed for the optimization and frequency calculation of 1-Re-H transition metal complex in THF. 64
B.6 Input sample job showing the commands needed for single point calculation of CO_2 molecule in THF at different levels of theory (in red) after optimizing first at M06L/W06. 65
B.7 Input sample job showing the commands needed for single point calculation of distorted CO_2 molecule in toluene. 66

B.8 Output sample output showing the polarizable continuum model used in all calculations 66
B.9 Input sample showing the commands needed for the optimization of the fixed geometry of transition state. 67
B.10 Input sample showing the commands needed for activation of the geometry of transition state. 68
B.11 Output sample showing the calculated imaginary frequency after the activation of the geometry in optimization of transition state. 68
B.12 Input sample showing the commands needed for the calculation of the intrinsic reaction coordinates for bridging hydride TS in 1-Re-H system. 69
B.13 Output sample showing the Energies along the reaction coordinates of the bridging hydride TS in 1-Re-H system as displayed in the output file. 70
B.14 Input sample showing the commands needed for the AIM calculation of 1-Re-H system. 71
B.15 Output sample showing the detected Bond Critical points and Delocalization indices parameter (DI) in AIM calculation of 1-Re-H complex. 72

List of Schemes

1.1 Classical Inner-sphere Aldehyde Insertion 1
1.2 Experimentally observed Ru-Alkoxide bond. 2

2.1 Associated TSs for CO_2 Insertion into 1-Re-H 12
2.2 Efficient Octahedral catalysts in inserting CO_2 12
2.3 An Associative Insertion Mechanism 13
2.4 Comparison of Borohydride Analog of i1, through geometry analysis and Delocalization index. 15
2.5 Computed KIE for ts1 in THF. 22
2.6 Computed KIE for ts2 in THF. 23
2.7 Computed KIE for TS_{cyc} in THF. 23
2.8 Methoxy substituted analog of 1-Re-H at the 4,4' position of bipyridyl ligand. 28

3.1 Hazari's Octahedral trans-Trihydride Complex (1-Ir-H) 32
3.2 Computed KIE for ts1 in THF. 35
3.3 Computed KIE for TS_{cyc} in THF. 36
3.4 General structure of a tridentate Pincer-Ligand 38

4.1 Series of Carbonyl compounds; **1**: Formaldehyde/**2**: Acetaldehyde/ **3**: carbon dioxide/**4**: Acetone/**5**: Dimethyl carbonate/**6**: Lactone/**7**: Ethyl acetate/**8**: N-methylacetamide/**9**: Methyl methylcarbamate/**10**: Urea/**11**: Dimethylurea. 46
4.2 Gusev's Octahedral Osmium *trans*-Dihydride Complex (1-Os-H) . 46
4.3 Insertion reaction into 1-Os-H 47
4.4 Thermodynamic Cycle for carbonyl compounds reduction 48
4.5 Thermodynamic Cycle 3 for energy barrier at ts1. 54

List of Tables

2.1 Variation in KIE of ts1 and TS_{cyc} upon scaling the harmonic frequencies with 5 different methods. 25
2.2 Computed solvent and substituent effects on the energy of the stationary points for CO_2 insertion in 1-Re-H, ΔG *in kcal/mol at 298 K and 1 M.*(- : indicates unlocated species) 27

3.1 Stretching vibrations of 1-Ir-H and TS_{cyc} *(cm^{-1})*, their force constant *(mDyne/A)*, and reduced masses *(amu)*. 37
3.2 The change in N–H bond stretching vibration frequency cm^{-1} at different stages of the reaction. 39
3.3 The variation in *trans* Ir-H bond length (A) and secondary α-KIE at different stages of the reaction in THF. 40

4.1 Electronic(ΔE), Gibbs Free Energy ΔG^o and Equilibrium Isotope Effect for the insertion reaction of different carbonyl compound. *Energies are in kcal/mol.* 47
4.2 Computed M06L-D3 Distortion Energies shown in thermodynamic cycles. 49
4.3 The electronic energy ($\Delta E^{\ddagger}$), Gibbs free energy ($\Delta G^{\ddagger}$),imaginary frequency, reduced mass (μ), KIE and some bond distances at ts1. 52
4.4 Computed M06L-D3 Free energies for stationary points along the PES of the reaction of 1-Os-H with all the substrates. Gibbs free energies are given in kcal/mol at 298 K and 1 M relative to the separated reactants. 53
4.5 Computed M06L-D3 for Energies in Cyle 3. 55

Chapter 1

Introduction

1.1 Introduction to Insertion Reactions

Inesrtion of unsaturated molecules such as olefins and carbonyl compounds into metal-hydride bonds is one of the most fundamental and characteristic reactions in transition metal chemistry. This reaction or its reverse deinsertion (β-hydride elimination) is a key step in a wide range of important catalytic transformations such as hydrogenation, hydroformylation and the water gas shift reaction. Conventionally, insertion reactions in coordinatively saturated complexes follow inner-sphere mechanisms that require an empty coordination site brought by ligand dissociation to bind the substrate directly to the metal at some stage of the reaction as illustrated in **scheme 1.1** [1, 2].

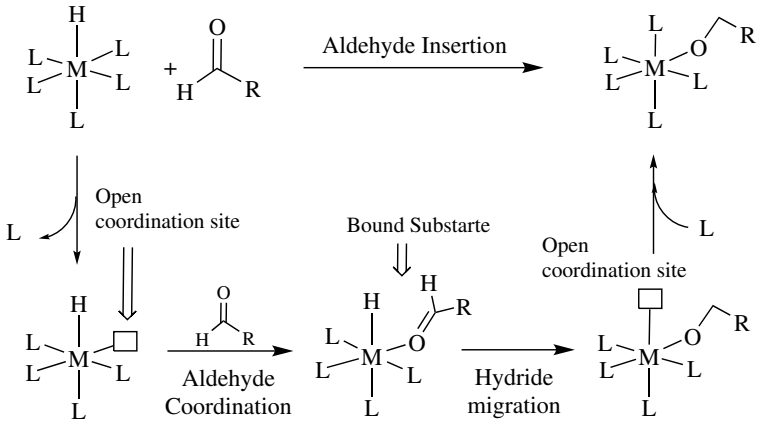

Scheme 1.1 – Classical Inner-sphere Aldehyde Insertion

In 1986, Sullivan and Meyer reported that carbon dioxide undergoes insertion into the Re-H bond of the octahedral complex *fac*-(bpy)Re(CO)$_3$H (bpy=2,2'-bipyridine) yielding a Re-formate product [3]. Through mechanistic and kinetic investigations, they argued their results supported a non-classical associative

mechanism where no vacant coordiantion site is required, they proposed the mechanism can have either a linear or a cyclic transition state (TS) in the rate-determining step (RDS). To what best known, this marks the first example of an associative insertion reaction mechanism.

Since then, there have been ample observations implicating associative insertion for CO_2 [4, 5, 6] as well as for other organic substrates. Concerning carbonyl group insertion (XYC=O), remarkably, Bergens and coworkers observed experimentally a *trans*-hydrido alkoxide product at very low temperature (-80 °C) when mixing stoichiometric amounts of acetophenone and the octahedral complex trans-dihydride [(BINAP)Ru-$(H)_2$(diamine)] as outlined in **scheme 1.2** [7]. Obviously, initial ligand dissociation and ketone coordination is unlikely in this system, where an associative mechanism is proposed to take place through a cyclic TS.

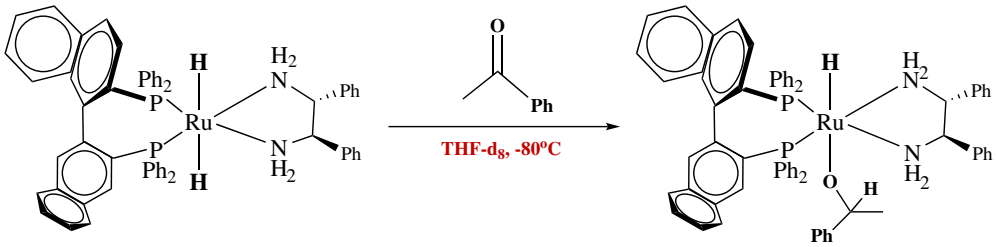

Scheme 1.2 – Experimentally observed Ru-Alkoxide bond.

Accordingly, Blum and Milstein provided experimental evidence for a non-classical mechanism for aldehyde de-insertion from an octahedral metal-methoxide complex that did not require an empty coordination site, and DFT calculations on this reaction supported a cyclic TS as rate determining [8]. Associative unsaturated molecules and especially CO_2 insertion into the M-H bond of octahedral catalysts has been the subject of several theoretical investigations. However, these studies provide a conflicting views about the RDS.

The aim of this thesis is to address the gap concerning the RDS in insertion mechanism of some unsaturated molecules such as carbon dioxide and other carbonyl compounds into octahedral transition metal hydride complexes where a review for previous mechanistic studies are elaborated in the introduction of each chapter. Detailed calculations of the outer sphere associative PES in this reaction will take place through quantum chemical methods and computational tools. In the next part of this introductory chapter, a brief introduction to kinetic isotope effect (KIE) as a tool for elucidating reaction mechanism will take place as well a discussion of the development of quantum methods, specifically Density Functional Theory (DFT).

1.2 Background of Isotope Effects

1.2.1 Discovery

The theory of isotopes or the fact that atoms coming in more than one weight can have same number of protons but different masses has been discovered since 1920, through spectral lines arising in the bands of simple molecules. By that time, the less-abundant isotopes of carbon, nitrogen, and oxygen had been disclosed. It was until 1931, the pioneering work of the chemist and physicist Harold C. Urey on isotopes who believed that isotopes of hydrogen —the lightest element— could be more important, led to his discovery of deuterium [9], for which he subsequently won the Nobel Prize [10]. Ever since the "heavy hydrogen" discovery came to light, isotopes were an active field of research. The rapid development of nuclear physics after 1931 was initiated by isotope research [11].

Before the discovery of deuterium, chemical properties were generally supposed to be determined by the number and configuration of the extranuclear electrons, quantities that are identical for isotopes of the same element. Thereafter, Eyring and Polanyi independently predicted the mass dependence of these properties, postulating that protonated and deuterated compounds should have different dynamic behavior in chemical reactions in much the same way that the heavier objects tend to move more slowly than lighter ones. This prediction has been amply verified [12], and the deuterium isotope effect has been found to be of great value in the study of the mechanisms of chemical reactions and in the development of the theories of rate processes. The superiority of the isotope method in mechanism detection lies mainly in the possibility of making the substitution within the very reacting center and with a minimum change in reaction's parameter. This was especially fruitful in investigations of complex physiological processes and in medicinal chemistry, as in the breakdown of fatty tissue and in cholesterol metabolism [13, 14].

1.2.2 Theoretical Basis of Kinetic Isotope effects

Kinetic Isotope Effects (KIE), which refers to the difference in dynamic behavior between isotopes, can be measured experimentally and theoretically to provide detailed analysis of the mechanism of reaction under investigation [15]. It is defined as the ratio of rates constants of the reaction of hydrogen over that of deuterium, **eq 1.1**.

$$KIE = \frac{k_H}{k_D} \tag{1.1}$$

Henry Eyring's "theory of absolute rates" [16, 17] expresses KIE as the exponential of difference of free energy of proteo and deutero reactions over RT, gas constant and temperature respectively, **(eq 1.2)**, where $\Delta G_H^{\ddagger}$ is free Energy for

proteo-reaction and $\Delta G_D^{\ddagger}$ is that for deuterium, however, an approximation of equal pre-exponential terms in rate equation of isotopic reactions is provided.

$$KIE = \frac{k_H}{k_D} = exp^{\frac{\Delta G_H^{\ddagger} - \Delta G_D^{\ddagger}}{RT}} \tag{1.2}$$

Understanding the major factors contributing to this quantum mechanical phenomenon arises from the Potential energy curve of vibration of the bond to hydrogen and that to deuterium shown in **figure 1.1**.

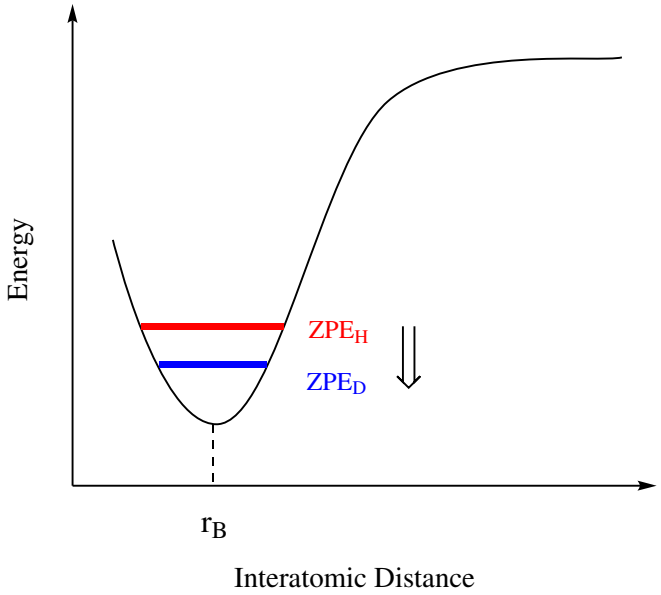

Figure 1.1 – Potential Energy Curve of Bond to Hydrogen/Deuterium.

Since the electronic structure of the two isotopes of the same element are identical, hence, the forces which hold the atoms together will be nearly independent of the changes in the masses of the atomic nuclei caused by isotopic substitution, then this curve is identical for both bonds, and the vibrational force constant k in Hook's law expression **eq (1.3)** could be treated as invariant under isotopic substitution, but the total vibrational frequency is mass dependent.

$$\upsilon = \frac{1}{2\pi c} \cdot \sqrt{\frac{k}{\mu}} \tag{1.3}$$

Even in it's ground state or at absolute zero, an oscillator (bond) retains a certain amount of vibrational energy, commonly referred to as zero-point vibrational energy (ZPE), **eq 1.4**, which is dependent upon the vibrational frequency, **eq 1.3**, and hence on masses.

$$ZPE = \frac{1}{2} \cdot \frac{1}{2\pi c} \cdot \sqrt{\frac{k}{\mu}} \tag{1.4}$$

Therefore, different isotopes will encounter different ZPE. Simple math of the described equation above, provides that the ZPE is inversely proportional to the square root of the mass and that the heavy isotope will always end with the smaller ZPE.

In a chemical reaction, considering the curve relating the potential energy of a system with the distance along the reaction coordinates **figure 1.2**, on top of which resides the transition state (activated complex), the barrier to reach this TS from the starting reactants is E_a. Difference in width of curves in reactant and TS express different force constant of the bond being cleaved and that being formed. According to **eq 1.4**, the difference in zero point energy upon deuteration decreases with decreasing force constant and increasing reduced mass, therefore, bond with higher frequency encounters higher ΔZPE.

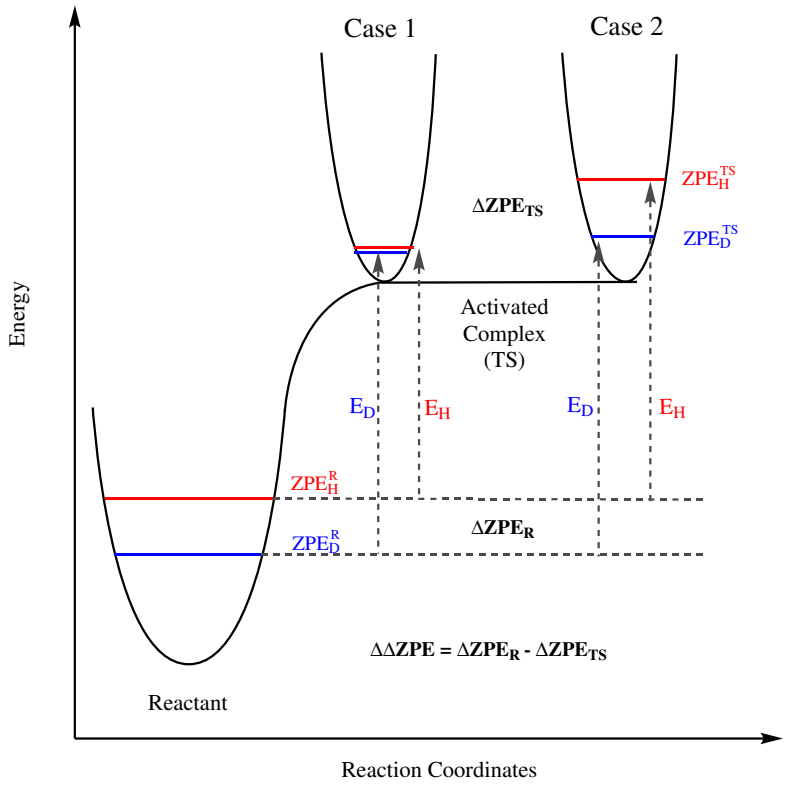

Figure 1.2 – Potential Energy Profile based on TST. *(E is the activation Energy reaching TS)*

However, the difference in zero-point energy in the TS in **figure 1.2** is also affected by the involvement of the assigned isotope sensitive bond in the reac-

tion coordinates near the activated complex. Hence, it is this involvement that determines the scope of the difference of zero point energy in the reactant and TS, thus ΔΔZPE.

In a rate process and according to the quasi-thermodynamic conventional transition state theory (TST)[18], scientists treated KIE in the harmonic approximation, where it is expressed as result of the partition function ratio of translational, rotational and vibrational energies, simplified in **eq 1.5**.

$$KIE = (\frac{Q^{R*}Q^{TS}}{Q^{R}Q^{TS*}})_{rot}.(\frac{Q^{R*}Q^{TS}}{Q^{R}Q^{TS*}})_{trans}.(\frac{Q^{R*}Q^{TS}}{Q^{R}Q^{TS*}})_{vib}.exp^{\frac{-\Delta\Delta ZPE}{RT}} \tag{1.5}$$

At low temperature, the exponential term, which is a purely enthalpy factor expressing the effcet of difference in ZPE between reactant and TS (ΔΔZPE), dictates the nature and significance of KIE, and considered the heart of isotope effect.

The first two terms in **eq 1.5** are the mass-moment of Inertia (MMI) term, which is the contributions from rotational and translational motions, critical incase of isotope effect in reactions involving molecules of small mass such as H_2. The third term is the contribution of vibrational motion, which are the thermal and entropy contributions, mainly dominates at high T. This will result in KIE being expressed as :

$$KIE = MMI.EXC.EXP \tag{1.6}$$

As shown in case (1) in **figure 1.2** and at room temperature, assuming the bond to be cleaved in the reaction to be relatively weak in the activated complex in comparison to the reactants, then the effect of zero-point energy on the rate becomes apparent ($E_D > E_H$), and the proteo-reaction will be more favored. However, in other cases: such as case (2) there is a considerable difference in zero-point energy in the activated complex which will in part cancel the difference in zero-point energy in the reactant, compensating it's effect and thus resulting in less-significant KIE.

From case 2 arises two legitimate types of KIE; **i)** The **Normal** KIE (KIE>1) resulting when $|\Delta ZPE_{TS}| < |\Delta ZPE_{React}|$ and **ii)** The **Inverse** KIE (KIE<1) resulting when $|\Delta ZPE_{TS}| > |\Delta ZPE_{React}|$.

It is shown that isotope effects are probes for force constant changes at the position of isotopic substitution. A quick analysis of **eq 1.5** shows that isotope effect will tend to be normal (light faster than heavy) if force constants in the transition state are smaller than in reactant and inverse if the opposite situation holds.

Simplistically, while the force constant of the bond in reactant and TS determines the nature of KIE, it is the strength of the involved bond in the activated complex what determines it's significance. So the treatment of vibrations in the assigned transition states and determining their KIE will be a key feature in

elucidating reaction mechanisms through investigating the stages where the new bond is formed and the old bond is cleaved, thus, specifying the most possible rate determining step (RDS) of the reaction under investigation.

1.2.3 Classifications of Isotope Effects

Isotope effects are categorized as either primary or secondary. Primary isotope effects are rate changes due to isotopic substitution at a site of bond breaking in the rate determining step of a reaction. Secondary kinetic isotope effects are rate changes due to isotopic substitutions at a site other than the bond breaking site in the rate determining step of the reaction. In other words, it occurs when the atom being substituted is not directly involved in reaction center.

Like primary-KIE, the magnitude of secondary-KIE is determined by vibrational factors, while unlike it, secondary KIE tends to be much smaller. However, it is still very useful in elucidating reaction mechanisms [19]. Normal secondary KIEs are generally observed at atoms undergoing a weakening of their bonds in the transition state, while inverse secondary KIE can result from crowding of an atom at the transition state.

From such simple assumptions, KIEs can be interpreted qualitatively to provide valuable information about the nature of atoms being transferred and/or the geometry of transition state.

1.3 Introduction to Computational Chemistry

1.3.1 Theories Behind Computing

Computational Chemistry is considered as more "recent" addition to the plethora of approaches developed to aid in the continuous search for the origins of chemical phenomena. In mechanistic studies,the tremendous progress in the development of hardware, software, and theoretical methods allowed scientists to gain detailed information about mechanism of chemical reactions, by studying the nature of transition states directly, allowing therefore the analysis of the origins of selectivity or the study of more complex reactivity scenarios, such as those related to catalysis as well as property prediction.

It all starts by studying the electronic structure of atoms and molecules to describe their motion. Exploring the electronic structure and the properties of many-electron systems can be done by means of solving the famous Schrödinger equation (SE), **eq 1.7**:

$$H\Psi = E\Psi \tag{1.7}$$

where H is the Hamiltonian of the system (which takes into account five contributions to the total energy of a system: the kinetic energies of the electrons and nuclei, the attraction of the electrons to the nuclei, and the interelectronic and

internuclear repulsions), E is the energy of the system, and Ψ is the many-electron wave function. Theoretical chemists approach the above equation in two different manners, in a time-dependent **eq 1.8** and time-independent **eq 1.9** fashion which begins by assuming the separability of the space and time coordinates.

$$i\hbar\frac{\partial\psi(x,t)}{\partial t} = -\frac{\hbar^2}{2m}\frac{\partial^2\psi}{\partial x^2} + V(x,t)\Psi(x,t) \tag{1.8}$$

$$-\frac{\hbar^2}{2m}\frac{\partial\psi(x)}{\partial x^2} + V(x,t)\Psi(x,t) = E\Psi(x) \tag{1.9}$$

where i is the imaginary unit, $\hbar$ is Planck's constant divided by 2π, and V is the potential operator.

Solving the Schrödinger equation essentially means to find a wave function solution (Ψ) that specifies which positions of all the electrons in a molecule are more likely and which are less likely. But unfortunately, solving it fully for systems with more electrons than a hydrogen atom is computationally impossible, however, quantum mechanics (QM) algorithms can approximate it. To that extent, an enormous amount of effort has been expended on developing mathematical and theoretical techniques in solving SE based on quantum mechanics approximations and their implementation into computer programs. **Figure 1.3** shows important milestones since the early period of quantum mechanics implemented in computational chemistry nowadays.

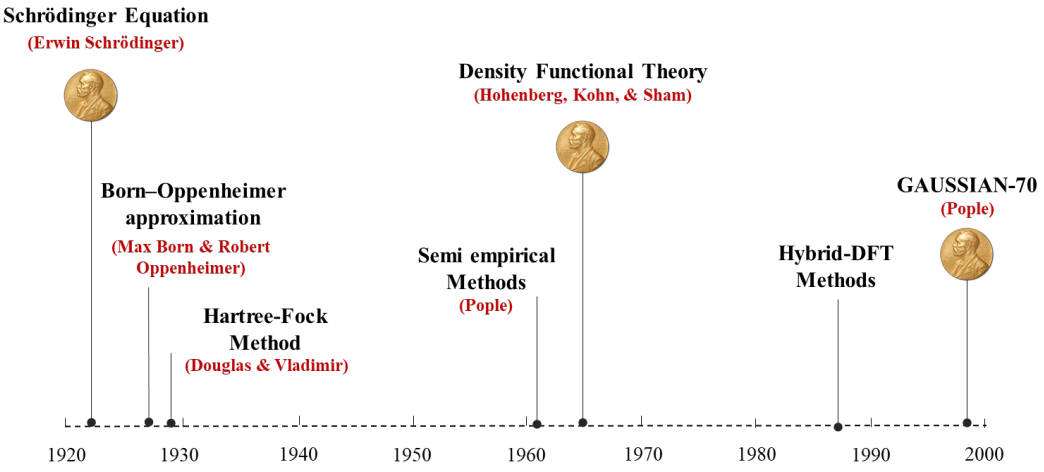

Figure 1.3 – Milestones in quantum mechanics contributions to Computational Chemistry.

In 1928, Douglas R. Hartree introduced "self-consistent field method (SCF)" [20], which was later augmented by Vladimir A. Fock to be known as the Hartree-Fock (HF) method [21]. HF makes the fundamental approximation that each

electron moves in the static electric field created by all of the other electrons - thus neglecting electron correlation- and then proceeds to optimize orbitals (wave-functions) for all of the electrons in a self-consistent fashion subject to variational principle. It was defined as a stepping stone on the way to more sophisticated theories toward the ultimate rigor of solving the Schrödinger equation thus predicting properties and energies.

In the early 60s, a new standpoint toward the electronic interaction in molecules is possessed, which was later known as the electron density. It originates from the dependence of the hamiltonian operator on the total number of electrons in a molecules, therefore, integrating this density over all space gives the total number of electrons, **eq 1.10** [22].

$$N = \int \rho(r).dr \tag{1.10}$$

Assuming the variation principle approximation and Born-Oppenheimer's which assumes fixation of the nuclei's position and separation from electronic interactions, Hohenberg, Kohn, and Sham represented the first effort to define the Density Functional theory (DFT). It is known as using functionals (function of a function) by which energies and properties can be obtained from the electron density function of the system under study. Interestingly this density ($\rho(r)$) started to emerge as a useful physical observable among computational researchers. Despite it's introduction a few decades before, in 1998, the Nobel Prize in Chemistry was divided equally between Walter Kohn "for his development of the density-functional theory" and John A. Pople "for his development of computational methods in quantum chemistry-*Gaussian-70*" [23].

DFT is now used in studies of numerous chemical problem areas, from calculating the geometrical structure of molecules (i.e. bonding distance and angles) to mapping chemical reactions, which is dealt with as bond formation/cleavage occurring due to changes in electronic states of molecules along a potential energy surface (PES).

In organometallic reactions, those involving transition metal complexes as catalysts, such as polymerization of olefins [24], dehydrogenation of alcohols [25], ammonia synthesis [26] and CO_2 hydrogenation using homogeneous catalysts [27], the mechanism involves more than one intermediate and transition state, therefore, the development of highly active catalysts is related to correctly understanding the complicated mechanisms. This is where alot of DFT calculations are employed.

1.3.2 Methods of Inquiry

This thesis is for purely theoretical work. DFT electronic structure calculations were done using quantum chemical software- *Gaussian16*[28]. The main procedure to start DFT calculations is determining the level of theory which is what signifies the hamiltonian used to apply a certain approximation and the basis set,

describing mathematically the molecular orbital within a system in which the theory is conducted. Unless otherwise specified, all geometry optimizations and frequency calculations were done at the popular M06L-D3 level of theory developed by Truhler and coworkers [29], and is proven to have balance between accuracy and time for transition metals and organometallic compounds[30]. The basis set used for main group elements is def2tzvp, while all metals incorporated additional associated effective core potential (ECP), which is a method used to reduce the scope of the electronic structure problem for heavy elements, by treating only their valence electrons. The calculations are linked and compared to available experimental work. To set the most optimal experimental solvent conditions, the universal continuum solvation model (SMD) is used [31], which is based on the quantum mechanical charge density of a solute molecule interacting with a polarizable continuum description of the solvent such as: THF, acetone, acetonitrile and toluene employed in this study. The thermal and entropy terms to the Gibbs free energy were computed at 298.15 K and 1 M concentrations. The harmonic frequencies were used to calculate the KIEs without any scaling. As a proof of concept, scaling frequencies by 0.95 is done, and results obtained this way did not show any significant change. Gaussview 5 visualization software was utilized for visualization of optimized geometries, vibration frequencies and intrinsic reaction coordinates (IRCs) [32]. Quantum Theory of Atoms in Molecules (QTAIM) was done using the Müller approximation [33] as implemented in AIMALL program ultilized for calculations of Delocalization index parameter (DI), for located Bond critical points (BCP) in some optimized molecules [34].

Chapter 2

Mechanistic DFT Study on CO_2 Insertion into Re-H Bond of $(bpy)Re(CO)_3H$

2.1 Aim and Background of the Study

Predictions on the increase in earth's temperature upon increase in the concentration of CO_2 was first estimated by the Swedish Nobel laureate Svante Arrhenius in 1896 [35]. Scientists for decades had shown that carbon dioxide traps heat and thus functions as green house gas causing global warming. The problem is accelerating bringing the world to irreversible climate change. The latest in this attempt was the 2021 nobel prize in physics which was awarded to Syukura Manabe for his accurate predictions of consequences of carbon dioxide accumulation in the atmosphere, and the foundation of current climate models [36, 37].

CO_2 is the product of combustion of fossil fuels, it is relatively inert, non-toxic and highly abundant gas. Therefore, a high driving force is required to mitigate its release into the atmosphere. The demands for green and sustainable chemistry have driven in recent years interest in utilizing the abundant CO_2 as a carbon feedstock for synthesis in renewable energy [38], for hydrogen storage [39], and the main precursor for preparation of organic compounds synthesised on large industrial scales [40].

Current research in this area uses heterogeneous catalysts based on transition metals for electrocatalytic conversion, however, most displayed little selectivity to the product between methane, carbon monoxide, and formic acid. In practice, these metals are either too expensive or have limited lifetimes but currently being operated and improved on a pilot scale [41, 42, 43]. Alternatively, homogeneous molecular organometallic complexes may be employed as catalysts for hydrogenation of carbon dioxide to formic acid. A lot of 2nd and 3rd row

transition metals have shown to be active for carbondioxide hydrogenation. The first step in the catalytic cycle of such reactions is proposed to be the insertion of CO_2 into the metal-hydride bond to generate a metal-formate bond, **eq 2.1**, which is believed to be a key step in the proposed mechanism of CO_2 reduction. Therefore, understanding the insertion mechanism is of fundamental interest and can be important to catalyst design.

$$M - H + CO_2 \longrightarrow M - OCHO \tag{2.1}$$

In their study in 1986, Sullivan and Meyer reported CO_2 undergoes insertion into the Re-H bond of the octahedral complex *fac*-(bpy)Re(CO)$_3$H (1-Re-H; bpy=2,2'-bipyridine) yielding a Re-formate product (1-Re-OCHO) [3]. The kinetics of the reaction in aprotic solvents followed a second order rate law, and the rates were sensitive to the solvent as well as to substitution at the 4,4'-bpy positions but not to the presence of additives like PPh_3 and NEt_3. As mentioned in the previous chapter, Sullivan and Meyer argued the results supported a non-classical associative mechanism that can have either a linear or a cyclic transition state (TS) in the rate determining step (RDS) as shown in **scheme 2.1**.

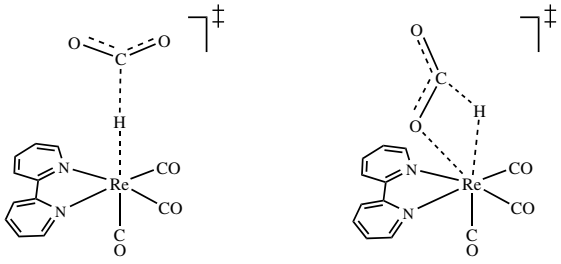

Scheme 2.1 – Associated TSs for CO_2 Insertion into 1-Re-H

Octahedral metal-hydride complexes are among the most investigated catalysts and electrocatalysts used in this context. For Example, Nozaki who's been a leader in this area of chemistry, discovered the pyridyl pincer ligated complex PNP-Ir(H)$_3$ (**scheme 2.2**) to catalyze CO_2 reduction to the formate anion in water using H_2 as reductant and KOH as a proton acceptor and invoked a catalytic cycle that begins with CO_2 insertion [27].

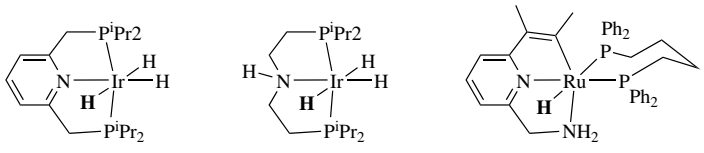

Scheme 2.2 – Efficient Octahedral catalysts in inserting CO_2

The reaction has been the subject of several experimental and theoretical investigations. However, there have been conflicting views about the rate-determining step of this fundamental step. DFT investigations by Ahlquist on the Nozaki catalyst calculated a mechanism that starts with a transition state **ts1** yielding an intermediate species **i1** described as a C-H bound formate intermediate as outlined in **scheme 2.3** [44, 45].

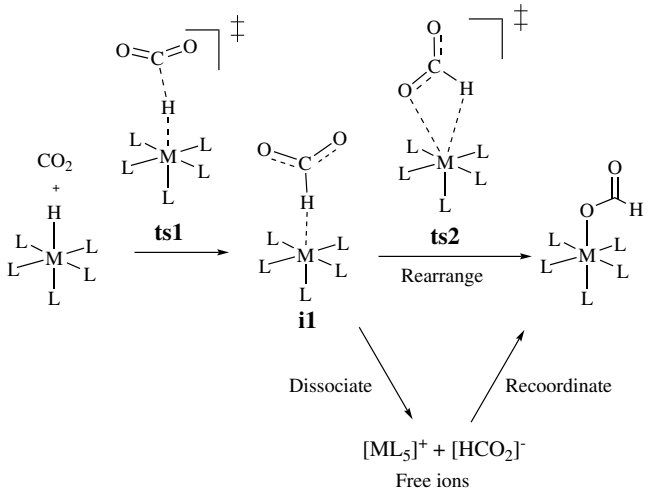

Scheme 2.3 – An Associative Insertion Mechanism

From i1 two distinct routes were considered to arrive to the final C-O bound formate product: **(i)** intramolecular rearrangement via cyclic transition state ts2 or **(ii)** dissociation into free ions followed by recoordination by one of the C-O formate bonds. The computed ts2 "the cyclic TS" imparted an activation barrier of 8.0 kcal/mol to the rearrangement route. An exergonic dissociation of i1 "the ion-pair" in water was presumed to be barrierless and was hence concluded to be the more plausible rearrangement route. This implies ts1 is the RDS for CO_2 insertion. Another study on the Nozaki catalyst by Yang calculated ts1 and assumed barrierless dissociation of i1 in water but did not calculate ts2 [46]. The same protocol was adopted in calculations by Hazari and coworkers on CO_2 insertion into an amino pincer analog of the Nozaki catalyst in THF **(scheme 2.2)** [47]. However, these investigations did not calculate TSs for the proposed dissociation of i1. This is a thorny problem for electronic structure methods because the entropy of dissociation of a ligand from a complex is highly favorable for the products but not necessarily for the dissociation TS which is often not possible to locate on the PES. The energy of ts2 in **scheme 2.1** might as well be lower than other points on the free energy surface leading to full dissociation into separated ions. Furthermore, calculations by Morokuma on the Nozaki catalyst in water and by Waymouth on a ruthenium catalyst with an amino pincer ligand in THF (**scheme 2.2**) both predicted ts1 and ts2 to have similar energies [48, 49].

Some studies reported only ts1 and skipped the question of the rearrangement of i1 altogether [50, 51], while other studies reported only ts2 [52, 53].

The mechanism of CO_2 insertion in 1-Re-H was the subject of computational study by Li and coworkers[54], which identified only a cyclic transition state. Remarkably, in this case the intrinsic reaction coordinate (IRC) originating from this TS was reported to connect the reactants "smoothly" with the products. Concerted CO_2 insertion in a metal-hydride bond was also reported in studies by Baiker and coworkers on the hydrogenation catalyst $[Ru(dmpe)_2H_2]$[52, 55]. However, these conclusions had been based on geometries optimized in the gas phase. Recent studies on the associative reactions between organic carbonyl substrates and bifunctional hydrogenation catalysts have shown the solvent can profoundly change the details of the outer-sphere potential energy surface [56, 57].

The extensive kinetic data uniquely available for CO_2 insertion in **1-Re-H** makes it an ideal system to address the associative PES. The previous calculations on this system were done as part of a more elaborate theoretical investigation of the mechanism of photocatalytic reduction of CO_2 by the chloro catalyst *fac*-$(bpy)Re(CO)_3Cl$ in the presence of triethylamine. The computed results were not discussed in details and no comparisons were made with the experimental data. The experiments included measurements of substantially inverse kinetic isotope effects (KIEs) 0.52 – 0.58 depending on the solvent. However, no attempts were made to use the observed KIEs to distinguish between the linear and Cyclic TSs proposed for 1-Re-H in **scheme 2.1**.

The aim of this chapter is to use DFT methods to investigate the associative mechanism for CO_2 insertion in 1-Re-H in details through isotope effect and Potential Energy Surface calculations, where both Linear and cyclic TSs are located, which allowed us to conduct side-by-side comparison of the involved transition states in the reaction along the available experimental data.

2.2 Results and Discussion

2.2.1 Energy Profile in THF

The stationary points identified on the associative PES in the reaction between CO_2 and 1-Re-H in THF are summarized in **figure 2.1**. Gibbs free energies (B) and Electronic Energies with solvent correction (A) are given relative to the separated reactants in kcal/mol. The calculations in THF identify a minimum i1 at an early stage of the PES in which the hydride is "sandwiched" between the metal and the carbon of CO_2. The Re-H and C-H bond distances in i1 are r_{Re-H} = 2.06 Å and r_{C-H} = 1.23 Å. i1 may at first suggest formation of an ion-pair in which the formate anion has been produced by hydride transfer from the metal but is still subject to an "extreme" degree of C-H activation by agostic bonding to a square pyramidal metal fragment. However, the common range for CH–M

agostic bond distances is 2.3 – 2.9 Å [58], much longer than r_{Re-H} in i1. In fact, in i1 Re-H is stretched by just 0.27 Å compared to the reactant 1-Re-H, and the C-H bond is still significantly longer than in the free formate anion, 1.23 vs 1.14 Å.

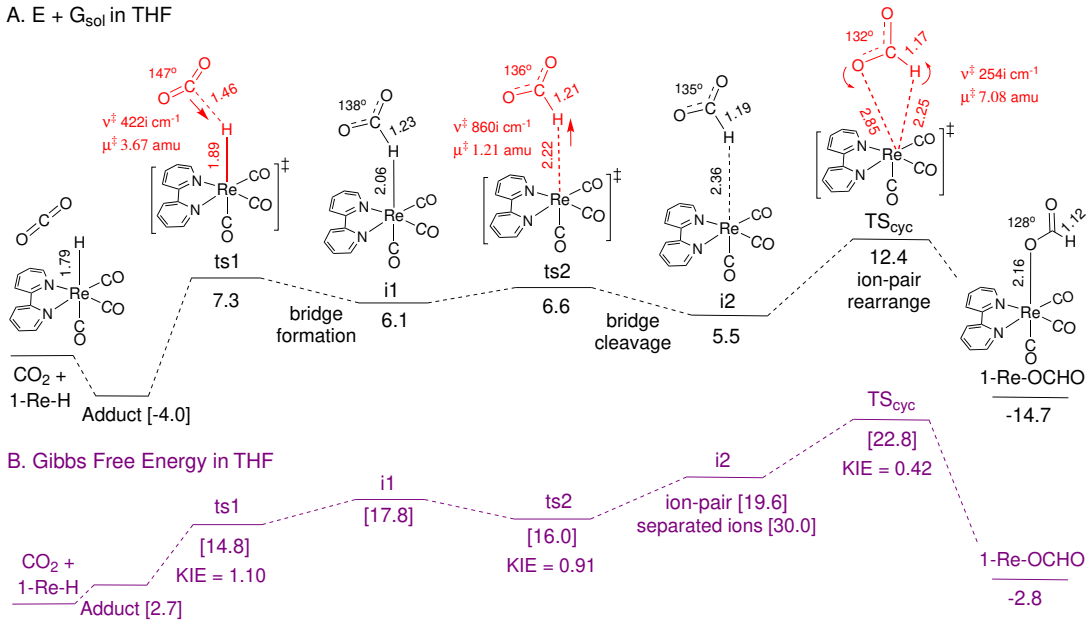

Figure 2.1 – Calculated M06L-D3 (A):E_{Solv}+G and (B): Gibbs free energy profile for CO_2 insertion into 1-Re-H in THF; in kcal/mol at 298 K and 1 M. Some bond distances are given in Å.

For a comparison, the borohydride adduct given in **scheme 2.4** is calculated to have a Re-H bond distance of 2.07 Å, a significantly stretched B-H bond (1.26 Å) and a bent Re-H-B angle (134^0).

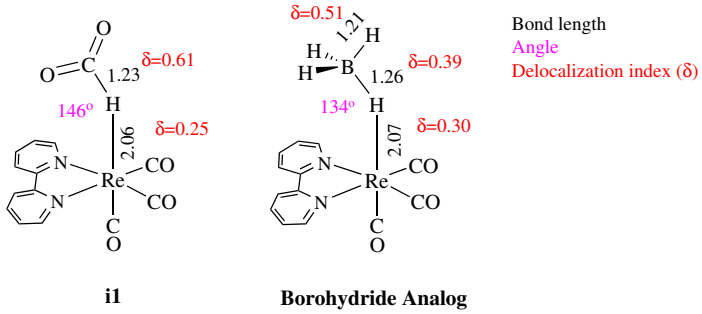

Scheme 2.4 – Comparison of Borohydride Analog of i1, through geometry analysis and Delocalization index.

Analysis of the electron density in the given adduct using the Quantum Theory of Atoms in Molecules (QTAIM) identifies a Bond Critical Point (BCP) in

the Re–HBH_3 bond. The Delocalization Index (DI) between the Re and H atoms of the Re–HBH_3 bond is 0.30 (δ values in scheme 2.4). This is a substantial value implying a significant degree of 2-electron sharing in the Re-H bond [34] which can be interpreted in terms of an appreciable bond order [59, 60] as expected from a bridging hydride. The intermediate i1 of interest also has a significantly bent Re-H-CO_2 angle, 146^0, and a Re–HCO_2 bond with a BCP and a substantial DI value, 0.25. By analogy with the borohydride complex, therefore, i1 may be classified as an organometallic bridging hydride complex. This means i1 can be viewed to be the product of a step involving addition of CO_2 to the hydride end of the intact Re-H bond, not the product of a hydride transfer step cleaving the Re-H bond to give an ion-pair species.

Consistently, the computed "linear" ts1 for this step is characterized by a very long C–H distance, 1.46 Å, and a Re-H bond that is barely stretched relative to the reactant; r_{Re-H} = 1.89 Å vs 1.79 Å. The intrinsic reaction coordinate (IRC) shown in **figure 2.2** reveals CO_2 approaches the Re-H bond at a significantly bent C-Re-H angle, not linearly, reaching 141° in ts1 and 146° in i1. For convenience, we continue to refer to ts1 as the "linear" TS. The reaction coordinate of ts1 is discussed further in the kinetic isotope effects section.

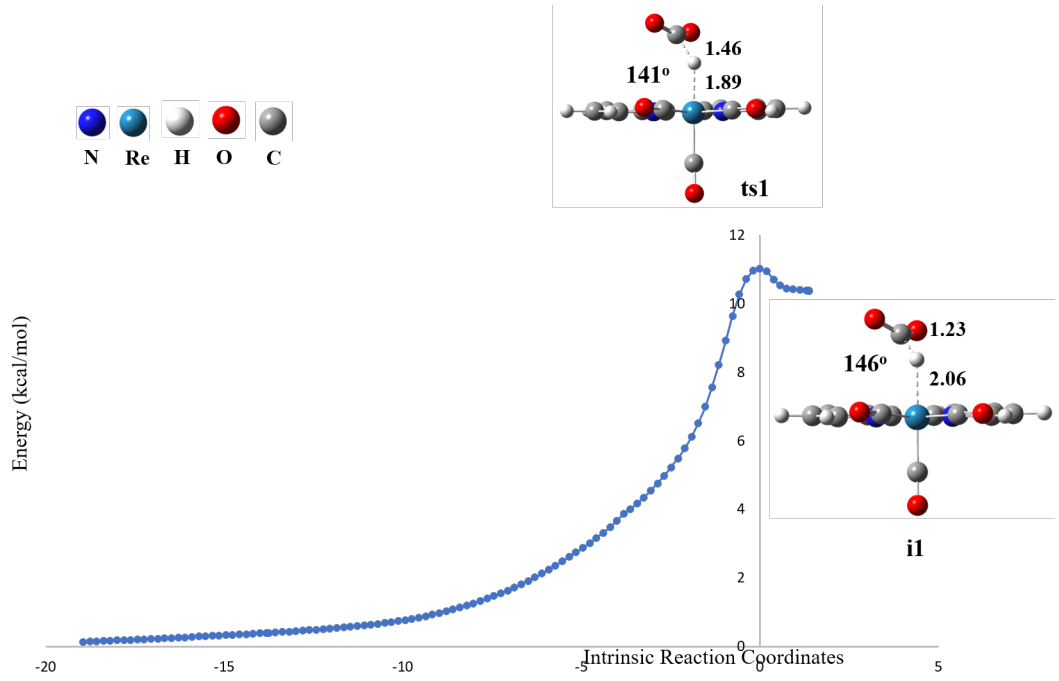

Figure 2.2 – Computed IRC plot for the Linear transition state "ts1" located on PES of CO_2 insertion into 1-Re-H in THF, bond length in Å.

As shown in **figure 2.1-A**, the electronic energy of ts1 is only 1.2 kcal/mol higher than i1. However, when the vibrational terms are included, the Gibbs free energy of i1 comes to be 3.0 kcal/mol above ts1, **figure 2.1-B**. This means i1 is

unlikely to be an observable intermediate in THF because there is no barrier for CO_2 dissociation. The reason we discuss i1 in these great details here is to stress that this species is *not a hydride transfer product.*

Further calculations in THF identified i2, the second intermediate located on the PES. The Re-H and C-H bond distances in i2 are r_{Re-H} = 2.36 Å and r_{C-H} = 1.19 Å. The Re-H bond at i2 is stretched by 0.57 Å when compared to the reactant 1-Re-H. Now, the metal-hydride bond is more consistent with the common range of CH–M agostic bond distances discussed earlier. This means that i2 could be now viewed as the product of the step involving metal-hydride bond cleavage forming an "ion-pair" where the C-H bond formed at i2 is still subjected to an agostic interaction with the metal.

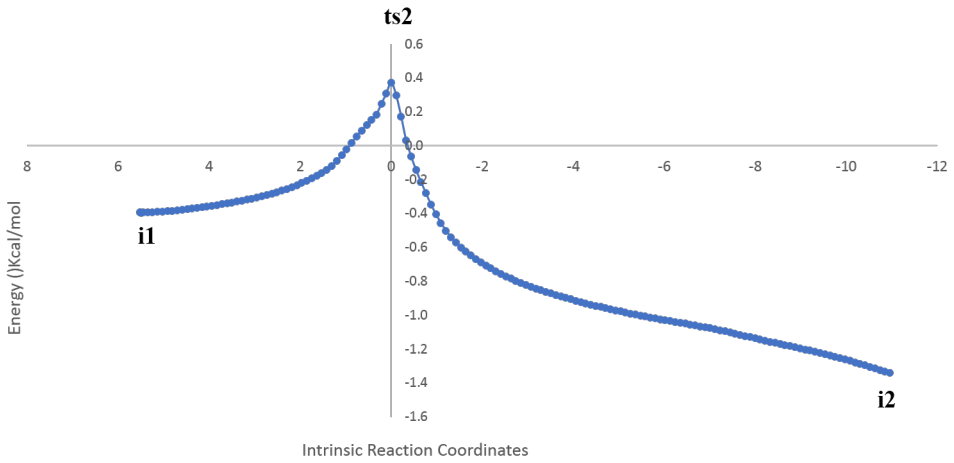

Figure 2.3 – Computed IRC plot for the second Linear transition state "ts2" located on PES of CO_2 insertion into 1-Re-H in THF, bond length in Å.

A computed second "Linear" transition state ts2 for this step is located and characterized by an imaginary frequency of 860i cm^{-1} consistent with motion of Re-H bond stretching vibration. The intrinsic reaction coordinate (IRC) for ts2 shown in **figure 2.3**, the variation in the Re-H bond along the IRC shows full cleavage of the Metal hydride bond starting from the bridged Complex i1. As shown in **figure 2.1-A**, the electronic energy of ts2 is only 0.5 kcal/mol higher than i1. However, when the vibrational terms are included, the Gibbs free energy of both i1 and i2 comes to be 1.8 kcal/mol and 3.6 kcal/mol above ts2, **figure 2.1-B**. This means that i1, ts2 and i2 all have similar energies. This is not surprising, since these three species differ by minor changes in the position of the hydride between the metal and CO2.

Starting with i1, the subsequent transformation leading to the final Re-formate product is computed to be highly exergonic: $\Delta G^{\ddagger}$ = -20.6 kcal/mol. The cyclic TS (TS_{cyc}) provides a direct route for this transformation. TS_{cyc} is characterized by an imaginary frequency of 255i cm^{-1} for a vibration that exchanges C-H and

C-O bond coordination of the formate anion to the metal as confirmed by IRC calculations, **figure 2.4**.

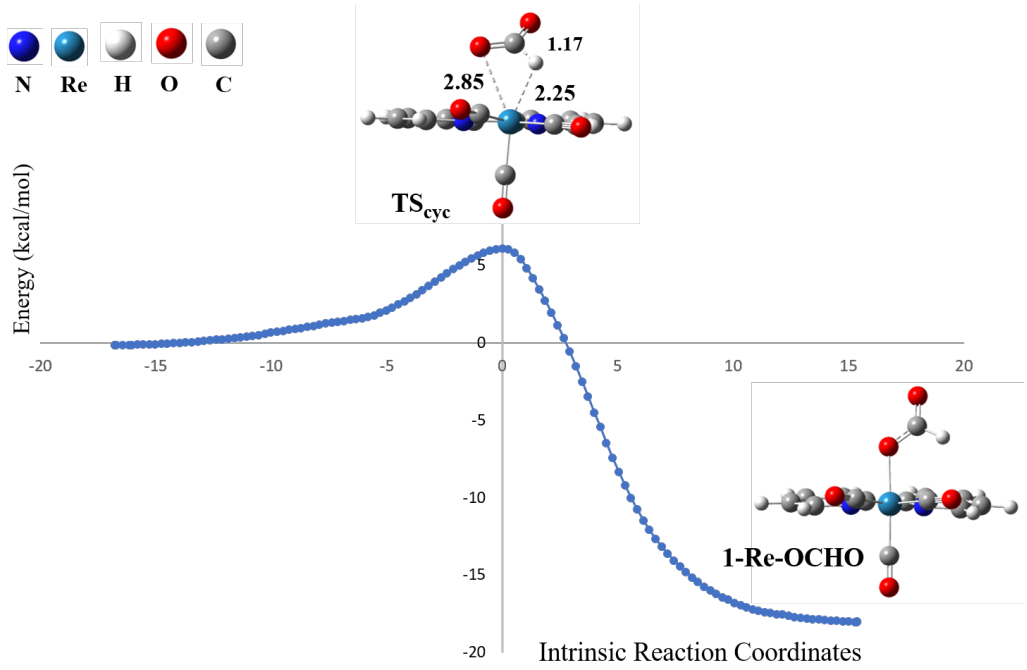

Figure 2.4 – Computed IRC plot for the Cyclic transition state "TS$_{cyc}$" located on PES of CO_2 insertion into 1-Re-H in THF, bond length in Å

The C-H bond in TS$_{cyc}$ is contracted to 1.17 Å but it is still pointed to the metal at 2.25 Å with a C-H-Re angle of 107º, suggesting some degree of C-H agostic bonding. The distance between the metal and the oxygen in the four membered ring of the reaction center, on the other hand, is long: 2.85 Å. Along these parameters, what is striking here in that the initial linear transition states (ts1 and ts2) and intermediates (i1 and i2) have very similar energies, and the IRC of TS$_{cyc}$ in THF concertedly links i1 to 1-Re-OCHO. This means that in effect, CO_2 insertion in this system effectively proceeds concertedly via a cyclic TS. This indicates that once the bridging species i1 is formed, TS$_{cyc}$ represents an early TS to reach the final low energy product. Consistently, the activation free energy from i1 to TS$_{cyc}$ is low, $\Delta G^{\ddagger} = 5.0$ kcal/mol.

The highest point on the Gibbs free energy profile in **figure 2.1** is 22.8 kcal/mol for TS$_{cyc}$ (at 298 K and 1M). Perhaps just fortuitously, this value is in excellent agreement with the experimental activation free energy of 23.0 kcal/mol determined at 298 K in THF from an Eyring plot. The computed energy of ts1 on the other hand is only 14.8 kcal/mol while that of ts2 is 16.0 kcal/mol. The dissociation of i1 into free ions is uphill by 12.2 kcal/mol, so dissociation won't compete with TS$_{cyc}$ in THF even if it was barrierless. Given that ts1 and ts2 don't lead to an energy well on the Gibbs free energy surface, the full results in

figure 2.1 imply CO_2 insertion into Re-H bond in 1-Re-H proceeds effectively concertedly in THF via TS_{cyc}.

Moreover, the reaction between CO_2 and 1-Re-H was computed in the gas phase, the IRC originating from TS_{cyc} was reported to connect the separated reactants smoothly with the product 1-Re-COHO, as reported previously by Li and coworkers[54].

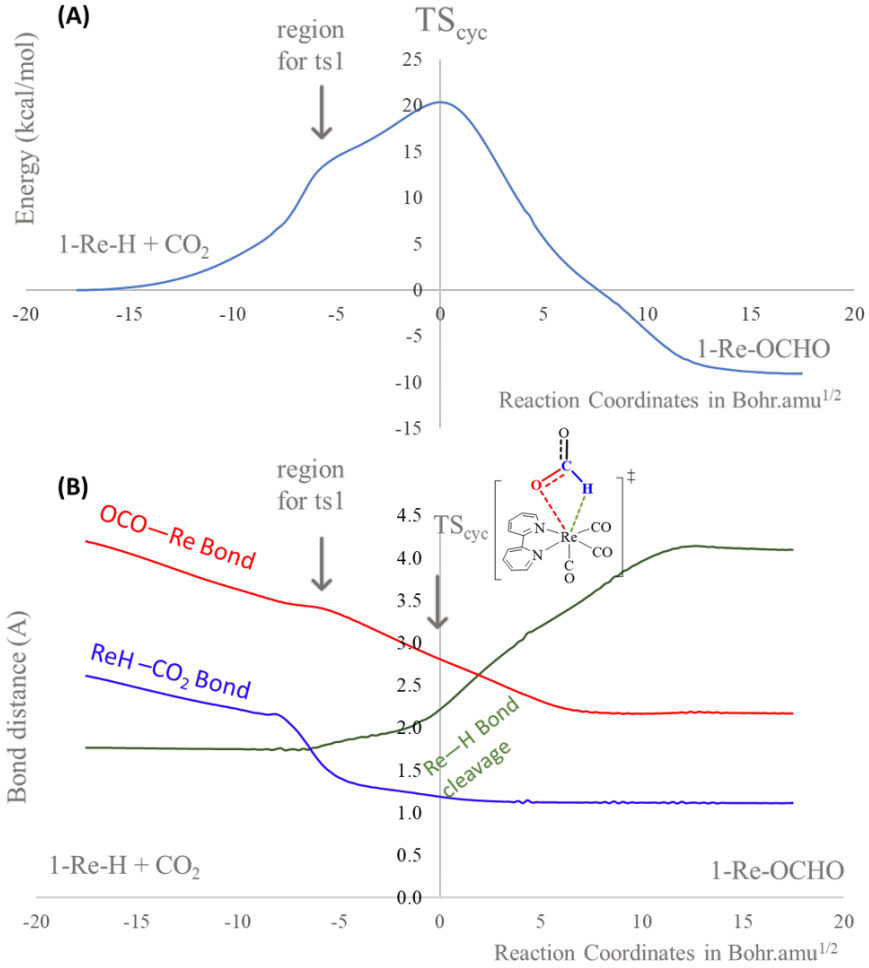

Figure 2.5 – Energy and selected parameters on the gas phase IRC for CO_2 insertion in 1-Re-H. *The reference point for the energy is the combined reactants as converged from the IRC.*

Our attempts to optimize ts1, i1, ts2 and i2 in gas phase weren't fruitful. Consistently, after TS_{cyc} location, it's calculated IRC shows no other stationary points, this is given in **Figure 2.5-A**. Although there are no more stationary points for other TSs and intermediates in the gas phase, the IRC features a shoulder at the early stage of the reaction where these species are expected to be

formed. The changes in the Re–H and H–CO_2 bond distances along the gas IRC as plotted in **Figure 2.5-B** illustrate how CO_2 initially bridges to the hydride in the ts1 segment, and how appreciable Re–H bond cleavage begins only afterwards in the ts2 segment.

Interestingly, unlike the H–CO_2 bond which shows to be formed in a great extent prior to TS_{cyc} and the Re–H bond which we previously showed that it cleaves largely in the ts2 region, the distance between the metal and one of the oxygen atoms of CO_2 decreases almost linearly along the IRC until the final formate product is formed. When combined, the two IRCs originating from ts1 and TS_{cyc} identified in THF shown in reveal net changes in the geometric parameters that are, overall, similar to the ones plotted in **Figure 2.5-A**. An effectively concerted CO_2 insertion in THF as inferred from the Gibbs free energy profile in **figure 2.1** is therefore not unreasonable.

In order to verify that the above finding in THF as a solvent is not an artifact of M06L-D3, the level of theory at which the calculations were conducted, and due to the difference in the nature of the species located on the potential energy surface of the reaction, we calculated the energy profile at the ωB97XD functional after geometry optimization, results are shown in **figure 2.6**. As shown, the calculated profile at this level enforces the above conclusion and predicts the energy of TS_{cyc} to be 21.7 kcal/mol, also close to the experimental, while that of ts1 is much lower at 13.1 kcal/mol, while no ts2 was located on this PES using ωB97XD functional.

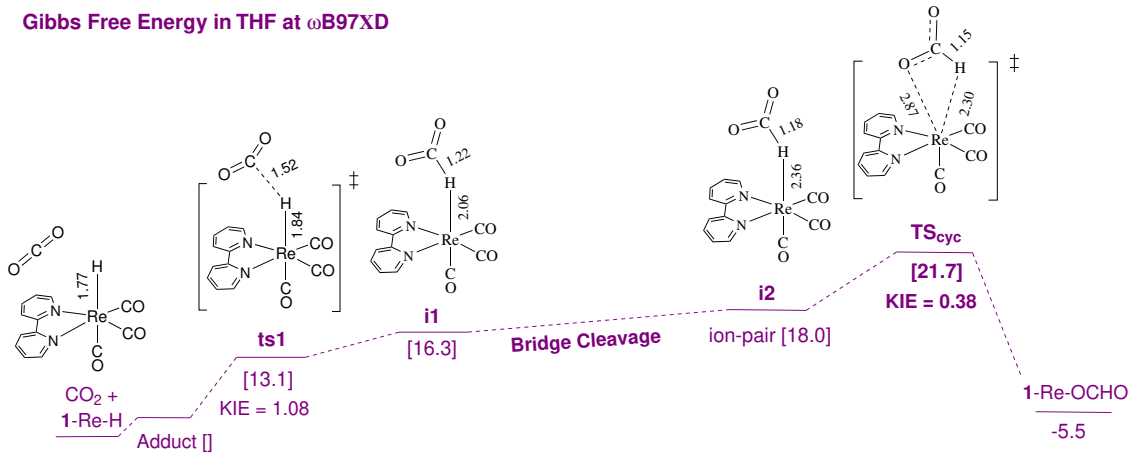

Figure 2.6 – Calculated ωB97XD Gibbs free energy profile for CO_2 insertion in 1-Re-H in THF; in kcal/mol at 298 K and 1 M. Some bond distances are given in Å.

Methodically, two additional functionals were used to calculate the Gibbs free energy profile of CO_2 insertion into 1-Re-H, which are: M06 [61] and B3LYP [62], both with and without dispersion, through single point calculation using geometries from the main M06L-D3 functional used. The conclusion continues

supporting a concerted mechanism for this reaction through TS_{cyc} which showed the highest point on the computed profiles (**figure-2.7**).

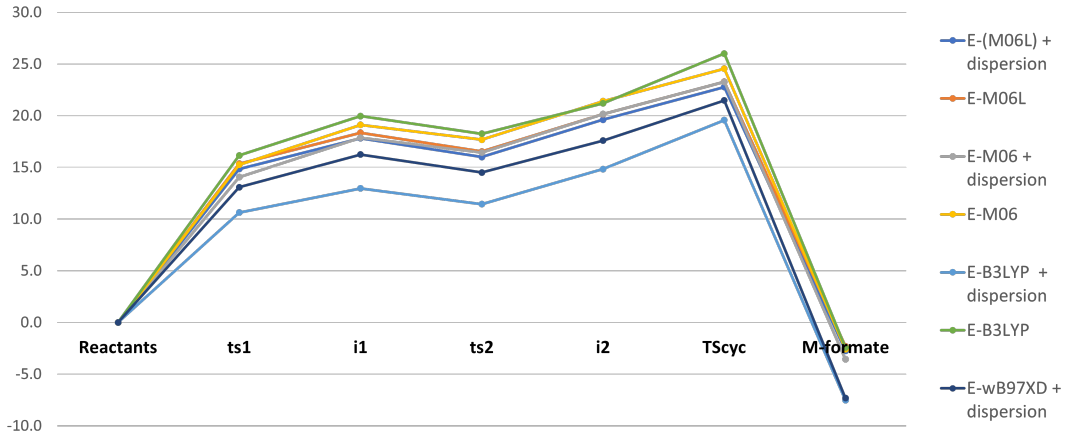

Figure 2.7 – Variation of the Energy Profile of the Reaction of CO_2 insertion into *fac*-(bpy)$Re(CO)_3H$ at different levels of theory in THF

2.2.2 Computed Kinetic Isotope Effect

The computed KIE for the initial step of CO_2 addition to 1-Re-H in THF via ts1 and its components are summarized in **scheme 2.5**.

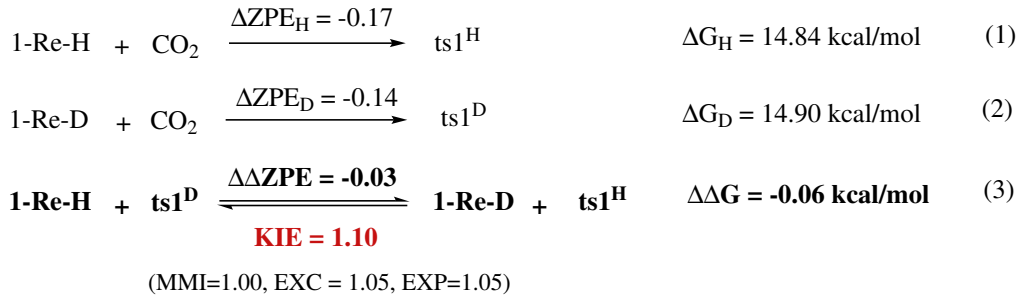

Scheme 2.5 – Computed KIE for ts1 in THF.

The barriers for the proteo and deutero reactions via ts1^H (eq 1) and ts1^D (eq 2) are very similar, $\Delta G^{\ddagger}$ = 14.84 and 14.90 kcal/mol, respectively. This means deuteration has a very minor unfavorable effect on the reaction rates of this step, leading to a very small normal KIE = 1.10, eq 3. The MMI, EXC and EXP components are all near unity for this KIE.

We at first found the absence of a KIE for ts1 to be quite intriguing because we thought this TS was for a "hydride transfer" step as been introduced in literature, so we expected the reaction coordinate to be dominated by the stretching vibrational mode of the Re-H bond being broken [63]. If this was true, the stretching mode of 1-Re-H would have become the loose vibration in ts1 ($\nu^{\ddagger}$). Because $\nu^{\ddagger}$ is a "lost" vibration in the TS with an imaginary frequency, the different ZPEs from the Re-H and Re-D stretching vibrations in the reactant would have contributed to a significantly negative $\Delta\Delta ZPE^{\ddagger}$ and a substantial normal KIE. It was this lack of a significant KIE that lead us to examine the nature of ts1 more closely. Thus, we find the actual $\nu^{\ddagger}$ in ts1 to have a reduced mass of 3.67 amu, and a motion that can be related to one of the translational modes of the free CO_2 molecule, consistent with a reaction in which CO_2 is adding to the Re-H bond. The vibrations in ts1 continue to include a distinct mode for Re-H stretching having a reduced mass near 1.0 amu and a frequency (1571 cm^{-1}) close to that in 1-Re-H (1642 cm^{-1}). Accordingly, $\nu^{\ddagger}$ in ts1 is not highly sensitive to isotope substitution of the hydride, dropping from 422i cm^{-1} to 387i cm^{-1} upon deuteration. For comparison, doubling the mass of the CO_2 carbon atom in ts1 lowers $\nu^{\ddagger}$ by 132i cm^{-1}, down to 290i cm^{-1}. The fact that the Re-H isotope sensitive vibrations in the reactant remain as real Re-H vibrations in ts1 can explain the lack of a KIE in the given step.

However, the stretching vibration was shown to be lost at ts2, the second "Linear" transition state that wasn't reported before in mechanistic studies on

CO_2 insertion into octahedral complexes. Upon deuteration, the imaginary frequency drops from $\nu^{\ddagger}$ = 860i cm^{-1} at ts2^H to 650i cm^{-1} at ts2^D. Despite the decrease in the imaginary frequency that is witnessed only at ts2 step, this step still didn't show significant KIE as illustrated in **scheme 2.6**. The barriers for the proteo and deutero reactions via ts2^H (eq 4) and ts2^D (eq 5) are observed to be very similar, $\Delta G^{\ddagger}$ = 16.00 and 15.64 kcal/mol, respectively. This means deuteration has a very minor favorable effect on the reaction rates of this step, leading to a very small inverse KIE = 0.91, eq 6. This inverse KIE could be explained in one way due to the partially formed C-H bond at ts2 step right before full cleavage of the Re-H bond. The partially formed C-H bond at ts2 mitigates the effect of imaginary frequency on yielding significant KIE. This inverse nature of KIE is fully consistent with step involving asymmetric bridged hydride cleavage. However, the experimentally reported KIE is much more inverse than that calculated for ts2.

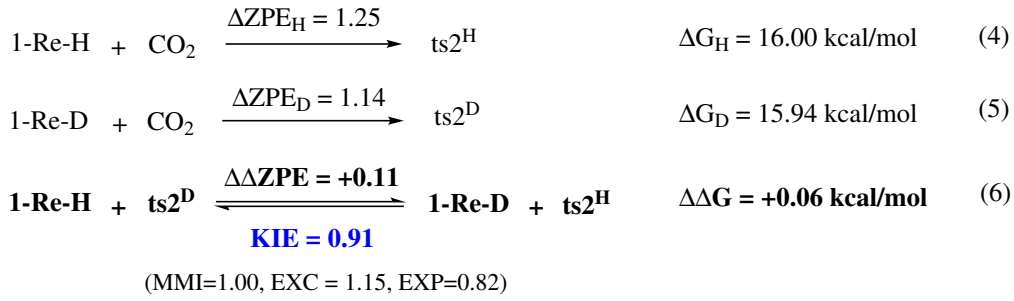

Scheme 2.6 – Computed KIE for ts2 in THF.

An altogether different condition applies for the KIE in TS$_{cyc}$ as summarized in **scheme 2.7**. Upon deuteration of the metal hydride, the activation free energy defined from the separated reactants to TS$_{cyc}$ is lowered from 22.76 to 22.24 kcal/mol, eqn's 7 and 8 respectively. The resulting $\Delta\Delta G^{\ddagger}$ = +0.52 kcal/mol leads to KIE = 0.42 in eq 9. The given KIE is driven by a positive $\Delta\Delta ZPE^{\ddagger}$ = +0.55 kcal/mol, which gives EXP = 0.40. The EXC term (1.05) mitigates the EXP term slightly, while the MMI term does not contribute to the KIE.

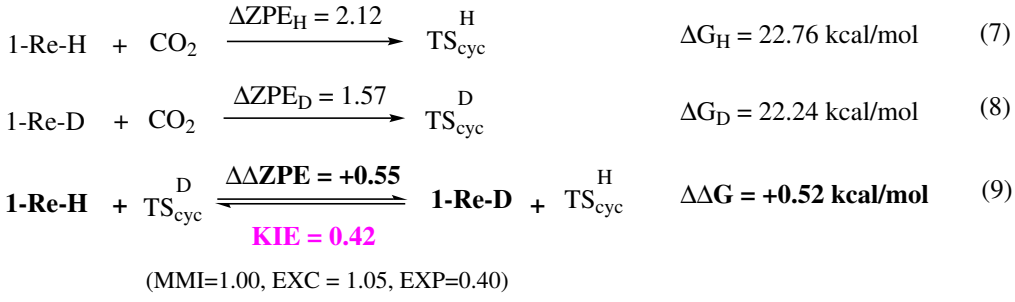

Scheme 2.7 – Computed KIE for TS$_{cyc}$ in THF.

The reaction coordinate characterizing TS_{cyc} corresponds to a rotation, or a slippage, of the intact formate anion over the square pyramidal cationic fragment. The imaginary frequency for this motion is again insensitive to deuteration: $\nu_{H}^{\ddagger}$ = 255i cm^{-1} vs $\nu_{D}^{\ddagger}$ = 246i cm^{-1}. In contrast to ts1 and ts2, however, in the transformation from 1-Re-H to TS_{cyc} the Re-H bond is totally lost and a new C-H bond is totally formed. The KIE in this case is determined by the different vibrational frequencies of the Re-H and C-H bonds which we elucidate for the stretching mode with the aid of **figure 2.8**.

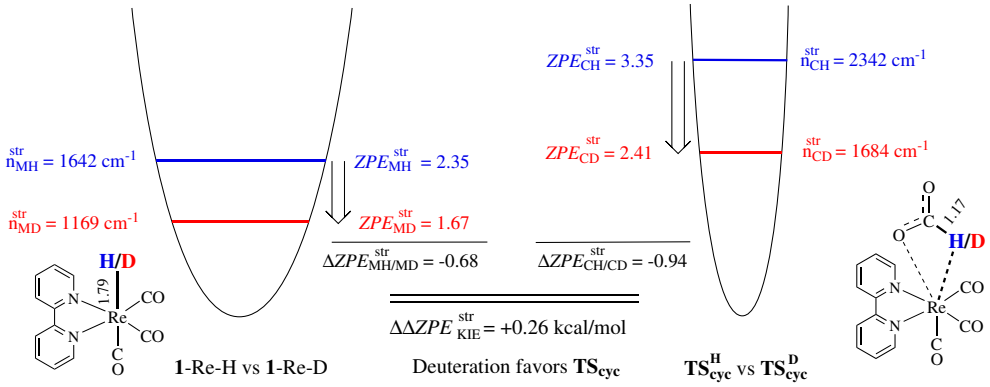

Figure 2.8 – Contribution of the Re-H and C-H stretching vibrations to the KIE of TS_{cyc}.

The frequency of the Re-H stretching vibration in the proteo reactant is ν^{str}_{MH} = 1642 cm^{-1} while the stretching frequency of the C-H bond in TS_{cyc} is ν^{str}_{CH} = 2342 cm^{-1}. Both modes have reduced masses near 1.0 amu, so the different frequencies originate from different force constants f^{str}_{MH} = 1.72 vs f^{str}_{CH} = 3.35 mDyne/Å, which is expressed in **figure 2.8** using different curvatures for the harmonic vibrational curves as explained in the previous chapter. These frequencies make different contributions to the ZPE of 1-Re-H and TS_{cyc}: ZPE^{str}_{MH} = 2.35 vs ZPE^{str}_{CH} = 3.35 kcal/mol. Upon deuteration these frequencies are lowered to ν^{str}_{MD} = 1169 and ν^{str}_{CD} = 1684 cm^{-1}, and their contributions to ZPE are lowered to ZPE^{str}_{MD} = 1.67 and ZPE^{str}_{CD} = 2.41 kcal/mol. Deuteration, therefore, causes a greater stabilizing effect on the ZPE of TS_{cyc} than on 1-Re-H, leading to a contribution of $\Delta\Delta ZPE$ = +0.26 kcal/mol in eq 6 from the stretching mode alone. Additional contributions from the bending modes lead to the final $\Delta\Delta ZPE$ of +0.55 kcal/mol.

To sum, the insensitivity of $\nu^{\ddagger}$ to deuteration and the higher frequencies of the C-H vibrations in TS_{cyc} compared to the Re-H vibrations in the reactant can explain why the KIE in **scheme 2.6** is inverse.

The experimental KIE for CO_2 insertion into 1-Re-H in THF is 0.58 ± 0.03. Clearly, an inverse KIE would be incompatible with a mechanism in which ts1 or ts2 is rate-determining. On the other hand, the KIE of 0.42 computed for

the cyclic TS (TS_{cyc}) is in good agreement with the experiment. The ωB97XD functional gives KIE = 0.38. Differences between computed and measured KIE of these magnitudes are not unexpected since, for example, the calculations use harmonic vibrational frequencies. Thus, the computed energy of TS_{cyc} as well as the computed KIE support a cyclic TS as the RDS in the given system.

KIE wasn't utilized before either experimentally or computationally for elucidating the mechanism of CO_2 insertion into octahedral complexes other than the one for 1-Re-H discussed in details in this chapter. Another inverse KIE is known for a CO_2 insertion in a square planar nickel-hydride complex, 0.61 in THF or 0.79 in CH_3CN [64]. Interestingly, Murray and coworkers have recently studied CO_2 insertion into the bridging metal hydride bonds of $[L_nFe_3(\mu\text{-}H)_3]^{3+}$ clusters and measured KIEs of 1.09 and 1.50 depending on the steric bulk of the ligands in the clusters [65, 66].

In an attempt to validate our calculated KIE, scaling harmonic frequencies in eqs (3) and (9) were done by a factor of 0.95, by increasing lower vibrations to 50 cm^{-1} and to 100 cm^{-1} showed no significant effect, KIE results shown in **table 2.1** for ts1 and for TS_{cyc}.

Table 2.1 – Variation in KIE of ts1 and TS_{cyc} upon scaling the harmonic frequencies with 5 different methods.

		$KIE_{unscaled}$	KIE_{50}	KIE_{100}	$KIE_{*0.95}$	$KIE_{50*0.95}$	$KIE_{100*0.95}$
TS_{cyc}	THF	0.42	0.42	0.42	0.44	0.44	0.44
	Acetone	0.42	0.42	0.42	0.44	0.44	0.45
	MeCN	0.30	0.30	0.28	0.32	0.32	0.30
ts1	THF	1.10	1.10	1.10	1.10	1.10	1.10
	Acetone	1.15	1.15	1.15	1.15	1.15	1.15
	MeCN	1.05	1.05	0.99	1.06	1.06	1.00

2.2.3 Computed Solvent and Substituent Effects

Experimentally, the kinetics of CO_2 insertion in 1-Re-H exhibited a large dependence on the solvent with the second-order rate constant increasing in the order **1.97×10^{-4} (THF) < 2.52×10^{-3} (Acetone) < 5.44×10^{-2} (Acetonitrile)**, in $M^{-1}s^{-1}$. Using the experimental activation free energy determined from the Eyring plot in THF as a reference (23.0 kcal/mol at 298 K) the rate constants afford activation energies of 21.5 kcal/mol in acetone and 19.7 kcal/mol in acetonitrile. The experimental study also included kinetics data for the effect of a few substituents at the 4,4' positions of the bipyridyl ligand. The greatest effect was found for the methoxy substituents (-OMe) which increased the reac-

tion rates by approximately three orders of magnitude compared to the parent complex, corresponding to a barrier of 21.3 kcal/mol. In this section we examine if these effects can be reproduced by the computed associative mechanism.

The dielectric constants for the solvents used are Ds = 7.3 (THF), 20.7 (Acetone) and 36.1 (CH_3CN). For comparison, the computed Energy profile along with some assigned geometric parameters are elaborated in **figure 2.9** (A) in THF, (B) in Acetone, and (C) in CH_3CN. The computational and experimental results are summarized in **table 2.2**.

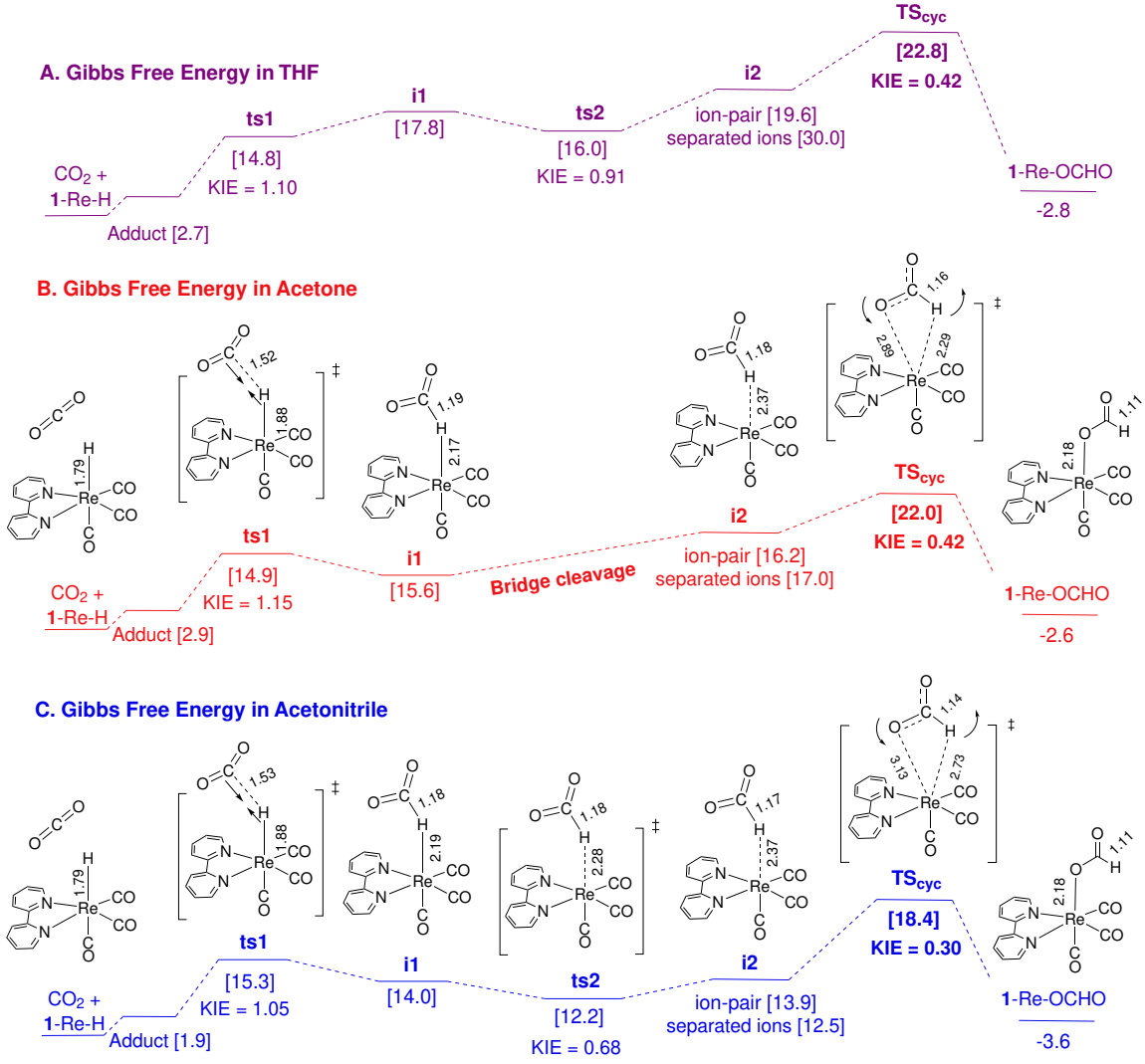

Figure 2.9 – Calculated M06L-D3 Gibbs free energy profile for CO_2 insertion in 1-Re-H. (A) in THF, (B) in Acetone, and (C) in CH_3CN; in kcal/mol at 298 K and 1 M. Some bond distances are given in Å.

Despite the wide range of Ds values, changing the solvent continuum applied in the calculations exerts very minor effects on the energy of ts1: 14.7 (THF),

14.9 (Acetone) and 15.3 (CH_3CN), in kcal/mol. This is not surprising, since ts1 is an early TS that does not introduce any significant changes in the character of the bonds characterizing the two reactants.

The computed energy of TS_{cyc} relative to the separated reactants, on the other hand, decreases uniformly as Ds increases: $\Delta G^{\ddagger} = 22.8$ (THF), 22.0 (acetone) and 18.4 (CH_3CN), kcal/mol. This is the same effect observed experimentally. The solvent effects on TS_{cyc} most likely follow from some degree of ion-pair character acquired in TS_{cyc}. This is evident in the computed geometry of TS_{cyc} which exhibits increased separation of the formate anion with increased Ds, especially in acetonitrile where the Re– HCO_2 distance is increased to 2.73 Å (**figure 2.9-C**). In the gas phase $\Delta G^{\ddagger}$ for TS_{cyc} is increased to 26.7 kcal/mol. Despite that ts2 was located in THF and acetonitrile only, it's barrier decreased from 16.0 kcal/mol to 12.2 kcal/mol as Ds of solvent increases. Same solvent effect was observed on i2, which exhibit highest stabilization in CH_3CN the most polar solvent, resulting in it being more stable than the bridged hydride species i1, supporting it's ion-pair character. The aprotic solvents are also computed to exert pronounced effects on the energy of i1 following ts1. As a consequence, i1 has a higher free energy than ts1 in both THF and acetone, but the order is reversed in acetonitrile, although the difference between the two species remains small, 1.3 kcal/mol.

Table 2.2 – Computed solvent and substituent effects on the energy of the stationary points for CO_2 insertion in 1-Re-H, ΔG *in kcal/mol at 298 K and 1 M.*(- : indicates unlocated species)

Solvent	ts1	i1	ts2	i2	TS_{cyc}	1-ReOCHO	ΔG_{ions}	$\Delta G^{\ddagger}_{exp}$
	Solvent effects on $(bpy)Re(CO)_3H$							
THF	14.8	17.8	16.0	19.6	**22.8**	-2.8	30.0	**23.0**
Acetone	14.9	15.6	-	16.2	**22.0**	-2.7	17.5	**21.5**
MeCN	15.3	14.0	12.2	13.9	**18.4**	-3.6	12.5	**19.7**
	Effect of 4,4'-OMe substitution							
THF	14.4	17.0	-	18.9	**21.7**	-3.9	28.3	**21.3**

Experimentally, the given solvents exert minor effects on the KIE, with THF and acetone giving similar values, 0.58 ± 0.03 vs 0.55 ± 0.11, while acetonitrile gives a slightly more inverse KIE: 0.52 ± 0.05. The calculations capture this trend qualitatively yielding KIE = 0.41 (THF), 0.42 (acetone) and 0.30 (CH_3CN). Although the effect of acetonitrile appears to be exaggerated, the result is still overall, satisfactory. The gas phase calculations afford KIE = 0.48.

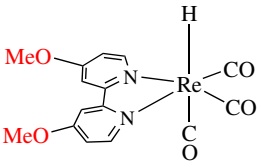

Scheme 2.8 – Methoxy substituted analog of 1-Re-H at the 4,4' position of bipyridyl ligand.

Calculations on CO_2 insertion into the C-H bond of the 4,4'-OMe substituted analog of 1-Re-H (**scheme 2.8**) in THF shows TS_{cyc} reproduces the observed favorable effects of substitution on the reaction rate in THF fairly accurately: $\Delta\Delta G^{\ddagger}_{comp}$ = -1.1 kcal/mol vs $\Delta\Delta G^{\ddagger}_{exp}$ = -1.7 kcal/mol. Interestingly, a much smaller effect is computed for the given substitution on ts1, $\Delta\Delta G^{\ddagger}_{comp}$ = -0.4 kcal/mol, while no ts2 was located on the PES of the reaction. The detailed Gibbs Free Energy Profile is shown in **Figure 2.10**.

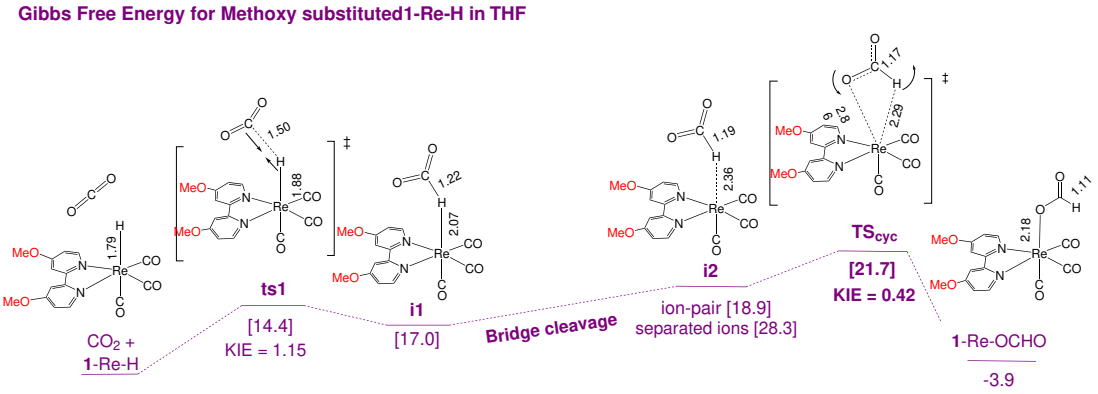

Figure 2.10 – Calculated M06L-D3 Gibbs free energy profile for CO_2 insertion in Methoxy substituted analog of 1-Re-H in THF; in kcal/mol at 298 K and 1 M. Some bond distances are given in Å.

Table 2.2 also includes data for the thermodynamics of the hydride transfer reaction from 1-Re-H to CO_2 leading to the separated formate ion and five coordinate metal cation fragment (ΔG_{ions}). In THF, ΔG_{ions} = +30.0 kcal/mol, much higher than TS_{cyc}, so the mechanism involving dissociation of the ion pair forming free ions are unlikely to compete with TS_{cyc} in THF.

Hydride transfer in acetone and acetonitrile, on the other hand, affords ΔG_{ions} = +17.5 and +12.5 kcal/mol, respectively, 4.5 and 6.0 kcal/mol lower than TS_{cyc}. What is important to our study is the kinetics of CO_2 insertion, so whether the free ions in the more polar solvent will be involved as intermediates in the mechanism depends on whether their formation encounters a barrier or not. Starting with i2 as the reference point, free ion formation in acetonitrile is almost ergoneutral (-1.4 kcal/mol). In contrast, the transformation from i2 to the final formate

product 1-Re-OCHO is highly exergonic (-17.5 kcal/mol). As mentioned in the introduction, the entropy of dissociation favors the thermodynamics of the free ions. However, formation of the free ions from i2 still requires cleavage of the Re-H bond, further bending of the CO_2 angle and pulling of the formate anion out from the metal center of the cation fragment before the favorable effect of the dissociative entropy is exerted. These are the same requirements needed to reach TS_{cyc}. In fact, the computed geometry of TS_{cyc} in acetonitrile is characterized by quite long Re–HCO_2 (2.73 Å) and long Re–OCHO (3.31 Å) bond distances indicating a very early transition state with increased ion-pair character (**figure 2.9**).

Our attempts to identify a TS for free ion formation from i2 have not been successful. The problem is that as the Re–HCO_2 bond is stretched in the course of TS geometry optimization, the formate anion tips and coordinates one of the two oxygens to the metal. These features of the dissociative PES obtained by static DFT calculations may not conclusively rule out a role for free ion formation in the insertion mechanism. A more complete investigation of the dissociative PES by dynamic calculations that account explicitly for the acetone and acetonitrile molecules of the solvent is beyond the scope of the present study. However, assuming dissociation of the formate ion from i2 to be completely barrierless is also too simplistic and would provide computed activation free energies in acetone and acetonitrile that are way too low compared to the experimentally observed ones. Given that the barrier from i2 to TS_{cyc} in acetonitrile is only 4.5 kcal/mol, there seems to be no obvious advantages for free ion-formation and re-coordination over the direct highly exergonic intermolecular reaction. Note that in the experimental study, Sullivan and Meyer raised the possibility of a role for free ions in the mechanism of CO_2 insertion in 1-Re-H in acetonitrile but ruled it out based on results from trapping experiments.

2.2.4 Conclusion

Previous results from kinetics and mechanistic experiments by Sullivan and Meyer provided compelling evidence that carbon dioxide insertion into the metal hydride bond of the octahedral complex *fac*-(bpy)$Re(CO)_3H$ (1-Re-H) proceed by a non-classical associative mechanism that does not require an empty coordination site to initially bind CO_2 to the metal, but still left the question about the involved TS open (**a** or **b** in the study).

In the present chapter we conducted a more detailed DFT investigation on the PES of the reaction of carbon dioxide insertion into 1-Re-H systems where we compared the computed results with the available experimental data. When a polarizable continuum representing THF, acetone and acetonitrile is applied during geometry optimization, the calculations identify a linear ts1 and a cyclic TS_{cyc}. Detailed analyses of the reaction coordinates and isotope effects reveal ts1 mediates an initial stage of the reaction that anchors the carbon of CO_2 to the

metal-hydride bond. The reaction identifies a minimum for the bridged species followed by a distinct TS for hydride transfer (ts2) that leads to an ion-pair minimum between the formate anion and a cationic metal fragment (i2) that rearranges by TS_{cyc} to give the final product. ts1, i1, ts2 and i2 all have similar free energies and are significantly lower than the cyclic TS.

Consideration of TS_{cyc} as the RDS accurately reproduces the available experimental data, including the magnitude of activation free energies in the two systems, solvent effects, substituent effects and KIEs. In contrast, assuming ts1 to be the RDS leads to barriers, solvent effects and KIEs that are all inconsistent with the experiments. These results appear to follow because initial step of the reaction involving ts1 represents a step that "bridges" CO_2 to the Re-H bond.

Prior to TS_{cyc}, C-H bond formation is nearly completed but it is still pointing to the metal. Although a C-O bond from CO_2 is part of the four membered ring of the reaction center, the Re–OHCO bond distance is still long, so TS_{cyc} may still be best classified as mediating an outer-sphere mechanism in the sense that there is no pre-coordination of CO_2 to the metal.

Chapter 3

Effect of Hydrogen Bonding and *trans*-Hydride on CO_2 Insertion into Metal-Hydride Bond

3.1 Introduction

As concluded in **Chapter 2**, the DFT calculations of the PES of the reaction of CO_2 insertion into Rhenium hydride bond of (bpy)Re(CO)$_3$H showed the rate determining step is without ambiguity in full support of cyclic transition state (TS_{cyc}), this is what led to an experimentally inverse kinetic isotope effect observed by Sullivan and Meyer[3]. Also, we showed that ts1 is an early transition state involving a step that "bridges" CO_2 to the Re-H bond. This proposition represents a new understanding to how CO_2 activation reaction through homogeneous transition metal catalysts is initiated.

The catalyst used in the previous experiment is one of those organometallic complexes to be described as "clean" due to the lack of cooperation possibility of any of it's ligands in the insertion reaction, and the lack of a strong sigma donor ligand trans to the metal–hydride bond weakening it and assisting it's cleavage, all what helped in clearer elucidation of the reaction mechanism.

This led us to question the validity of our conclusion when using one of today's frontier transition metal octahedral catalysts efficiently used in reaction of CO_2 hydrogenation, which is Hazari's Iridium(III) trihydride complex that carries a tridentate pincer ligand [47], **scheme 3.1**.

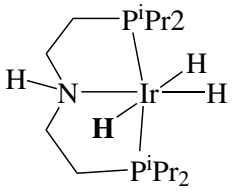

Scheme 3.1 – Hazari's Octahedral trans-Trihydride Complex (1-Ir-H)

The choice of this catalyst is a key step in investigating the generality of our proposition under specific catalytic variables. First due to to: **i)** Presence of a characteristic hydride trans to the metal-hydride bond involved in the reaction, these strong segma donors are scientifically believed to have great effect assisting the dissociation of the groups trans to them[67], a phenomenon known as "Trans-Effect", and **ii)** Amine arm of the pincer ligand which could be involved in stabilizing the insertion of CO_2 through hydrogen bonding with one of the 2 oxygen atoms of CO_2.

Both hydrogen bonding and trans effect are to be examined through Potential Energy Surface calculations, geometric parameters analysis and Isotope Effect.

3.2 Results and Discussion

3.2.1 Free Energy Profile

We started our study by calculating the Free Energy profile for the reaction between CO_2 and 1-Ir-H. The stationary points located on the PES of this reaction are summarized in details in **Figure 3.1**. Calculations were done in THF continuum as a solvent.

As found in the previous chapter, the calculations started by identifying a linear transition state ts1. This TS is characterized by an imaginary frequency $534i$ cm^{-1} and coordinates involving motion of the hydride between the metal and the carbondioxide (further analysis of ts1 frequencies will be done in Isotope effect's section of this chapter). It is also characterized by an Ir–H and C–H bond distances of $r_{Ir-H} = 1.75$ Å and $r_{C-H} = 1.65$ Å. These parameters indicate that only 0.05 Å lengthening in the Ir–H bond occurs at ts1, this barely stretching relative to the reactant 1-Ir-H (1.70 Å), is consistent with significantly long C–H bond. Thus, no full cleavage of Ir-H bond occurs at ts1, however, ts1 yields an intermediate i1 at an early stage of the PES in which the hydride is "sandwiched" between the metal and the carbon of CO_2 at distances $r_{Ir-H} = 2.00$ Å, still inconsistent with common range for CH–M agostic bond distances discussed in previous chapter, and $r_{C-H} = 1.20$ Å, still significantly longer than in a free formate anion (1.21 A vs 1.14 A). This is all in indicative of i1 being viewed as the product of a step involving addition of CO_2 to the hydride end of the intact

Ir-H bond, not the product of a hydride transfer step cleaving the Ir-H bond to give an ion-pair species. As shown in **figure 2.1-A**, the electronic barrier of ts1 is only 1.7 kcal/mol higher than the reactants. However, when the vibrational terms are included the Gibbs free energy increases to 9.8 kcal/mol.

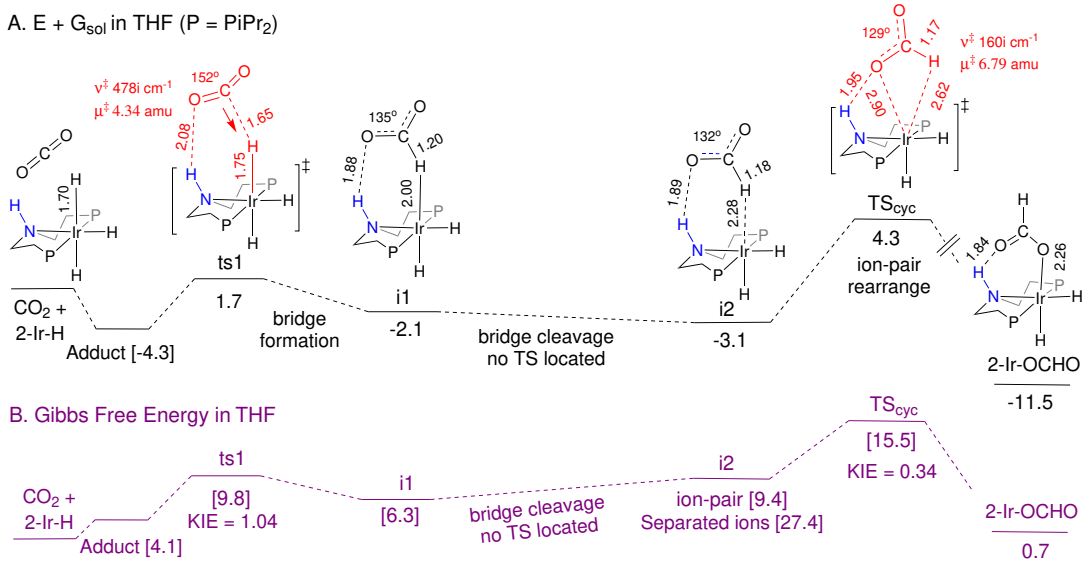

Figure 3.1 – Calculated M06L-D3 (A):E$_{Solv}$+G and (B): Gibbs free energy profile for CO_2 insertion into 1-Ir-H in THF; in kcal/mol at 298 K and 1 M. Some bond distances are given in Å.

The IRC for ts1 shown in **figure 3.2** is observed to link the initial adduct of the reactants to i1.

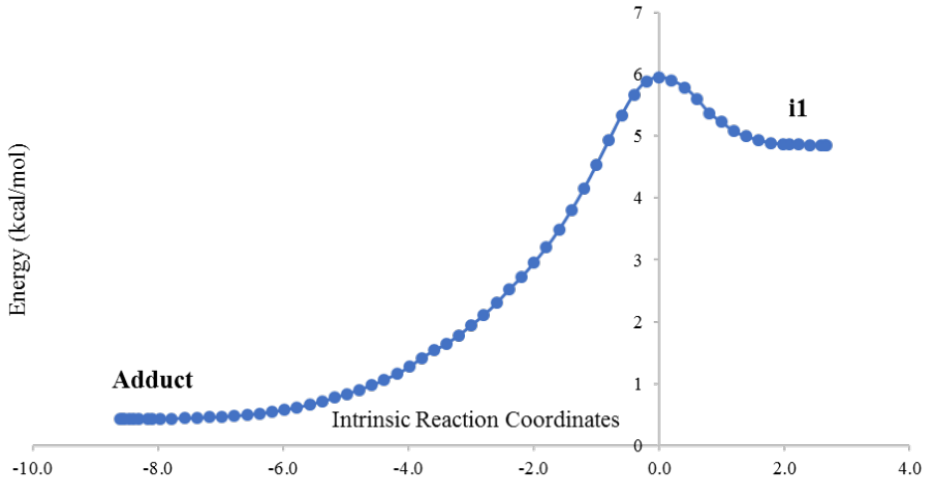

Figure 3.2 – Computed IRC plot for the linear transition state "ts1" located on PES of CO_2 insertion into 1-Ir-H. Energy in kcal/mol.

Further calculation in THF identified i2, the second intermediate located on the PES. The Ir-H and C-H bond distances in i2 are r_{Re-H} = 2.28 Å and r_{C-H} = 1.18 Å. The Ir-H bond at i2 is stretched by 0.58 Å when compared to the reactant 1-Ir-H. Now, the metal-hydride bond is more consistent with the common range of CH–M agostic bond distances discussed earlier. This means that i2 could be now viewed as the product of the step involving Metal-hydride bond cleavage forming an "ion-pair" where the C-H bond formed at i2 is still subjected to an agostic interaction with the metal. The attempt to locate a transition state for the cleavage of the bridged species i1 yielding i2 weren't successful. This means that no saddle point appears along the valley connecting i1 and i2, therefore, no genuine transition state for hydride transfer is shown. Next, the calculations identified a second TS which is TS_{cyc} with the C-H and C-O bonds of the formate anion making a four membered ring with the metal at 2.62 Å and 2.90 Å, respectively. The C-H bond in TS_{cyc} has been fully formed, since it is in great agreement with that of a formate anion (1.15 Å vs 1.14 Å). TS_{cyc} is characterized by an imaginary frequency of 160 i cm^{-1} for a vibration that exchanges C-H and C-O bond coordination to the metal. The IRC computed in THF confirms TS_{cyc} connects i2 and the product 1-Ir-OCHO as shown in **figure 3.3**.

The highest Energy point on Gibbs Free Energy profile for CO_2 insertion into 1-Ir-H is the cyclic transition state TS_{cyc}. At this TS the fomate is already formed, however, the C-H bond is still pointing to the metal at 2.62 Å. The barrier for this TS is computed to be 15.5 kcal/mol, just fortuitously this value is also now in excellent agreement with the experimental activation free energy of 14.3 kcal/mol determined at 298 K in THF by Hazari and coworkers [64]. The barrier for ts1 is computed to be 9.8 kcal/mol, much off that reported experimentally.

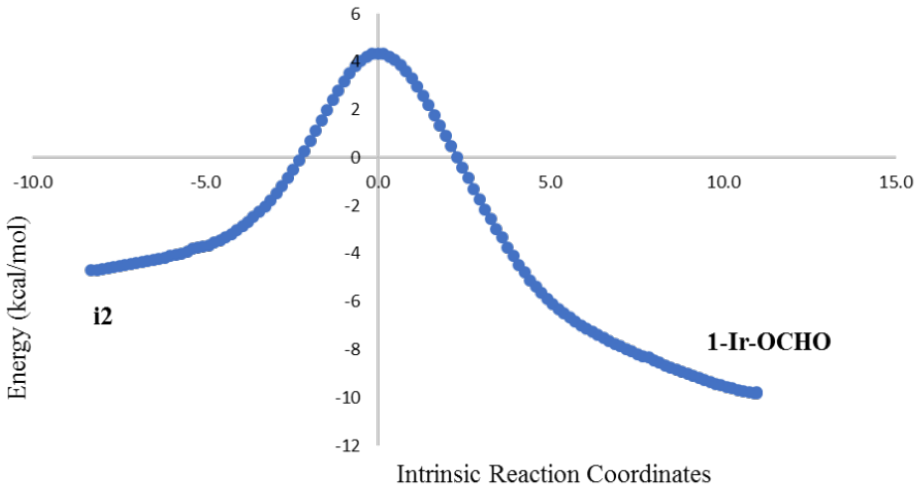

Figure 3.3 – Computed IRC plot for the Cyclic transition state "TS_{cyc}" located on PES of CO_2 insertion into 1-Ir-H. Energy in kcal/mol.

3.2.2 Computed Primary Kinetic Isotope Effect

As done earlier, we started by calculating the kinetic Isotope Effect for ts1, results summarized in **scheme3.2**.

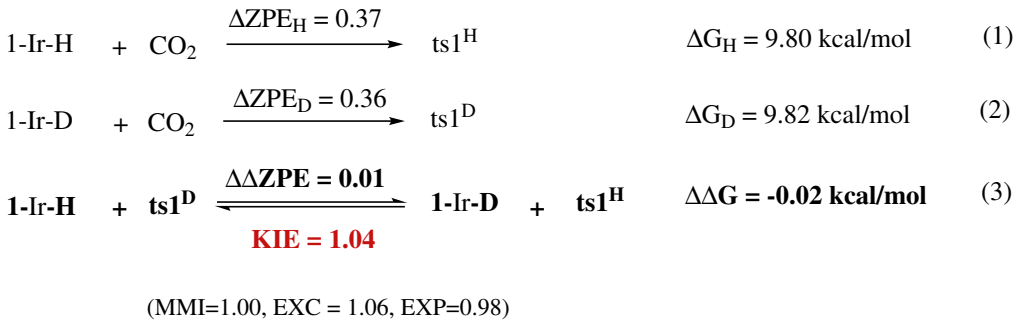

Scheme 3.2 – Computed KIE for ts1 in THF.

The barriers for proteo and deutero reactions via ts1^H (eq 1) and ts1^D (eq2) respectively, differ only by -0.02 kcal/mol, which means that deuterium substitution shows some minor unfavorable effect on the rate of the reaction reaching this TS. This leads to the small and non-considerable normal kinetic Isotope Effect (1.04), even less significant than that reported for ts1 in 1-Re-H (Chapter 2). This absence of a significant KIE for ts1 still supports the proposition that no hydride transfer is initiated at this stage of the reaction.

The imaginary frequency ($\nu^{\ddagger}$) is considered the loose vibration in any reaction, i-freq in ts1 has a reduced mass $\mu = 4.34$ amu, and a motion that can be related to one of the translational modes of the free CO_2 molecule, consistent with a reaction in which CO_2 is adding to the Ir-H bond. However, this vibration was not highly sensitive to isotope substitution where it only drops from $478i$ cm^{-1} in ts1^H to $450i$ cm^{-1} in ts1^D upon deuteration. The vibrational analysis for ts1 continued to reveal a distinct symmetrical and asymmetrical stretching vibrations for the *trans*-Hydrides in ts1 at 2017 cm^{-1} and 1613 cm^{-1} respectively, of reduced masses of 1.01 amu and 1.35 amu respectively. Still locating these 2 isotope sensitive vibrations means that they remained as real modes at this stage of the reaction which compensates ΔZPE resulted from the reactant (1-Ir-H) upon deuteration, therefore resulting in a non significant $\Delta\Delta$ZPE = +0.01 kcal/mol, explaining the small KIE at this given step where the metal-hydride bond isn't yet dissociated, and no full "hydride transfer" is possessed when reaching i1.

However, Upon deuteration the activation free energy reaching TS_{cyc} from the separated reactants decreases from 15.55 kcal/mol to 14.91 kcal/mol, eq's 4 and 5 respectively, **scheme 3.3**.

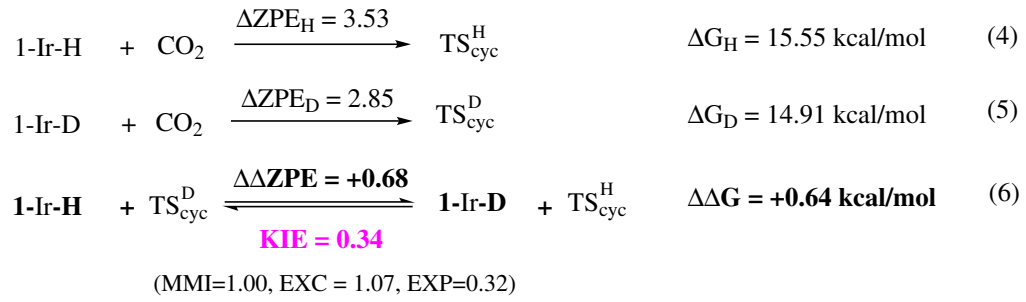

Scheme 3.3 – Computed KIE for TS_{cyc} in THF.

The resulting $\Delta\Delta G^{\ddagger} = 0.64$ kcal/mol leads into a substantial inverse KIE = 0.34 in eq 6. Again, this given KIE is dominated by the EXP term which results from a significantly positive $\Delta\Delta ZPE^{\ddagger} = +0.59$. The imagianry frequency of TS_{cyc} doesn't show any sensitivity toward deuteration where it only drops from $160i\text{cm}^{-1}$ in TS^{H}_{cyc} to $155i$ cm^{-1} in TS^{D}_{cyc}. Also, the IRC in **figure 3.3** shows that the reaction coordinates characterizing TS_{cyc} corresponds to the slippage of intact formate anion over the metal. In contrast to ts1, it was clearer that in the transformation from 1-Ir-H to TS_{cyc}, the Ir–H bond is lost and a new C–H bond is formed. The substantial KIE in this case is determined by the different vibrational frequencies of the Os-H and C-H bonds. The stretching vibrations of these two bonds are shown in **figure 3.4** below, where their contribution to $\Delta\Delta ZPE$ is considered.

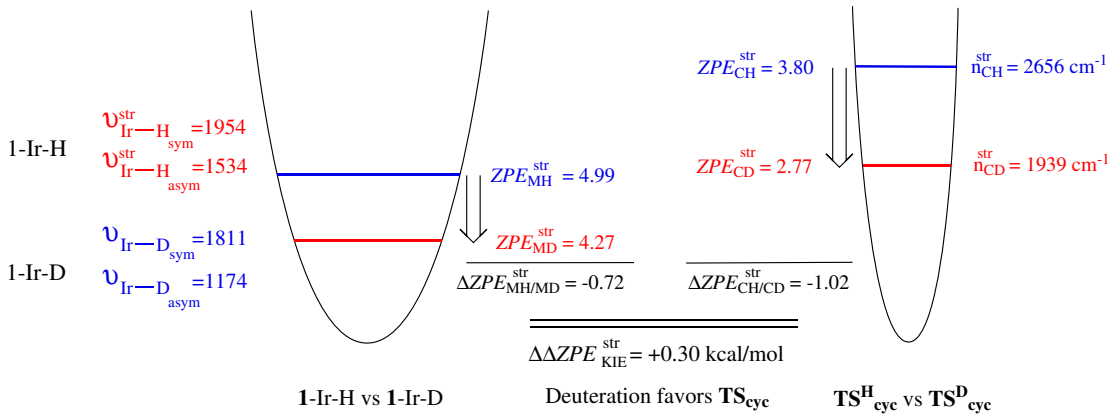

Figure 3.4 – Contribution of the Ir-H and C-H stretching vibrations to the KIE of TS_{cyc}. ZPE in kcal/mol, Stretching vibrations in cm^{-1}.

The symmetric and asymmetric stretching vibrations in the proteo reactant

are 1954 cm^{-1} and 1534 cm^{-1} respectively, while the frequency of stretching vibration of the formed C-H bond at TS^{H}_{cyc} is 2656 cm^{-1}. These vibrations have a reduced masses near 1.00 amu. Therefore, the different frequencies originate from different force constants as shown in **table 3.1**.

Table 3.1 – Stretching vibrations of 1-Ir-H and TS_{cyc} *(cm^{-1})*, their force constant *(mDyne/A)*, and reduced masses *(amu)*.

	Frequency (cm^{-1})	**Force Constant (mDyne/Å)**	**Reduced Mass (amu)**
$\nu_{Ir\text{-}H\text{-}sym}$	**1954**	2.67	1.00
$\nu_{Ir\text{-}H\text{-}asym}$	**1534**	1.41	1.02
$\nu_{C\text{-}H}$	**2656**	4.40	1.06

These frequencies result in different contributions to zero point energy in the reactant and TS_{cyc}: ZPE^{str}_{MH} = 4.99 kcal/mol **vs** ZPE^{str}_{CH} = 3.34 kcal/mol. Upon deuteration these frequencies are lowered where the symmetrical Ir-D stretch becomes 1811 cm^{-1}, asymmetrical stretch: 1174 cm^{-1} and the C-D bond stretch: 1939 cm^{-1}. This stabilization results in lowering their contribution to zero point energy in deutero-reactant to ZPE^{str}_{MD} = 4.27 kcal/mol and in TS^{D}_{cyc} to ZPE^{str}_{CD} 2.77 kcal/mol.

Deuteration, therefore, causes a greater stabilizing effect on the ZPE of TS_{cyc} than on 1-Ir-H, leading to a contribution of $\Delta\Delta ZPE^{str}$ = +0.30 kcal/mol in eq 6, from the stretching mode alone. Additional contributions from the bending modes lead to the final $\Delta\Delta$ZPE of +0.68 kcal/mol.

Thus, this higher frequency of C–H bond at TS_{cyc} and it's greater contribution to $\Delta\Delta$ZPE, together with the insensitivity of the imaginary frequency to deuteration explains the inverse nature of KIE in **scheme 3.3**.

3.2.3 Hydrogen Bonding Effect

Pincer Ligands are a class of chelating agents that bind tightly to three adjacent coplanar sites of a transition metal in a meridional configuration[68], **scheme 3.4**. Such ligands offer the ability to fine tune the electronic and the steric properties about the metal center, thereby increasing the scope of their applications. The research on modification of the pincer ligands to elucidate reaction mechanisms has been the interest of numerous researchers[69, 70].

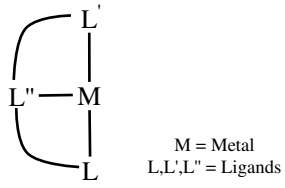

Scheme 3.4 – General structure of a tridentate Pincer-Ligand

Modifications have been made on the pincer-ligand site to improve the rate determining step in CO_2 hydrogenation reactions reaching the final formic acid product via involvement of the ligand in the reaction. In consideration that the rate Determining step in these reactions is the displacement of formate by H_2 (Hydrogenolysis)[71]. Pathak and coworkers[72], tested the incorporation of an N–H functionality in pincer ligand by calculating 2 pathways for the reaction, **ligand assisted** where the hydrogen is said to only stabilize the formate moiety vs **ligand participation** where the amine proton is totally transferred, the latter being very similar to that proposed by Noyori for asymmetric ketone hydrogenation[73].

Considering the first step of hydrogenation, CO_2 insertion into metal-hydride, the hydrogen bond donor atom incorporated in a pincer ligand is also believed to assist insertion. In this context, Hazari and coworkers, demonstrated experimentally and computationally that the presence of a hydrogen bond donor atom in the secondary coordination sphere of the Ir(III) trihydride complex lowers the kinetic barrier of the reaction with CO_2, by comparing the stability of formate anion via N-H..O hydrogen bond interactions at **ts1** considered as the "Hydride Transfer" and rate determining step. This study didn't illustrate any effect on the cyclic transition state $\mathbf{TS}_{cyc}$[47].

Figure 3.5 reproduces and compares the M06L-D3 Gibbs free energy profiles for CO_2 insertion into 1-Ir-H(blue) and 1-Re-H(red) of the previous chapter where no hydrogen bonding is present.

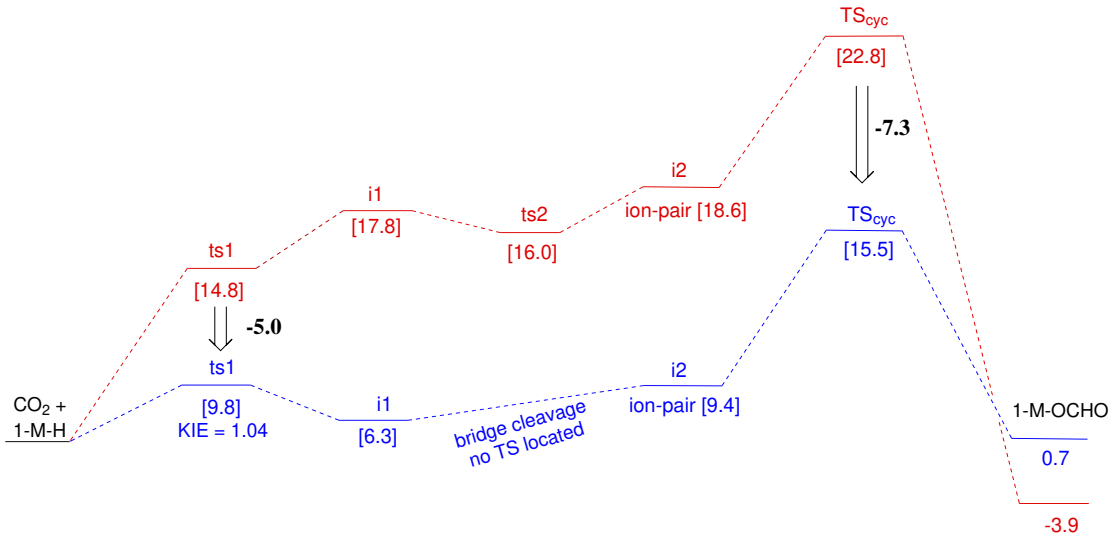

Figure 3.5 – Computed Gibbs Free Energy Profile for CO_2 insertion into 1-Re-H (red) and 1-Ir-H (blue). Energy in kcal/mol.

The energy barrier for ts1 is 14.8 kcal/mol in 1-Re-H which drops to 9.8 kcal/mol in 1-Ir-H, thus resulting in stabilization of 5 kcal/mol. However, the energy barrier for TS_{cyc} is observed to decrease from 22.8 kcal/mol in 1-Re-H system to 15.5 kcal/mol in 1-Ir-H which results in stabilization of around 7.3 kcal/mol, greater than that of ts1.

This difference in energy could be first attributed to the stabilization of the distorted CO_2 moiety in the later by hydrogen bonding interaction. The N–H stretching vibration in the assigned amine arm are shown in **table 3.2**.

Table 3.2 – The change in N–H bond stretching vibration frequency cm^{-1} at different stages of the reaction.

	$\nu_{stretch}$ of N-H (cm^{-1})
1-Ir-H	**3464**
ts1	**3418**
i1	**3217**
i2	**3171**
TS_{cyc}	**3389**

The stretching vibration is observed to slightly decrease from 3464 cm^{-1} at 1-Ir-H to 3418 cm^{-1} at ts1, then it reaches minimum at i2, the species encountering ion-pair character, thus is expected to get stabilized through hydrogen bonding. However, the bond's frequency then increases from 3171 cm^{-1} at i2 to 3389 cm^{-1}

when reaching TS_{cyc} revealing low effect on the cyclic transition state, therefore, hydrogen bonding interaction with oxygen is minimized at this step.

3.2.4 Trans-Hydride Effect

The second factor that can have a direct effect on the energy barrier of the reaction is the Trans-Effect. The hydride is classified as the ligand with the strongest effect, meaning it will strongly impact the ligand trans to it, by disfavoring it's presence. The trans-effect was elaborated also by Hazari in the same study on 1-Ir-H [47], who emphasized the effect of trans-ligand on the thermodynamics of CO_2 insertion into 1-Ir-H, by examining the effect of different trans ligands on the natural bond orbital (NBO) charge of the transferred hydride, in consideration that the rate-determining step is the nucleophilic attack of hydride on CO_2 and that step being ts1, therefore more nucleophilic hydrides have lower kinetic barriers. This study didn't explain the effect of trans-H on the cyclic transition state's barrier as it is not calculated.

This led us to question the importance of the trans-ligand in affecting the RDS of CO_2 insertion reaction, through comparing this effect on ts1 and TS_{cyc} using what is defined earlier as secondary isotope effect. The Secondary Isotope Effect (α-KIE) was calculated and shown in table 3.3, along with the trans-Ir-H bond length at the different stationary points on the PES of the reaction.

Table 3.3 – The variation in *trans* Ir-H bond length (A) and secondary α-KIE at different stages of the reaction in THF.

	trans $\mathbf{r_{Os\text{-}H}}$	**α-KIE**
ts1	**1.65**	**0.92**
i1	**1.58**	**0.83**
i2	**1.56**	**0.72**
$\mathbf{TS_{cyc}}$	**1.55**	**0.61**

A significant secondary isotope effect (α-KIE) is resulted revealing the involvement of the *trans*-H in the reaction coordinates. *trans*-Ir-H bond contractions start at ts1, where the bond length decreases from 1.70 Å in the reactant to 1.65 Å at this step, resulting in 0.92 α-KIE. However, the secondary kinetic isotope effect decreases reaching the maximum inverse at TS_{cyc}, α-KIE = 0.61, consistent with the the highest bond contraction meaning the shortest r_{IrH} = 1.55 Å, considered the step where the hydride fully cleaves and CO_2 starts inserting, this effect favored the bridge cleavage and thus resulted in the decrease in the kinetic barrier of the reaction. For completeness we include the equilibrium isotope effects (EIE) at i1 and i2 minima in **table 3.3**.

Despite TS_{cyc} not showing any evidence of hydrogen-bonding with the amine proton incorporated in the secondary coordination sphere of the pincer ligand, it still results in a higher kinetic barrier stabilization than that of ts1 when compared to 1-Re-H system. Our computed results suggest an explanation for this kinetic stabilization. TS_{cyc} is shown to receive the highest trans-Hydride effect by encountering the most inverse α-KIE, thus, evidently supporting our previous proposition that the reaction is to be proceed concertedly through TS_{cyc}, considered as the rate-determining step, thus resulting in the observed metal-formate product.

3.2.5 Computed Solvent Effect

The stationary points calculated on the associative PES for CO_2 insertion in the hydride of 1-Ir-H are summarized in **figure 3.6**.

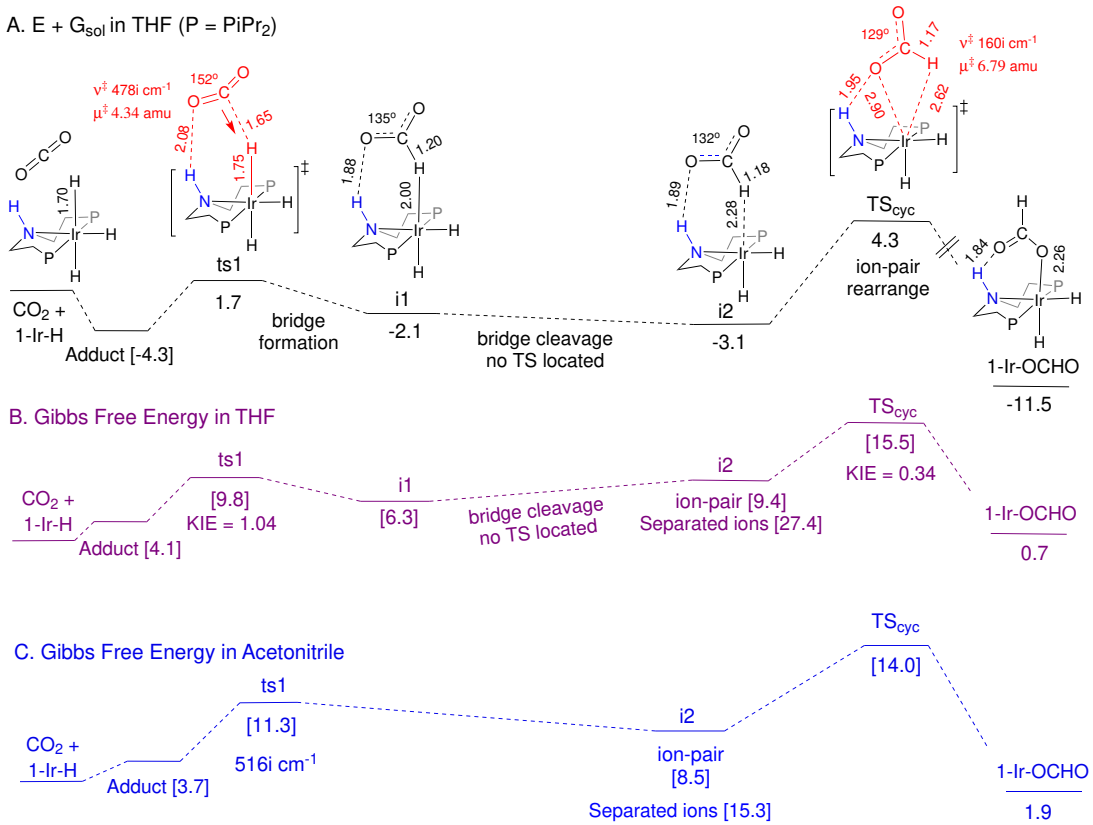

Figure 3.6 – Calculated minima and TSs on the associative PES for CO_2 insertion in 1-Ir-H in THF(A and B) and CH_3CN (C). Bond distances are given in Å. Gibbs free energies are given in kcal/mol at 298 K and 1 M relative to the separated reactants. KIE values are kinetic isotope effects defined relative to the separated reactants.

As before, the PES starts with ts1 for addition of CO_2 to the intact Ir-H bond of 1-Ir-H. This is true in both the gas phase and in a solvent continuum. When the calculations are done in THF, the bridged species i1 and the ion-pair species i2 were both fully optimized and characterized by normal mode analyses as true minima, but ts2 that is expected to connect the two minima could not be optimized. In acetonitrile, on the other hand, the IRC originating from ts1 leads at first to a plateau where i1 is expected to be found, and then proceeds directly into ion-pair i2 as shown in **figure 3.7**. In both solvent continuums, the insertion reaction following i2 is completed via TScyc.

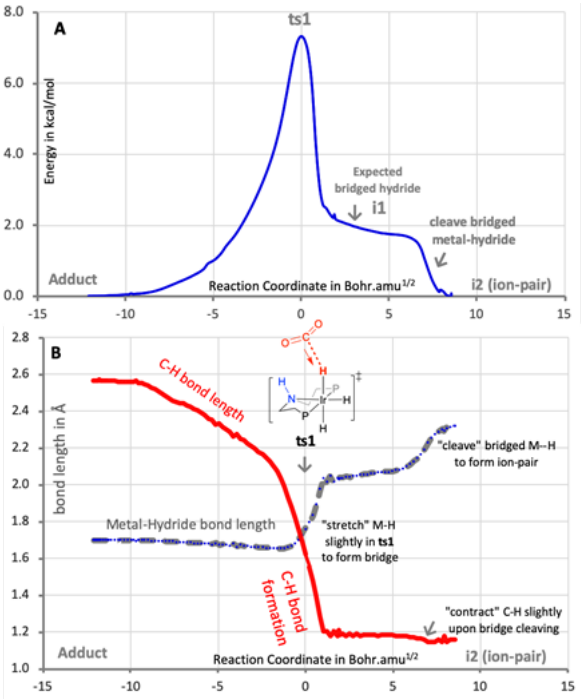

Figure 3.7 – IRC originating from ts1 in the reaction between 2-Ir-H and CO_2 in acetonitrile.

The highest energy point on the insertion Gibbs free energy surfaces in **figure 3.6-B** and C is TS_{cyc}. The computed $\Delta G^{\ddagger}$ for the transformation from the separated reactants 1-Ir-H and CO_2 to TS_{cyc} in THF is 15.5 kcal/mol. This is in excellent agreement with an experimental value of 14.3 kcal/mol determined from an Eyring plot. The computed $\Delta G^{\ddagger}$ for TS_{cyc} is lowered to 14.0 kcal/mol in acetonitrile. Significantly, for this system the computed free energy of the separated ions from dissociation of i2 in acetonitrile is 15.3 kcal/mol, slightly higher than TS_{cyc} **figure 3.6-C**

3.3 Conclusion

In this chapter, we investigated how hydrogen bonding and trans-hydride ligand might influence the associative PES for CO_2 insertion and especially the rate determining step. We conducted a more detailed DFT investigation of the associative PES in Iridium (III) tri-hydride octahedral complex. When a polarizable continuum representing THF or acetonitrile is applied during geometry optimization, the calculations identify a linear TS, resembling ts1 in previous chapter. This TS is similar to the one reported in many studies. Analysis of the reaction coordinates reveals ts1 mediates a preparatory stage of the reaction that bridges the carbon of CO_2 to the metal-hydride bond, and not a TS for hydride transfer. This view is unambiguously evident in the reaction of 1-Re-H where the calculations identify a minimum for the bridged species followed by a distinct TS for hydride transfer (ts2). The calculations predict the cyclic TS to be rate limiting in this system as well. Accepting this result accurately reproduces the experimental kinetics data available for 1-Ir-H, including the magnitude of activation free energy, and solvent effect. In contrast, assuming ts1 to be rate limiting affords barriers and solvent effects that are all inconsistent with the experiment. TS_{cyc} has a nearly fully formed C-H bond, while both the H and an O atoms of the resulting formate unit are weakly bound at the coordination site originally occupied by the hydride. Although a C-O bond is part of the four membered ring, TS_{cyc} may still be best classified as mediating an outer-sphere mechanism in the sense that there is no pre-coordination of CO_2 to the metal.

1-Ir-H is a prototype of octahedral metal hydride complexes with an amino ligand functionality that can interact with a carbonyl group in an associative mechanism. Given that the similar RDSs for 1-Re-H which lacks the amino functionality and 1-Ir-H, it is reasonable to expect that other insertions of CO_2 into metal-H bonds, at least those of d^6 octahedral hydrides, may generally proceed through analogous TS_{cyc} with k^2-H,O-formate character.

Chapter 4

Structure - Activity Study of Insertion Reaction of a Series of Carbonyl Compounds

4.1 Introduction

In the Previous two chapters we conducted a mechanistic study on the reaction of carbon dioxide insertion into a metal-hydride bond of octahedral transition metal complexes forming metal-formate products. Using kinetic isotope effect and potential energy surface calculations, we provided a new perspective toward how this elementary reaction is initiated, where CO_2 approaches hydride with a bent angle through **ts1** resulting in the formation of a newly characterized "bridging species" known as **i1**. This step is completely different from the initial conventional "Hydride Transfer" step mostly discussed in literature where nucleophilic attack of the hydride on CO_2 initiates the reaction resulting in ion-pair formation, thus, ts1 is attributed as hydride transfer TS and i1 as ion-pair minimum. Failure in locating a second linear TS involving full cleavage of the metal-hydride bond (ts2 in Chapter 2) supports this proposition.

However, insertion is not limited to carbon dioxide, other unsaturated organic substrates like olefins and some carbonyl groups undergo insertion into a metal hydride bond that are proposed to proceed through associative mechanism. A mechanistic study by Hasanayn and Morris for acetophenone hydrogenation via *trans*-[Ru(H)$_2$(diamine)(diphosphine)] system verified an energetically favorable route suggesting the formation of Ruthenium-alkoxide product via a hydride-transfer step from the metal to the ketone followed by reorganization of the alkoxide within the intact ion pair as simplified in **figure 4.1** [74]. The reaction is proposed to proceed through an outer sphere associative mechanism where no vacant coordination cite is required.

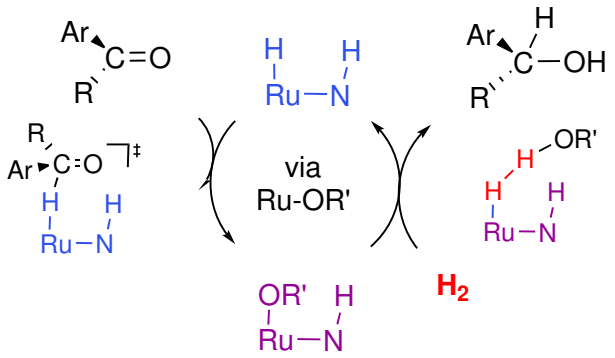

Figure 4.1 – Ketone hydrogenation mechanism involving carbonyl insertion into ruthenium-hydride bond.

Moreover, one of the proposed routes for hydrogenation of methyl acetate by Hasanayn and coworkers into *trans*-[Ru(H)$_2$(PNN)(CO)] catalyst identified the coordination of the terminal oxygen of the hemiacetaloxide formed post hydride transfer to yield the octahedral 2-Ru-HemAc as shown in **figure 4.2**, where no ligand dissociation is proposed as well [75].

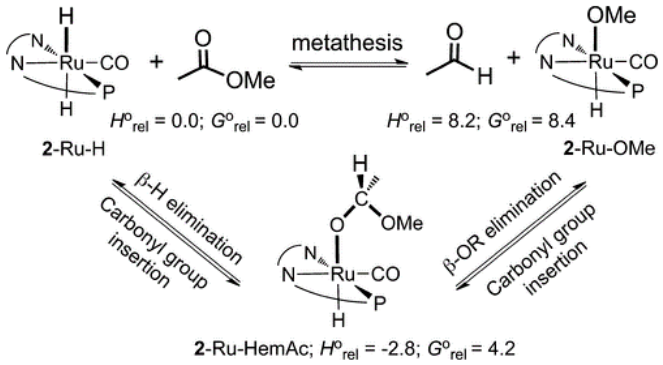

Figure 4.2 – Metal alkoxide mediated mechanism for hydrogenation of ester. Energies are given in kcal/mol

In this chapter, we focus on examining our proposition on the initial stage of the bridging species formation in insertion reaction of various classes of carbonyl compounds (XYC=O, where X,Y = H, Me, OMe, OEth, NH_2, NHMe) and CO_2 shown in **scheme 4.1**, including aldehydes, ketone, carbonate, lactone, ester carboxamide, carbamate and urea. Some that showed facile insertion.

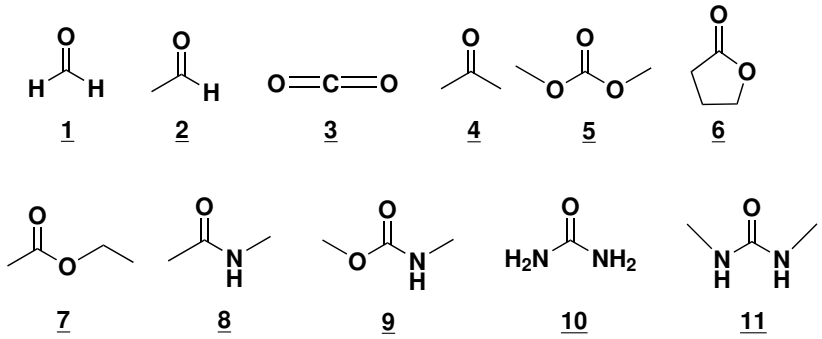

Scheme 4.1 – Series of Carbonyl compounds; **1**: Formaldehyde/**2**: Acetaldehyde/ **3**: carbon dioxide/**4**: Acetone/**5**: Dimethyl carbonate/**6**: Lactone/**7**: Ethyl acetate/**8**: N-methylacetamide/**9**: Methyl methylcarbamate/**10**: Urea/**11**: Dimethylurea.

Specifically, using Gusev's octahedral Osmium *trans*-dihydride complex *trans*-[$Os(H)_2(CO)$ $PyCH_2NH$-$CH_2CH_2NHPtBu_2$] (**Scheme 4.2** ;1-Os-H), one of the frontier catalysts utilized for hydrogenation of aldehydes and esters [76], we will conduct a DFT-based comprehensive investigation on the insertion mechanism of these organic compounds into Os–H bond, through thermodynamic study of the net reaction. A kinetic study will be conducted through analysis of computed transition states and along the PES of reaction for each substrate with 1-Os-H. Also, we aim at using energy decomposition cycles to explain the different propensities of these compounds to undergo reduction.

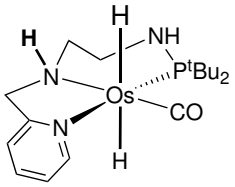

Scheme 4.2 – Gusev's Octahedral Osmium *trans*-Dihydride Complex (1-Os-H)

4.2 Results and Discussion

4.2.1 Thermodynamics of Insertion

We started our investigation by a thermodynamic study of the net insertion reaction of the different carbonyl compounds into Os-H bond of 1-Os-H forming a metal-alkoxide product (1-Os-OCHXY), a general reaction is shown in **scheme 4.3**.

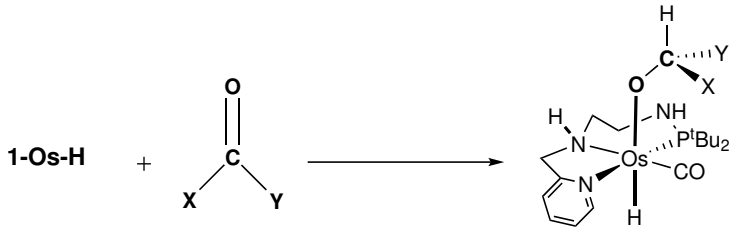

Scheme 4.3 – Insertion reaction into 1-Os-H

The Gibbs free energy (ΔG^o) and the electronic Energy (ΔE) are computed in a polarizable continuum representing toluene as solvent. These energies along with equilibrium isotope effect of the equilibrium reaction of the proteo and deutero 1-Os-H are shown in **table 4.1**.

Table 4.1 – Electronic(ΔE), Gibbs Free Energy ΔG^o and Equilibrium Isotope Effect for the insertion reaction of different carbonyl compound. *Energies are in kcal/mol.*

Substrate	ΔE	ΔG°	EIE
1- Formaldehyde	-30.0	-15.5	0.29
2- Acetaldehyde	-22.6	-7.4	0.28
3- CO_2	-18.8	-6.5	0.33
4- Acetone	-17.7	-0.8	0.26
5- Dimethyl carbonate	-8.7	5.3	0.26
6- Lactone	-7.5	7.0	0.25
7- Ethyl acetate	-5.8	9.5	0.27
8- N-methylacetamide	-4.5	11.1	0.28
9- Methyl methylcarbamate	-2.9	12.9	0.27
10- Urea	4.0	18.0	0.26
11- Dimethyl urea	3.5	19.2	0.26

As shown above, the equilibrium isotope effect (EIE) is computed to be highly inverse for all the substrates considered. This result can be attributed in a straightforward way to the fact that the vibrational frequencies of the C-H bond being formed in the assigned reactions are much higher than that of Os-H bond being cleaved. Energies were arranged in order of decreased exoergicity as obtained by calculations, different carbonyl compounds showed very different affinity to insert into Os-H bond of the complex, where the reaction's energies spanned a range of around 35 kcal/mol indicating different propensities of these

substrates to get reduced. The most favorable insertion was for that of formaldehyde with highly exoergic free energy of -15.5 kcal/mol, while the least favorable was that of Dimethylurea with insertion free energy of 19.2 kcal/mol.

However, the variation in the EIE (K_H/K_D) was essentially minor. This was totally unexpected because one would normally associate the more favorable reaction with the formation of a much "stronger" C-H bond that would yield the more inverse EIEs. Counterintuitively, the computed data in **table 4.1** reveal opposite trend, where Dimethylurea, the least favorable inserted species resulted in very similar inverse EIE to that of Formaldehyde (0.26 for vs 0.29). This means that, the C–H formed after Dimethylurea insertion is of same strength as that of Formaldehyde insertion, despite the great difference in their net reactions energies. This is a counterintuitive finding because, generally, more exoergic reactions are expected to yield stronger bonds, that have higher frequencies.

To rationalize why the more favorable insertion doesn't form stronger C–H bonds or why the energy of insertion/reduction isn't directly linked to the strength of the bond being formed. We constructed two thermodynamic cycles to split the energy of the reduction reaction into several terms. These two cycles are outlined in **scheme 4.4**.

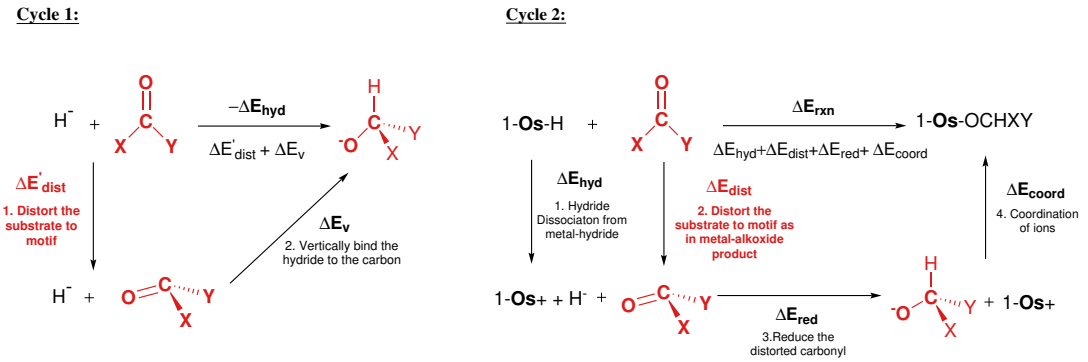

Scheme 4.4 – Thermodynamic Cycle for carbonyl compounds reduction

In Cycle 1, the structural and electronic energy of the complex itself are excluded, where the reaction studied is the reduction of the carbonyl compounds through binding of H^- to the carbon of carbonyl. Therefore, -ΔE_{hyd} of this reaction is split into two terms; **i)** A distortion energy ($\Delta E'_{dist}$), which is the energy required to distort the structure of the carbonyl compound from planar to trigonal pyramidal geometry attained at it's alkoxide form, and **ii)** The "vertical" (or adiabatic) energy (ΔE_v) for hydride binding to the distorted organic substrate.

In Cycle 2, we studied the net insertion reaction, where the Electronic energy of insertion (ΔE_{rxn}) is split into four terms; **i)** ΔE_{hyd} representing the affinity of the complex to donate a hydride forming a metal cation (which is constant value characterizing the complex), **ii)** ΔE_{dist} which is the energy required to distort the structure of the carbonyl compound from planar to trigonal pyramidal geometry

attained at the metal-alkoxide product, **iii)** ΔE_{red} is the energy of the reaction involving binding the hydride to the distorted carbonyl, and **iv)** ΔE_{coord} which is the energy required to coordinate both the metal cation and alkoxide anion forming metal-alkoxide product. The computed energies are shown in **table 4.2.**

As shown in **table 4.2**, for Cycle 1, the distortion energies ($\Delta E'_{dist}$) are computed to vary considerably among the organic substrates. The lowest $\Delta E'_{dist}$ is that of formaldehyde at 32.6 , which encounters hydrogens as substituents to the carbonyl. However, at the other end are structures involving amido groups substituents such as Dimethylurea which requires much higher distortion energy of 70.1 kcal/mol. The overall range of the computed distortion energies is 37 kcal/mol. Most remarkably and according to the shown computed data, some of the substrates that strongly disfavor reduction have high distortion energy. For example, the net reaction energy for reducing formaldehyde is much favored than that of Dimethylurea: ΔE_{rxn} = -24.1 and 5.1 kcal/mol, respectively. Accordingly, the distortion energy required by formaldehyde is much lower than that of Dimethylurea: $\Delta E'_{dist}$ = 32.6 vs 70.1 kcal/mol. However, the vertical energy required to bind the hydride to the distorted carbonyl (ΔE_v) are -68.2 kcal/mol for Formaldehyde and -77.2 kcal/mol for Dimethylurea. This means that the distorted Dimethylurea in fact favors reduction (forming C–H bond) by nearly 9 kcal/mol compared to the distorted formaldehyde, thus resulting in C–H bond of very similar strength, therefore invariant EIE. However, there is no systematic correlation between the distortion energies and the net reduction energies.

Table 4.2 – Computed M06L-D3 Distortion Energies shown in thermodynamic cycles.

	Cycle 1				*Cycle 2*					
Substrate	$\Delta E'_{dist}$	ΔE_v	$-\Delta E_{hyd}$	$-\Delta G_{hyd}$	ΔE_{hyd}	ΔE_{dist}	ΔE_{red}	ΔE_{coord}	ΔE	$\Delta G°$
1- Formaldehyde	32.6	-68.2	-35.6	-24.1	89.8	43.0	-78.6	-84.2	-30.0	-15.5
2- Acetaldehyde	36.0	-64.3	-28.4	-16.4	89.8	45.7	-74.0	-84.0	-22.6	-7.4
3- CO_2	53.8	-92.4	-38.6	-29.1	89.8	58.4	-97.0	-70.0	-18.8	-6.5
4- Acetone	38.5	-62.0	-23.5	-10.8	89.8	47.7	-71.2	-84.0	-17.7	-0.8
5- Dimethyl carbonate	58.7	-84.4	-25.7	-13.9	89.8	59.7	-85.4	-72.7	-8.7	5.3
6- Lactone	51.0	-71.7	-20.7	-10.3	89.8	67.2	-87.9	-76.6	-7.5	7.0
7- Ethyl acetate	51.0	-72.2	-21.2	-9.3	89.8	56.1	-77.3	-74.4	-5.8	9.5
8- N-methylacetamide	58.4	-71.5	-13.1	-1.1	89.8	49.3	-62.4	-81.1	-4.5	11.1
9- Methyl methylcarbamate	66.6	-83.4	-16.8	-5.2	89.8	55.7	-72.5	-75.9	-2.9	12.9
10- Urea	68.5	-76.3	-7.8	3.5	89.8	66.4	-74.1	-78.0	4.0	18.0
11- Dimethyl-Urea	70.1	-77.2	-7.2	5.1	89.8	66.0	-73.1	-79.1	3.5	19.2

Cycle 2 starts with removing a hydride from 1-Os-H complex. This step is endoergic by ΔE_{hyd}= 89.9 kcal/mol. Similarly as Cycle 1, the distortion energies (ΔE_{dist}) are computed to vary considerably among the organic substrates. Also, The lowest ΔE_{dist} is for that of formaldehyde at 43.0, while the highest is that of Dimethylurea at 66.0 kcal/mol. After distorting, Formaldehyde and

Dimethylurea showed reduction energies of ΔE_{red} = -78.2 and -73.1 kcal/mol respectively, while coordination energies ΔE_{coord} = -84.2 and -79.1 kcal/mol respectively. Therefore, both have very similar tendency to get reduced first, and then coordinate with the square pyramidal osmium cation (1-Os+) form of the complex forming metal-alkoxide product, thus, the only factor contributing to their very different reaction energies and plays an important role in their different propensities to insert into metal-hydride bond is suggested to be "distortion".

Evidently, the presence of an amino group at the carbonyl carbon greatly increases the distortion energy. The distortion at hand involves primarily pyramidalization of the three substituents at the carbonyl carbon. This presumably raptures the conjugation achieved when there is a substituent with a lone pair. In the case of ureas, the distortion involves both pyramidalization at the carbonyl carbon as well as the nitrogen centers, which can explain the very high distortion energy. In other words, when there is an amino group connected to the carbonyl, π-conjugation greatly stabilizes the carbonyl motif around the carbon, disfavoring thereby the interaction with a hydride thus reduction.

4.2.2 Mechanism of Insertion

Our investigations on carbonyl compounds insertion into Os-H bond of 1-Os-H suggests that a major factor in determining the thermodynamic favorability of reduction is "Distortion Energies" of the substrates. To direct our proposition, we performed additional calculations on the mechanism of insertion to probe the distortion's effect on the pathway of the reaction along with examining the RDS. We started our mechanistic study by locating the stationary points along the PES of reaction of two substrates with 1-Os-H that showed very different distortion energies, Formaldehyde and Dimethylurea. Gibbs free energy profiles are shown in **figure 4.3**.

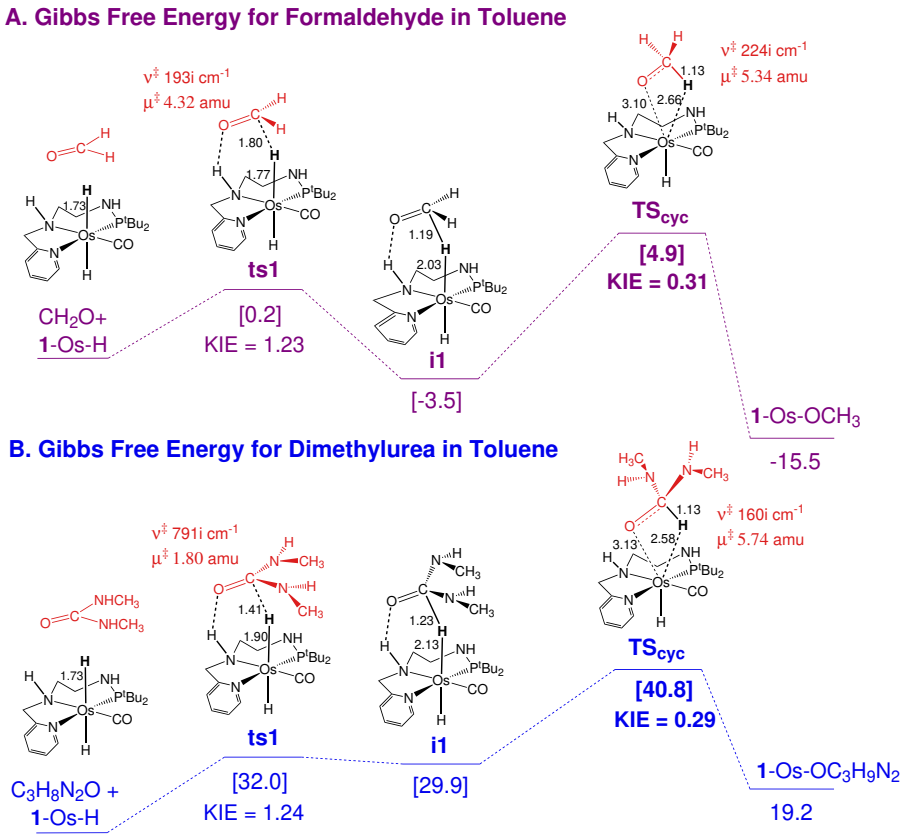

Figure 4.3 – M06L-D3 Gibbs Free Energy profile for insertion of Formaldehyde (A), and Dimethylurea (B) in toluene.

Both profiles start by locating the first linear transition state on the PESs of the reactions in toluene. These TSs showed barely stressed Os–H bond at 1.77 Å for Formaldehyde and 1.90 Å for Dimethylurea when compared to the reactant 1-Os-H (1.73 Å). However, the C-H bond is observed to be shorter for Dimethylurea than that of formaldehyde (1.80 Å vs 1.41 Å) indicating a greater interaction for the former at this stage of the reaction, but yet, much larger

than a fully formed C–H bond at formate (1.14 Å), then they are both still characterized as ts1. The barriers for these TSs varry considerably from 0.2 kcal/mol for Formaldehyde to 32.0 kcal/mol for Dimethylurea while the kinetic isotope effect was essentially invariant as illustrated in **figure 4.3**. This transition state connects the initial reactants to i1, the first minimum on the PES. According to the previously discussed details, by analogy to i1 reported in chapters 2 and 3, this minimum is considered a bridging hydride minimum, where the hydride is sandwiched between osmium and carbon of the carbonyl.

The electornic energy along with gibbs free energy, the kinetic isotope effect (KIE), and some assigned geometric parameters of ts1 computed for all the carbonyl compounds are shown in **table 4.3**.

Table 4.3 – The electronic energy ($\Delta E^{\ddagger}$), Gibbs free energy ($\Delta G^{\ddagger}$),imaginary frequency, reduced mass (μ), KIE and some bond distances at ts1.

Substrate	$\Delta E^{\ddagger}$	$\Delta G^{\ddagger}$	*i*-freq	μ	$r_{Os—H}$	$r_{C—H}$	KIE
1- Formaldehyde	**-10.5**	**0.2**	193	4.32	1.77	1.80	**1.23**
2- Acetaldehyde	**-6.1**	**5.5**	495	2.09	1.80	1.64	**1.37**
3- CO_2	**-0.3**	**8.2**	534	2.82	1.78	1.66	**1.19**
4- Acetone	**0.4**	**13.3**	592	1.89	1.89	1.53	**1.46**
5- Dimethyl carbonate	**6.0**	**18.2**	630	2.31	1.84	1.47	**1.17**
6- Lactone	**3.4**	**15.2**	737	1.79	1.90	1.43	**1.35**
7- Ethyl acetate	**5.8**	**19.1**	676	1.89	1.90	1.42	**1.35**
8- N-methylacetamide	**7.3**	**20.3**	236	2.48	2.01	1.32	**1.12**
9- Methyl methylcarbamate	**14.6**	**27.9**	653	2.00	1.87	1.50	**1.30**
10- Urea	**19.1**	**30.8**	811	1.81	1.88	1.42	**1.27**
11- Dimethyl-Urea	**20.0**	**32.0**	791	1.80	1.90	1.41	**1.24**

We continued our investigations to locate the second transition state known as the cyclic TS. Computed TS_{cyc} connects i1, the bridging intermediate to the final metal-alkoxide product. Same TS was calculated for all the studied carbonyl compounds and are all characterized by an imaginary frequency representing a vibration that exchanges C-H and C-O bond coordination of the formed alkoxide anion to the metal. This *i*-freq were observed to be insensitive to isotope substitution of the hydride by deuterium. The computed stationary points along the PESs of the insertion reaction of all substrates with 1-Os-H are shown in **table 4.4**

Moreover, no distinct hydride transfer transition state (ts2) were located for all these substrates, indicating the vanish of such step when a bridging hydride is formed and a shallow surface near these points. Therefore, after formation of the bridging species characterized by a lower barrier, the reaction is expected to proceed through concomitant cleavage of Os–H bond and formation of Os–O bond through what we discussed earlier as slippage or cyclic TS, therefore

resulting in insertion, not through a conventional hydride transfer mechanism. As shown in **table 4.4**, the free energy of the separated ions that can form by dissociation of all i1s in toluene is computed to be endoergic and much higher than TS_{cyc} for all the substrates. Therefore, this rules out any proposed role for free ions in mediating associative carbonyl compounds insertion into metal hydride bond in Gusev's system. Ion-pair formation, dissociation and re-coordination is, therefore, unlikely to be viable.

Consistently, TS_{cyc} is observed to be the highest point on the PES of all the substrates as shown in **table 4.4**, therefore indicating that if reduction reaction is to take place for these carbonyl compounds, then it is expected to proceed through the characteristic cyclic transition state (TS_{cyc}).

Table 4.4 – Computed M06L-D3 Free energies for stationary points along the PES of the reaction of 1-Os-H with all the substrates. Gibbs free energies are given in kcal/mol at 298 K and 1 M relative to the separated reactants.

Substrate	ts1	i1	TS_{cyc}	1-Os-OCHXY	Separated ions
1- Formaldehyde	0.2	-3.5	**4.9**	-15.5	54.2
2- Acetaldehyde	5.5	4.4	**12.9**	-7.4	61.4
3- CO_2	8.2	5.3	**13.6**	-6.5	51.2
4- Acetone	13.3	5.0	**18.5**	-0.8	66.3
5- Dimethyl carbonate	18.2	15.8	**21.2**	5.3	64.1
6- Lactone	15.2	15.9	**21.5**	7.0	69.1
7- Ethyl acetate	19.1	20.1	**28.0**	9.5	68.6
8- N-methylacetamide	20.3	21.4	**31.2**	11.1	76.6
9- Methyl methylcarbamate	27.9	27.1	**34.1**	12.9	73.0
10- Urea	30.8	29.7	**40.4**	18.0	82.0
11- Dimethyl-Urea	32.0	29.9	**40.8**	19.2	86.1

Despite showing that the reduction of the above studied substrates with 1-Os-H in toluene involves TS_{cyc} as RDS. The initial stage of the reaction commonly involves a preparatory step for activating the carbonyl compound through bridging species formation which is observed to encounter a smaller yet significant barrier. However, this barrier varies substantially when changing the carbonyl compound. Theoretically, the kinetic barrier for any transformation is the energy required for the structural and electronic reorganization to progress from a ground state to a transition state. As the energy varies substantially among the considered organic compounds we suggest that it falls from the bending required by this carbonyl prior to bridging the hydride with the metal. Thus assuming that this preparatory step (forming the bridge) is due to a bending barrier from the carbonyl.

We can test this assumption by constructing a thermodynamic cycle (Cycle 3) to dissect the reaction's energy into two energies. This cycle is outlined in **scheme**

4.5, where the Electronic Energy barrier ($\Delta E^{\ddagger}$) is split into; **i)** A distortion energy ($\Delta E"_{dist}$), which is the energy required to distort the structure of the carbonyl compound from planar to trigonal pyramidal geometry attained at the level of ts1, and **ii)** A vertical binding energy ($\Delta E"_{v}$), which is the energy required to react the hydride with the carbon of distorted carbonyl compound.

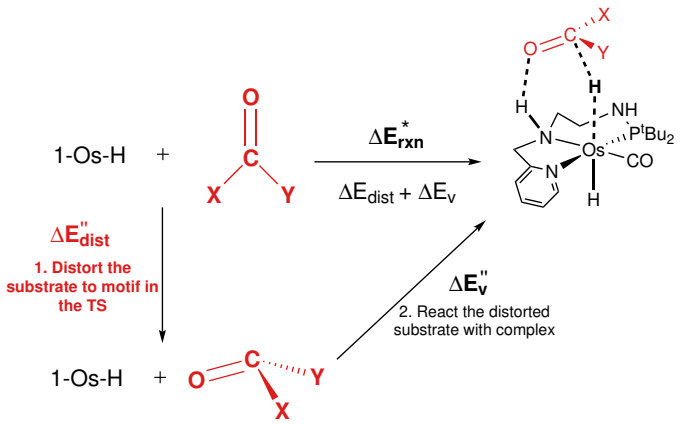

Scheme 4.5 – Thermodynamic Cycle 3 for energy barrier at ts1.

The computed M06L-D3 Energies of Cycle 3 are shown in **table 4.5**. The distortion energies ($\Delta E"_{dist}$) are shown to vary considerably among the organic substrates. Compounds with higher distortion energies showed higher reaction barriers, very consistent with the thermodynamics. Remarkably, a high percentage of distortion is attained at ts1 by compounds initially requiring higher distortion, thus favoring by that hydride bridging. This is supported by examining the energy required to react the distorted geometry of the organic substrates with hydride. $\Delta E"_{v}$ is highly exergonic and very comparable for all the compounds [spans a range of 7 kcal/mol]. In a more extreme scenario, compounds that showed unfavorable reduction experimentally and theoretically, are currently (after distorting) showing high susceptibility to react. For example, the distortion energy in the reaction of formaldehyde is much lower than that of Dimethylurea: ΔE_{dist} = 3.1 kcal/mol vs 34.7 kcal/mol. However, the vertical energy for hydride bridging to the distorted formaldehyde and the distorted Dimethylurea are -13.7 and -14.5 kcal/mol respectively. This means that the distorted Dimethylurea in fact favors hydride bridging by nearly 1 kcal/mol compared to the distorted formaldehyde.

Table 4.5 – Computed M06L-D3 for Energies in Cyle 3.

Substrate	$\Delta E"_{dist}$	$\Delta E"_{v}$	ΔE^{*}_{rxn}
1- Formaldehyde	3.1	-13.7	-10.5
2- Acetaldehyde	7.8	-14.0	-6.1
3- CO_2	14.2	-14.5	-0.3
4- Acetone	14.9	-14.5	0.4
5- Dimethyl carbonate	25.6	-19.6	6.0
6- Lactone	21.5	-18.1	3.4
7- Ethyl acetate	25.8	-20.0	5.7
8- N-methylacetamide	27.8	-20.5	7.3
9- Methyl methylcarbamate	33.7	-19.2	14.6
10- Urea	33.0	-13.9	19.1
11- Dimethyl-Urea	34.7	-14.5	20.2

After showing that the distortion energy dictates the thermodynamic favorability of reduction, currently, we showed that it dictates kinetics as well. Especially, distortion starts at an early stage of the reaction where the compound approaches the metal-hydride through a bent angle at ts1 resulting in what we defined earlier as a bridging species i1.

4.3 Conclusion

In this chapter, we were able first to represent a simple approach for explaining the different thermodynamic susceptibility of a series of carbonyl compounds to get reduced. Our calculations suggest that carbonyl compounds having donor group substituents and showing experimentally non facile insertion favor C–H bond formation to the same extent as experimentally facile ones. However, their high distortion energies prior to hydride binding dictate this transformation thus disfavoring insertion.

Kinetically, we were able to support our previous proposition in Chapters 2 and 3 on the involvement of a bridging species as a preparatory step in hydrogenation of carbonyls as well as carbon dioxide. In some cases the formation of this species was clear, in others, the C–H bond was more dissociative at the level of ts1, however, in all the above studied unsaturated compounds no trace for a distinct hydride transfer TS was located.

To clarify the origin of this observation we can think of the carbonyl group as a Lewis acid that are expected to accept pair of electrons. The first step in bridge formation is computed to be of a distinct barrier along the potential energy surface of the reaction. This barrier arises from the distortion of the carbonyl

compound and varies upon. When this barrier is attained, we expect an exoergic C–H bond partial formation, similar for all species prior to cleavage of a metal-hydride bond. However, M-H bond cleavage is concomitant with the C–O bond insertion through what we computed and explained as TS_{cyc}, the highest point and RDS, not through a hydride transfer TS forming an ion-pair species. This transformation is predicted to be barrierless where the PES leads directly to TS_{cyc}, as both ts2 and i2 weren't distinctly located.

In attempts to develop new and more efficient catalytic systems, the mechanism of hydrogenation of unsaturated molecules using organometallic transition metal-hydride complexes had been widely elucidated. Numerous studies focus on examining the hydricity of metal-hydrides since a more conventional mechanism is expected to start through nucleophlic attack of the hydride on the carbon. Simplistically, our calculations convey no support for a mechanism initiated by a "shoot" of hydride to the carbonyl. This finding is believed to redirect the understanding of what has been for a long time fundamentally misunderstood as a hydride transfer mechanism.

Chapter 5

Conclusion

Insertion reactions of unsaturated molecules into saturated octahedral transition metal complexes is proposed to proceed through an associative mechanism where no empty coordination site is required. However, probing the rate determining step for such process has been tedious, due to conflicting view about the nature of TS involved. The advancement in the development of hardware, software, and theoretical methods allowed scientists to gain detailed information about mechanism of chemical reactions using modern quantum chemical methods such as Density Functional Theory (DFT).

In this thesis, we utilized DFT methods to investigate the associative mechanism of insertion of unsaturated molecules into a metal-hydride bond of saturated octahedral d^6-transition metal complexes. We examined the associative outer-sphere potential energy of the reaction of carbon dioxide and carbonyl compounds insertion into three different metal hydride complexes.

Our first investigation pertained carbon dioxide insertion into rhenium hydride bond of *fac*-(bpy)$Re(CO)_3H$, a system by Sullivan and Meryer who proposed either a linear or cyclic TS as RDS. The full associative mechanism was studied, our calculations revealed that the initial stage of the reaction starts with a low energy linear TS (ts1) for formation of a bond between the carbon and the metal hydride bond leading to a bridged hydride species (i1). In analogy with an organometallic bridged borohydride intermediate that are known to perform such species and using QTAIM, we supported our proposition that i1 is more consistent with a hydride bridge. A second stage of the reaction involves cleavage of the bridged metal hydride bond and rearrangement of the resulting ion-pair intermediate via a cyclic transition state (TS_{cyc}). We showed that consideration of TS_{cyc} as RDS afforded activation free energies, solvent effects, substituent effects and KIE that are all in excellent agreement with the experiment.

Our second investigation explored the effect of hydrogen bonding and trans-hydride ligand on the RDS of the same given transformation. We concluded that the RDS in the reaction with $(^{iPr}P^{H}NP)Ir(H)_3$, a prototype of octahedral complexes also involved a cyclic TS. Moreover, accepting this finding, accurately

reproduced the available experimental kinetics data for this system. In contrast, assuming ts1, the linear TS, to be rate determining afforded barriers and solvent effects that are all inconsistent with the experiment.

A key point in such conclusion reveals a new fundamental understanding to a mechanism has been widely believed to be initiated through a "hydride transfer step" where a nucleophilic attack of the hydride on the carbon takes place. Our finding redirects this understanding and simplistically conveys no support for a mechanism initiated by a "shoot" of hydride to the carbonyl.

In the last part, we expanded our investigation into the mechanism of associative insertion of carbonyl compounds other than CO_2. We considered the insertion of eleven carbonyl compounds (XYC=O, where X,Y = H, Me, OMe, OEth, NH_2, NHMe) into Gusev's octahedral osmium dihydride (PNN)Os$(H)_2$(CO) catalyst. Different carbonyl compounds showed different susceptibility to get inserted (energies varied over a range of around 30 kcal/mol). However, the substrates that disfavored insertion afforded Equilibrium Isotope Effect (EIE) that were slightly more inverse than the more favored insertions. This meant that the less favored reactions result in formation of stronger C-H bonds. We rationalized this counterintuitive finding using thermodynamic cycles starting with distortion of the carbonyl moiety in the free substrates prior to formation of a C-H bond. We concluded that this result followed due to high "Distortion Energies" required by these substrates prior to reduction, and that the distorted substrates have comparable susceptibilities to reduction by formation of a C-hydride bond. Kinetically, calculations predicted an associative mechanism where TS_{cyc} is the RDS even if some reactions are uphill or prohibited, while ts1 is a preparatory step for forming bridging hydrdie intermediate. Therefore, we showed that distortion energies dictate both the kinetic and thermodynamic trends of these reactions. The results obtained in the present work provide new insights to understanding the associative mechanism for carbonyl group insertion into the M-H bond of octahedral complexes.

Appendix A

Abbreviations

EIE	Equilibrium Isotope Effect
IRC	Intrinsic Reaction Coordinates
KIE	Kinetic Isotope Effect
NBO	Natural Bond Orbital
PES	Potential Energy Surface
RDS	Rate Determining Step
THF	Tetrahydrofuran
TST	Transition State Theory
ZPE	Zero Point Energy

Appendix B

Job Script Samples

B.1 Optimization and Frequency Calculations

```
%chk=CO2
%mem=40GB
%NProcShared=28
#M06L/gen opt=(tight,calcfc) scrf=(smd,solvent=THF) freq integral=(grid=superfine)

Carbon dioxide

0 1
C,0,-0.35787019,0.11242598,-0.09220139
O,0,0.8011297299,0.11242598,-0.09220139
O,0,-1.5168701099,0.11242598,-0.09220139

C O 0
Def2TZVP
****
```

Figure B.1 – Input sample job showing the commands needed for the optimization and frequency calculation of the Carbon dioxide in THF.

```
Optimization completed.
  -- Stationary point found.
                 ----------------------------
                 !   Optimized Parameters   !
                 ! (Angstroms and Degrees)  !
--------------------------                  --------------------------
! Name  Definition          Value       Derivative Info.            !
--------------------------------------------------------------------------------
! R1    R(1,2)              1.159       -DE/DX =    0.0             !
! R2    R(1,3)              1.159       -DE/DX =    0.0             !
! A1    L(2,1,3,-2,-1)      180.0         -DE/DX =    0.0             !
! A2    L(2,1,3,-3,-2)      180.0         -DE/DX =    0.0             !
--------------------------------------------------------------------------------
GradGradGradGradGradGradGradGradGradGradGradGradGradGradGradGradGradGrad

                  Input orientation:
---------------------------------------------------------------------
Center     Atomic     Atomic          Coordinates (Angstroms)
Number     Number      Type          X         Y         Z
---------------------------------------------------------------------
    1          6          0     -0.357870    0.112426   -0.092201
    2          8          0      0.801146    0.112426   -0.092201
    3          8          0     -1.516887    0.112426   -0.092201
---------------------------------------------------------------------
            Distance matrix (angstroms):
            1        2        3
   1  C   0.000000
   2  O   1.159016   0.000000
   3  O   1.159016   2.318033   0.000000
Stoichiometry    CO2
Framework group  D*H[O(C),C*(O.O)]
Deg. of freedom    1
Full point group              D*H     NOp   8
Largest Abelian subgroup      D2H     NOp   8
Largest concise Abelian subgroup C2     NOp   2
```

Figure B.2 – Output sample showing the completed optimization for CO_2 in THF.

```
Harmonic frequencies (cm**-1), IR intensities (KM/Mole), Raman scattering
activities (A**4/AMU), depolarization ratios for plane and unpolarized
incident light, reduced masses (AMU), force constants (mDyne/A),
and normal coordinates:
                      1                      2                      3
                     PIU                    PIU                    SGG
Frequencies --    675.8268               675.8268              1386.9869
Red. masses --     12.8774                12.8774                15.9949
Frc consts  --      3.4654                 3.4654                18.1291
IR Inten    --     35.7896                35.7896                 0.0000
 Atom  AN      X      Y      Z        X      Y      Z        X      Y      Z
    1   6     0.38   0.80  -0.00     0.80  -0.38  -0.00     0.00  -0.00  -0.00
    2   8    -0.14  -0.30   0.00    -0.30   0.14  -0.00    -0.00   0.00   0.71
    3   8    -0.14  -0.30  -0.00    -0.30   0.14   0.00    -0.00   0.00  -0.71
                      4
                     SGU
Frequencies --   2458.1787
Red. masses --     12.8774
Frc consts  --     45.8463
IR Inten    --    775.1948
 Atom  AN      X      Y      Z
    1   6     0.00   0.00   0.88
    2   8    -0.00  -0.00  -0.33
    3   8    -0.00  -0.00  -0.33
```

Figure B.3 – Output Sample showing the frequency calculations of the CO_2 molecule in THF.

```
-------------------
- Thermochemistry -
-------------------
Temperature   298.150 Kelvin.  Pressure   1.00000 Atm.
Atom     1 has atomic number  6 and mass  12.00000
Atom     2 has atomic number  8 and mass  15.99491
Atom     3 has atomic number  8 and mass  15.99491
Molecular mass:    43.98983 amu.
Principal axes and moments of inertia in atomic units:
                          1         2         3
    Eigenvalues --     0.00000 153.45774 153.45774
          X           -0.00000   1.00000  -0.00000
          Y            0.00000   0.00000   1.00000
          Z            1.00000   0.00000  -0.00000
This molecule is a prolate symmetric top.
Rotational symmetry number  2.
Rotational temperature (Kelvin)      0.56442
Rotational constant (GHZ):          11.760510
Zero-point vibrational energy      31083.9 (Joules/Mol)
                                   7.42923 (Kcal/Mol)
Vibrational temperatures:    972.36   972.36  1995.56  3536.77
         (Kelvin)

Zero-point correction=                           0.011839 (Hartree/Particle)
Thermal correction to Energy=                    0.014453
Thermal correction to Enthalpy=                  0.015397
Thermal correction to Gibbs Free Energy=        -0.008849
Sum of electronic and zero-point Energies=           -188.642957
Sum of electronic and thermal Energies=              -188.640343
Sum of electronic and thermal Enthalpies=            -188.639399
Sum of electronic and thermal Free Energies=         -188.663645

                    E (Thermal)             CV                S
                     KCal/Mol        Cal/Mol-Kelvin    Cal/Mol-Kelvin
Total                    9.069              6.833             51.030
Electronic               0.000              0.000              0.000
Translational            0.889              2.981             37.270
Rotational               0.592              1.987             13.069
Vibrational              7.588              1.865              0.691
                      Q            Log10(Q)             Ln(Q)
Total Bot       0.117523D+05          4.070124          9.371807
Total V=0       0.327933D+10          9.515785         21.910904
Vib (Bot)       0.388004D-05         -5.411164        -12.459666
Vib (V=0)       0.108267D+01          0.034496          0.079431
Electronic      0.100000D+01          0.000000          0.000000
Translational   0.114679D+08          7.059482         16.255059
Rotational      0.264123D+03          2.421806          5.576414
```

Figure B.4 – Output Sample showing the Thermodynamic section calculations of the CO_2 molecule in THF.

```
%chk=Re-H
%mem=40GB
%NProcShared=28
#opt=(tight,calcfc) freq rM06L/genecp/W06 EmpiricalDispersion=GD3
   scrf=(smd,solvent=THF) nosym integral=(grid=superfine)

 1-Re-H complex in THF

0 1
Re                -5.16710137   -0.52412830   -1.00623167
H                 -5.16710137   -0.52412830    0.57376833
C                 -6.90149452    1.65897108   -0.69196732
C                 -4.79554052    2.86158508   -0.69196732
C                 -5.48162252    4.07588108   -0.69472832
C                 -6.87627552    4.08398008   -0.69607332
C                 -7.58423652    2.88392208   -0.69326632
C                 -7.64192552    0.39852708   -0.69071232
C                 -7.91870452   -1.87939192   -1.47545332
C                 -9.06168352   -2.01845492   -0.68837732
C                 -9.49613052   -0.95129592    0.09746868
C                 -8.79289352    0.25153708    0.09688868
H                 -3.69568452    2.85150808   -0.68869532
H                 -4.92465352    5.02392608   -0.69582632
H                 -7.42057052    5.03976308   -0.70046332
H                 -8.68454252    2.89468208   -0.69991632
H                 -7.57456252   -2.71818392   -2.09818132
H                 -9.61858152   -2.96654192   -0.68746632
H                -10.39587552   -1.05818092    0.72103268
H                 -9.13585952    1.08923108    0.72256968
N                 -5.49908252    1.65897108   -0.69196732
N                 -7.21055652   -0.67948692   -1.47720232
C                 -5.16710137   -0.52412830   -3.05623167
C                 -5.16710137   -2.57412830   -1.00623167
C                 -3.11710137   -0.52412830   -1.00623167
O                 -5.16710137   -0.52412830   -4.17163167
O                 -5.16710137   -3.68952830   -1.00623167
O                 -2.00170137   -0.52412830   -1.00623167

H C N O 0
Def2TZVP
****
Re 0
QZVP
****

Re 0
def2
```

Figure B.5 – Input sample job showing the commands needed for the optimization and frequency calculation of 1-Re-H transition metal complex in THF.

B.2 Single Point Calculations

```
%chk=CO2
%mem=78GB
%NProcShared=28
#M06L/gen/W06 EmpiricalDispersion=GD3 scf=(direct) scrf=(smd,solvent=THF)
integral=(grid=superfine)
opt=(calcfc,tight) freq

Carbondioxide

0 1
 C,0,-0.35787019,0.11242598,-0.09220139
 O,0,0.8011297299,0.11242598,-0.09220139
 O,0,-1.5168701099,0.11242598,-0.09220139

C O 0
Def2TZVP
****

--link1--
%chk=CO2
%mem=78GB
%NProcShared=28
#M06/gen/W06 EmpiricalDispersion=GD3 scf=(direct) scrf=(smd,solvent=THF)
integral=(grid=superfine)
geom=check guess=check

Carbondioxide

0 1

C O 0
Def2TZVP
****


--link1--
%chk=CO2
%mem=78GB
%NProcShared=28
#b3lyp/gen/W06 EmpiricalDispersion=GD3 scf=(direct) scrf=(smd,solvent=THF)
integral=(grid=superfine)
geom=check guess=check

Carbondioxide

0 1

C O 0
Def2TZVP
****

--link1--
%chk=CO2
%mem=78GB
%NProcShared=28
#wB97XD/gen scf=(direct) scrf=(smd,solvent=THF) integral=(grid=superfine)
geom=check guess=check

Carbondioxide

0 1

C O 0
Def2TZVP
****
```

Figure B.6 – Input sample job showing the commands needed for single point calculation of CO_2 molecule in THF at different levels of theory (in red) after optimizing first at M06L/W06.

```
%mem=72GB
%nprocshared=28
#freq rM06L/genecp/W06 EmpiricalDispersion=GD3
scrf=(smd,solvent=toluene) nosym integral=(grid=superfine)

C--O

0 1
O                  2.20833700   14.14746100    0.15200900
C                  1.51092600   14.80740300   -0.67136000
O                  0.66355700   15.68475300   -0.44461700

C O 0
Def2TZVP
****
```

Figure B.7 – Input sample job showing the commands needed for single point calculation of distorted CO_2 molecule in toluene.

```
 Polarizable Continuum Model (PCM)
 =================================
 Model                : PCM.
 Atomic radii         : SMD-Coulomb.
 Polarization charges : Total charges.
 Charge compensation  : None.
 Solution method      : Matrix inversion.
 Cavity type          : VdW (van der Waals Surface) (Alpha=1.000).
 Cavity algorithm     : GePol (No added spheres)
                        Default sphere list used, NSphG=   31.
                        Lebedev-Laikov grids with approx.  5.0 points / Ang**2.
                        Smoothing algorithm: York/Karplus (Gamma=1.0000).
                        Polarization charges: spherical gaussians, with
                                              point-specific exponents (IZeta= 3).
                        Self-potential: point-specific (ISelfS= 7).
                        Self-field    : sphere-specific E.n sum rule (ISelfD= 2).
 1st derivatives      : Analytical E(r).r(x)/FMM algorithm (CHGder, D1EAlg=3).
                        Cavity 1st derivative terms included.
 2nd derivatives      : Analytical E(r).r(xy)/FMM algorithm (CHGder, D2EAlg=3).
                        Cavity 2nd derivative terms included.
 Solvent              : TetraHydroFuran, Eps=   7.425700 Eps(inf)=   1.974025
```

Figure B.8 – Output sample output showing the polarizable continuum model used in all calculations

B.3 Transition State and IRC Calculations

```
%chk=ts1
%mem=40GB
%nprocshared=28
#opt=(modred) freq rM06L/genecp/W06 EmpiricalDispersion=GD3
scrf=(smd,solvent=THF) nosym integral=(grid=superfine)

Transition state for hydride bridging

0 1
 Re                -5.00979228   -0.47249984   -1.35383640
 H                 -4.98215121   -0.46064906    0.49481898
 C                 -7.08547228    1.77837116   -0.88419940
 C                 -4.98231328    2.69187416   -1.22273940
 C                 -5.45635928    3.97514616   -1.05087840
 C                 -6.80340028    4.15608616   -0.78311440
 C                 -7.62221028    3.04816616   -0.70129340
 C                 -7.88132428    0.55263116   -0.82119840
 C                 -7.87899228   -1.75562084   -1.02773540
 C                 -9.22867428   -1.83209184   -0.75590340
 C                 -9.92280728   -0.66085984   -0.50055640
 C                 -9.24229928    0.53937416   -0.53623140
 H                 -3.93788628    2.50490016   -1.43303940
 H                 -4.77552428    4.81071116   -1.12676340
 H                 -7.21197028    5.14751716   -0.64162640
 H                 -8.67609328    3.16723916   -0.49801240
 H                 -7.29777828   -2.64602184   -1.22722940
 H                 -9.71741428   -2.79555484   -0.74305540
 H                -10.98077628   -0.68105984   -0.27664740
 H                 -9.76361328    1.46397416   -0.33777640
 N                 -5.76815028    1.61037416   -1.14215340
 N                 -7.20880728   -0.59671984   -1.05866640
 C                 -5.07267728   -0.46267984   -3.33744940
 C                 -4.59175328   -2.33861784   -1.32677640
 C                 -3.12857128   -0.12678484   -1.37166440
 O                 -5.05390328   -0.49045384   -4.49427040
 O                 -4.35107928   -3.47458484   -1.28143240
 O                 -1.98819628    0.09355716   -1.35851540
 C                 -5.01155444   -1.29621897    1.86086471
 O                 -3.85684944   -1.38397597    2.00056571
 O                 -6.17239144   -1.33600397    1.98549671

1 2 F
2 29 F

H C N O 0
Def2TZVP
****
Re 0
QZVP
****

Re 0
def2
```

Figure B.9 – Input sample showing the commands needed for the optimization of the fixed geometry of transition state.

```
%chk=ts1
%mem=40GB
%nprocshared=28
#opt=(ts,noeigentest,tight,readfc,modred) freq rM06L/genecp/W06
EmpiricalDispersion=GD3
scrf=(smd,solvent=THF) nosym integral=(grid=superfine) geom=check

Activated Transition state for hydride bridging

0 1

1 2 a
2 29 a

H C N O 0
Def2TZVP
****
Re 0
QZVP
****

Re 0
def2
```

Figure B.10 – Input sample showing the commands needed for activation of the geometry of transition state.

```
Harmonic frequencies (cm**-1), IR intensities (KM/Mole), Raman scattering
 activities (A**4/AMU), depolarization ratios for plane and unpolarized
 incident light, reduced masses (AMU), force constants (mDyne/A),
 and normal coordinates:
                      1                      2                      3
                      A                      A                      A
 Frequencies --   -422.1135               28.2774               32.8095
 Red. masses --      3.6690                7.4027                8.8452
 Frc consts  --      0.3852                0.0035                0.0056
 IR Inten    --   2450.4331                0.0441                1.2860
  Atom  AN      X      Y      Z        X      Y      Z        X      Y      Z
     1  75     0.01   0.00  -0.00    -0.01   0.01  -0.03    -0.01  -0.00  -0.03
     2   1     0.50   0.07  -0.72    -0.04   0.01  -0.03     0.00   0.02  -0.04
     3   6     0.00  -0.00  -0.01    -0.01  -0.00   0.04    -0.00  -0.03   0.08
     4   6    -0.00  -0.01  -0.01    -0.06   0.03  -0.19    -0.03  -0.01   0.00
     5   6    -0.00  -0.01  -0.00    -0.06   0.03  -0.18    -0.01  -0.03   0.14
     6   6    -0.00  -0.00   0.00    -0.03   0.01  -0.03     0.01  -0.05   0.26
     7   6     0.00  -0.00   0.00    -0.01  -0.01   0.07     0.01  -0.05   0.22
     8   6     0.00  -0.00   0.00     0.01  -0.01   0.09    -0.00  -0.03   0.03
     9   6     0.01   0.00   0.01     0.00  -0.00  -0.04    -0.01  -0.02  -0.16
    10   6     0.00   0.00   0.00     0.03  -0.02   0.09    -0.01  -0.04  -0.16
    11   6    -0.00   0.00   0.01     0.05  -0.04   0.24    -0.00  -0.05  -0.04
    12   6     0.00  -0.00   0.00     0.04  -0.03   0.23     0.00  -0.05   0.05
    13   1    -0.00  -0.01  -0.01    -0.08   0.05  -0.31    -0.05   0.01  -0.09
    14   1     0.00  -0.01  -0.00    -0.09   0.05  -0.28    -0.01  -0.02   0.16
    15   1     0.00  -0.00   0.00    -0.03   0.00  -0.01     0.03  -0.07   0.37
    16   1     0.00  -0.00   0.00     0.01  -0.02   0.17     0.03  -0.08   0.30
    17   1     0.01   0.00   0.01    -0.01   0.01  -0.15    -0.02  -0.01  -0.24
    18   1     0.00   0.00  -0.00     0.04  -0.03   0.08    -0.01  -0.04  -0.24
    19   1    -0.00  -0.00   0.00     0.07  -0.06   0.35     0.00  -0.07  -0.03
    20   1     0.00  -0.00  -0.01     0.05  -0.05   0.34     0.01  -0.07   0.13
    21   7     0.00  -0.02  -0.02    -0.03   0.02  -0.06    -0.02  -0.01  -0.02
    22   7     0.02  -0.00   0.02    -0.01   0.00  -0.03    -0.01  -0.02  -0.06
    23   6    -0.08   0.01  -0.07     0.12   0.06  -0.04     0.02  -0.09  -0.04
    24   6    -0.00   0.01   0.01    -0.05   0.00  -0.04    -0.01  -0.00   0.07
    25   6    -0.00  -0.00  -0.00     0.03  -0.08   0.15    -0.00   0.00  -0.00
    26   8     0.00  -0.00  -0.08     0.21   0.11  -0.05     0.05  -0.16  -0.04
    27   8    -0.00   0.00   0.00    -0.08  -0.00  -0.06    -0.01  -0.01   0.16
    28   8     0.01  -0.00   0.00     0.07  -0.17   0.31     0.00  -0.00   0.03
    29   6    -0.23  -0.05   0.39    -0.03  -0.00  -0.04     0.04   0.18  -0.02
    30   8     0.02  -0.03  -0.06    -0.03  -0.00  -0.04    -0.23   0.14  -0.05
    31   8     0.04   0.04  -0.04    -0.04  -0.00  -0.03     0.31   0.29   0.03
```

Figure B.11 – Output sample showing the calculated imaginary frequency after the activation of the geometry in optimization of transition state.

```
%chk=ts1
%mem=40GB
%nprocshared=28
#IRC=(calcfc,maxcycles=200,maxpoints=100,recorrect=never,nogradstop) rM06L/genecp/W06
EmpiricalDispersion=GD3
scrf=(smd,solvent=THF) nosym integral=(grid=superfine)

IRC for Rransition State of hydride bridging in 1-Re-H

0 1
 Re,0,-4.9362057331,-0.515018271,-1.4371674681
 H,0,-4.7448002204,-0.4839720893,0.4434288452
 C,0,-7.0259823182,1.6933370766,-0.8267429766
 C,0,-4.9332334602,2.637461874,-1.1450524233
 C,0,-5.4128979199,3.9067086855,-0.8978715876
 C,0,-6.7579178999,4.0631687234,-0.6082926541
 C,0,-7.5690369699,2.9468749949,-0.5737808217
 C,0,-7.8107216273,0.459040369,-0.7864354121
 C,0,-7.7738353618,-1.852612463,-0.9740586734
 C,0,-9.1236247566,-1.9461172504,-0.7078461085
 C,0,-9.8364996885,-0.7814526308,-0.4775003627
 C,0,-9.1738463033,0.429121602,-0.5176995983
 H,0,-3.8902574869,2.4693475911,-1.3766376354
 H,0,-4.7379845542,4.7495723068,-0.9331646687
 H,0,-7.1712952508,5.0426056438,-0.4089776788
 H,0,-8.619596291,3.0447175943,-0.3443398137
 H,0,-7.1779302126,-2.7359857531,-1.1597911242
 H,0,-9.5973252212,-2.9166778747,-0.683427412
 H,0,-10.8968759886,-0.814544145,-0.2669404344
 H,0,-9.7106178259,1.3484989619,-0.3368982766
 N,0,-5.7130340899,1.5500031304,-1.1145870845
 N,0,-7.1243432881,-0.68239568,-1.0174061122
 C,0,-5.1306401148,-0.4961948292,-3.3541464869
 C,0,-4.473009219,-2.3756805543,-1.5241177338
 C,0,-3.0696721183,-0.1383895018,-1.6566998093
 O,0,-5.207608467,-0.498487696,-4.5096177131
 O,0,-4.1976566004,-3.4992242465,-1.5753427591
 O,0,-1.9441621862,0.0978280568,-1.7951393789
 C,0,-5.5213309061,-0.6367674259,1.6746334515
 O,0,-5.3916601902,-1.7742230734,2.0187743694
 O,0,-5.9871838196,0.438981224,1.9218268518

H C N O 0
Def2TZVP
****
Re 0
QZVP
****

Re 0
def2
```

Figure B.12 – Input sample showing the commands needed for the calculation of the intrinsic reaction coordinates for bridging hydride TS in 1-Re-H system.

```
Energies reported relative to the TS energy of       -1103.363329
 ------------------------------------------------------------------------------
    Summary of reaction path following
 ------------------------------------------------------------------------------
                       Energy    RxCoord
   1                  -0.01737 -18.95493
   2                  -0.01736 -18.76445
   3                  -0.01735 -18.57430
   4                  -0.01733 -18.38439
   5                  -0.01732 -18.19487
   6                  -0.01731 -18.00502
   7                  -0.01729 -17.81486
   8                  -0.01728 -17.62414
   9                  -0.01727 -17.43325
  10                  -0.01725 -17.24222
  11                  -0.01724 -17.05118
  12                  -0.01722 -16.86013
  13                  -0.01721 -16.66909
  14                  -0.01720 -16.47809
  15                  -0.01718 -16.28713
  16                  -0.01716 -16.09628
  17                  -0.01715 -15.90564
  18                  -0.01713 -15.71521
  19                  -0.01712 -15.52543
  20                  -0.01710 -15.33539
  21                  -0.01708 -15.14620
  22                  -0.01707 -14.95584
  23                  -0.01705 -14.76546
  24                  -0.01703 -14.57494
  25                  -0.01701 -14.38467
  26                  -0.01700 -14.19498
  27                  -0.01698 -14.00539
  28                  -0.01696 -13.81605
  29                  -0.01695 -13.75931
  30                  -0.01693 -13.56809
  31                  -0.01691 -13.37680
  32                  -0.01689 -13.18560
  33                  -0.01687 -12.99433
  34                  -0.01685 -12.80319
  35                  -0.01683 -12.61202
  36                  -0.01681 -12.42100
  37                  -0.01678 -12.23001
  38                  -0.01676 -12.03918
  39                  -0.01673 -11.84834
  40                  -0.01670 -11.65748
  41                  -0.01667 -11.46647
  42                  -0.01664 -11.27531
  43                  -0.01661 -11.08403
  44                  -0.01657 -10.89266
  45                  -0.01653 -10.70127
  46                  -0.01649 -10.50986
  47                  -0.01645 -10.31845
  48                  -0.01640 -10.12705
  49                  -0.01635  -9.93567
  50                  -0.01630  -9.74429
  51                  -0.01624  -9.55294
  52                  -0.01618  -9.36160
  53                  -0.01611  -9.17025
  54                  -0.01603  -8.97891
  55                  -0.01596  -8.78755
  56                  -0.01587  -8.59618
 ------------------------------------------------------------------------------

 Total number of points:                 55
 Total number of gradient calculations:  56
 Total number of Hessian calculations:    1
 IRC-IRC-IRC-IRC-IRC-IRC-IRC-IRC-IRC-IRC-IRC-IRC-IRC-IRC-IRC-IRC-IRC-IRC
```

Figure B.13 – Output sample showing the Energies along the reaction coordinates of the bridging hydride TS in 1-Re-H system as displayed in the output file.

B.4 AIM Calculations

```
%chk=1-Re-H
%mem=40GB
%NProcShared=28
#rM06L/genecp/W06 EmpiricalDispersion=GD3
 scrf=(smd,solvent=THF) nosym integral=(grid=superfine)
 output=wfx pop=NBO

Re-H chelate ligand in THF

0 1
 Re,0,-4.9790677878,-0.6143852142,-1.1434805853
 H,0,-4.8462177808,-0.6780313831,0.6426967653
 C,0,-7.0370999071,1.6412272547,-0.5799800751
 C,0,-4.9222622528,2.545475256,-0.8623361071
 C,0,-5.3908181136,3.8289476257,-0.6762366169
 C,0,-6.7414793838,4.0147497002,-0.4310291713
 C,0,-7.5682259722,2.9110334571,-0.3818836759
 C,0,-7.8450520114,0.4221281383,-0.5511649459
 C,0,-7.8559960695,-1.8862250332,-0.7542368223
 C,0,-9.2140568566,-1.9509662406,-0.525004856
 C,0,-9.9078129327,-0.7726211269,-0.3031959008
 C,0,-9.2160435906,0.421359392,-0.3168279819
 H,0,-3.8753095647,2.3549654731,-1.0566285499
 H,0,-4.7033759486,4.6611327399,-0.7249128314
 H,0,-7.1465091831,5.0064230374,-0.2811887278
 H,0,-8.6243611651,3.031501478,-0.1916282567
 H,0,-7.276191025,-2.7815268255,-0.9329091128
 H,0,-9.7102039904,-2.9107432085,-0.5227278529
 H,0,-10.9739331108,-0.7830658451,-0.1211878769
 H,0,-9.7363991636,1.3521270394,-0.1454933799
 N,0,-5.7170518027,1.4687917924,-0.8182857309
 N,0,-7.1765186733,-0.7325696666,-0.7709699411
 C,0,-5.1675073451,-0.5177380334,-3.092498452
 C,0,-4.572866511,-2.4791117861,-1.2748143555
 C,0,-3.1016232,-0.2814787647,-1.2999973103
 O,0,-5.2279806871,-0.4955583403,-4.2492210386
 O,0,-4.3346320736,-3.6129322548,-1.3546286956
 O,0,-1.9632912572,-0.070386461,-1.3897856744

H C N O 0
Def2TZVP
****
Re 0
QZVP
****

Re 0
def2

1-Re-H.wfx
```

Figure B.14 – Input sample showing the commands needed for the AIM calculation of 1-Re-H system.

Atom A	Atom B	2*D2(A,B)	DI(A,B)	%Deloc(A,B)	%Deloc(B,A)	
Re1	H2	1.9799766895E+01	7.2619837534E-01	2.6922600359E+00	2.4287414482E+01	(Bonded)
Re1	C3	7.4179040957E+01	2.6380182319E-02	9.7800150770E-02	2.3977154338E-01	
H2	C3	8.2210779308E+00	6.2626204602E-03	2.0945083881E-01	5.6921447895E-02	
Re1	C4	7.3514820149E+01	2.8001300155E-02	1.0381017628E-01	2.5680227860E-01	
H2	C4	8.1475985413E+00	6.1433396293E-03	2.0546153909E-01	5.6341084390E-02	
C3	C4	2.9967601266E+01	4.7976944575E-02	4.3606620714E-01	4.4000059351E-01	
Re1	C5	8.0576076809E+01	8.2079393793E-03	3.0429573954E-02	6.8688523325E-02	
H2	C5	8.9315272959E+00	1.5724193876E-03	5.2588938096E-02	1.3158864947E-02	
C3	C5	3.2827340726E+01	8.0840938019E-02	7.3476961769E-01	6.7652115837E-01	
C4	C5	3.1896676711E+01	1.3543767080E+00	1.2421102691E+01	1.1334164618E+01	(Bonded)
Re1	C6	8.0537312379E+01	1.0144191999E-02	3.7607909414E-02	8.4931981165E-02	
H2	C6	8.9262513780E+00	3.7448141180E-03	1.2524381179E-01	3.1353357878E-02	
C3	C6	3.2815950634E+01	7.2787735968E-02	6.6157343346E-01	6.0941340824E-01	
C4	C6	3.2519721505E+01	7.7729437590E-02	7.1286320911E-01	6.5078767532E-01	

Figure B.15 – Output sample showing the detected Bond Critical points and Delocalization indices parameter (DI) in AIM calculation of 1-Re-H complex.

Bibliography

[1] C. Tejel, M. A. Ciriano, and V. Passarelli, "Rhodium (iii)-catalyzed dimerization of aldehydes to esters," 2011.

[2] J. Mallah, M. Ataya, and F. Hasanayn, "Dimerization of aldehydes into esters by an octahedral d6-rhodium cis-dihydride catalyst: Inner-versus outer-sphere mechanisms," *Organometallics*, vol. 39, no. 2, pp. 286–294, 2020.

[3] B. P. Sullivan and T. J. Meyer, "Kinetics and mechanism of carbon dioxide insertion into a metal-hydride bond. a large solvent effect and an inverse kinetic isotope effect," *Organometallics*, vol. 5, no. 7, pp. 1500–1502, 1986.

[4] S. Kern and R. van Eldik, "Mechanistic insight from activation parameters for the reaction of a ruthenium hydride complex with co2 in conventional solvents and an ionic liquid," *Inorganic chemistry*, vol. 51, no. 13, pp. 7340–7345, 2012.

[5] J. Huang, J. Chen, H. Gao, and L. Chen, "Kinetic aspects for the reduction of co2 and cs2 with mixed-ligand ruthenium (ii) hydride complexes containing phosphine and bipyridine," *Inorganic chemistry*, vol. 53, no. 18, pp. 9570–9580, 2014.

[6] M. K. Whittlesey, R. N. Perutz, and M. H. Moore, "Facile insertion of co2 into the ru- h bonds of ru (dmpe) 2h2 (dmpe= me2pch2ch2pme2): Identification of three ruthenium formate complexes," *Organometallics*, vol. 15, no. 24, pp. 5166–5169, 1996.

[7] S. Takebayashi, N. Dabral, M. Miskolzie, and S. H. Bergens, "Experimental investigations of a partial ru–o bond during the metal–ligand bifunctional addition in noyori-type enantioselective ketone hydrogenation," *Journal of the American Chemical Society*, vol. 133, no. 25, pp. 9666–9669, 2011. PMID: 21634401.

[8] O. Blum and D. Milstein, "Hydride elimination from an iridium (iii) alkoxide complex: a case in which a vacant cis coordination site is not required," *Journal of Organometallic Chemistry*, vol. 593, pp. 479–484, 2000.

[9] H. C. Urey, F. G. Brickwedde, and G. M. Murphy, "A hydrogen isotope of mass 2 and its concentration," *Physical Review*, vol. 40, no. 1, p. 1, 1932.

[10] NobelPrize.org, "Harold C. Urey – Facts." Online; Fri. 10 Sep 2021.

[11] J. Reader and C. W. Clark, "A watershed year in nuclear physics," *Phys. Today*, vol. 66, no. 3, p. 44, 2013.

[12] H. Eyring and A. Sherman, "Theoretical considerations concerning the separation of isotopes," *The Journal of Chemical Physics*, vol. 1, no. 6, pp. 345–349, 1933.

[13] P. Jacob III, L. Yu, M. Wilson, and N. L. Benowitz, "Selected ion monitoring method for determination of nicotine, cotinine and deuterium-labeled analogs: absence of an isotope effect in the clearance of (s)-nicotine-3 , 3 -d2 in humans," *Biological mass spectrometry*, vol. 20, no. 5, pp. 247–252, 1991.

[14] T. G. Gant, "Using deuterium in drug discovery: leaving the label in the drug," *Journal of medicinal chemistry*, vol. 57, no. 9, pp. 3595–3611, 2014.

[15] M. Gomez-Gallego and M. A. Sierra, "Kinetic isotope effects in the study of organometallic reaction mechanisms," *Chemical reviews*, vol. 111, no. 8, pp. 4857–4963, 2011.

[16] H. Eyring, "The activated complex in chemical reactions," *The Journal of Chemical Physics*, vol. 3, no. 2, pp. 107–115, 1935.

[17] S. Glasstone, K. J. Laidler, and H. Eyring, "The theory of rate processes; the kinetics of chemical reactions, viscosity, diffusion and electrochemical phenomena," tech. rep., McGraw-Hill Book Company„ 1941.

[18] P. Pechukas, "Transition state theory," *Annual Review of Physical Chemistry*, vol. 32, no. 1, pp. 159–177, 1981.

[19] F. Hasanayn, A. Streitwieser, and R. Al-Rifai, "A computational study of the effect of bending on secondary kinetic isotope effects in sn2 transition states," *Journal of the American Chemical Society*, vol. 127, no. 7, pp. 2249–2255, 2005.

[20] D. R. Hartree, "The wave mechanics of an atom with a non-coulomb central field. part i. theory and methods," in *Mathematical Proceedings of the Cambridge Philosophical Society*, vol. 24, pp. 89–110, Cambridge university press, 1928.

[21] V. Fock, "Näherungsmethode zur lösung des quantenmechanischen mehrkörperproblems," *Zeitschrift für Physik*, vol. 61, no. 1-2, pp. 126–148, 1930.

[22] C. J. Cramer, *Essentials of computational chemistry: theories and models*. John Wiley & Sons, 2013.

[23] NobelPrize.org, "The Nobel Prize in Chemistry 1998." Online; Fri. 28 Sep 2021.

[24] W. Kaminsky and H. Sinn, *Transition metals and organometallics as catalysts for olefin polymerization*. Springer Science & Business Media, 2012.

[25] M. Bertoli, A. Choualeb, A. J. Lough, B. Moore, D. Spasyuk, and D. G. Gusev, "Osmium and ruthenium catalysts for dehydrogenation of alcohols," *Organometallics*, vol. 30, no. 13, pp. 3479–3482, 2011.

[26] Q. J. Bruch, G. P. Connor, N. D. McMillion, A. S. Goldman, F. Hasanayn, P. L. Holland, and A. J. M. Miller, "Considering electrocatalytic ammonia synthesis via bimetallic dinitrogen cleavage," *ACS Catalysis*, vol. 10, no. 19, pp. 10826–10846, 2020.

[27] R. Tanaka, M. Yamashita, and K. Nozaki, "Catalytic hydrogenation of carbon dioxide using ir (iii)- pincer complexes," *Journal of the American Chemical Society*, vol. 131, no. 40, pp. 14168–14169, 2009.

[28] M. J. Frisch, G. W. Trucks, H. B. Schlegel, G. E. Scuseria, M. A. Robb, J. R. Cheeseman, G. Scalmani, V. Barone, G. A. Petersson, H. Nakatsuji, X. Li, M. Caricato, A. V. Marenich, J. Bloino, B. G. Janesko, R. Gomperts, B. Mennucci, H. P. Hratchian, J. V. Ortiz, A. F. Izmaylov, J. L. Sonnenberg, D. Williams-Young, F. Ding, F. Lipparini, F. Egidi, J. Goings, B. Peng, A. Petrone, T. Henderson, D. Ranasinghe, V. G. Zakrzewski, J. Gao, N. Rega, G. Zheng, W. Liang, M. Hada, M. Ehara, K. Toyota, R. Fukuda, J. Hasegawa, M. Ishida, T. Nakajima, Y. Honda, O. Kitao, H. Nakai, T. Vreven, K. Throssell, J. A. Montgomery, Jr., J. E. Peralta, F. Ogliaro, M. J. Bearpark, J. J. Heyd, E. N. Brothers, K. N. Kudin, V. N. Staroverov, T. A. Keith, R. Kobayashi, J. Normand, K. Raghavachari, A. P. Rendell, J. C. Burant, S. S. Iyengar, J. Tomasi, M. Cossi, J. M. Millam, M. Klene, C. Adamo, R. Cammi, J. W. Ochterski, R. L. Martin, K. Morokuma, O. Farkas, J. B. Foresman, and D. J. Fox, "Gaussian˜16 Revision C.01," 2016. Gaussian Inc. Wallingford CT.

[29] Y. Zhao and D. G. Truhlar, "A new local density functional for main-group thermochemistry, transition metal bonding, thermochemical kinetics, and noncovalent interactions," *The Journal of chemical physics*, vol. 125, no. 19, p. 194101, 2006.

[30] C. J. Cramer and D. G. Truhlar, "Density functional theory for transition metals and transition metal chemistry," *Physical Chemistry Chemical Physics*, vol. 11, no. 46, pp. 10757–10816, 2009.

[31] A. V. Marenich, C. J. Cramer, and D. G. Truhlar, "Universal solvation model based on solute electron density and on a continuum model of the solvent defined by the bulk dielectric constant and atomic surface tensions," *The Journal of Physical Chemistry B*, vol. 113, no. 18, pp. 6378–6396, 2009.

[32] R. Dennington, T. A. Keith, and J. M. Millam, "Gaussview Version 6," 2019. Semichem Inc. Shawnee Mission KS.

[33] A. Müller, "Explicit approximate relation between reduced two-and one-particle density matrices," *Physics Letters A*, vol. 105, no. 9, pp. 446–452, 1984.

[34] F. Cortés-Guzmán and R. F. Bader, "Complementarity of qtaim and mo theory in the study of bonding in donor–acceptor complexes," *Coordination Chemistry Reviews*, vol. 249, no. 5-6, pp. 633–662, 2005.

[35] P. S. Arrhenius, "Xxxi. on the influence of carbonic acid in the air upon the temperature of the ground," *The London, Edinburgh, and Dublin Philosophical Magazine and Journal of Science*, vol. 41, no. 251, pp. 237–276, 1896.

[36] S. Manabe and R. T. Wetherald, "Thermal equilibrium of the atmosphere with a given distribution of relative humidity," 1967.

[37] NobelPrize.org, "The Nobel Prize in Physics 2021." Online; Fri. 6 Oct 2021.

[38] M. Aresta, *Carbon dioxide as chemical feedstock*. John Wiley & Sons, 2010.

[39] F. Joó, "Breakthroughs in hydrogen storage—formic acid as a sustainable storage material for hydrogen," *ChemSusChem: Chemistry & Sustainability Energy & Materials*, vol. 1, no. 10, pp. 805–808, 2008.

[40] S. Dabral and T. Schaub, "The use of carbon dioxide (co2) as a building block in organic synthesis from an industrial perspective," *Advanced Synthesis & Catalysis*, vol. 361, no. 2, pp. 223–246, 2019.

[41] K. Hara, A. Kudo, and T. Sakata, "Electrochemical reduction of carbon dioxide under high pressure on various electrodes in an aqueous electrolyte," *Journal of Electroanalytical Chemistry*, vol. 391, no. 1, pp. 141–147, 1995.

[42] C. W. Li and M. W. Kanan, "Co2 reduction at low overpotential on cu electrodes resulting from the reduction of thick cu2o films," *Journal of the American Chemical Society*, vol. 134, no. 17, pp. 7231–7234, 2012.

[43] A. Álvarez, A. Bansode, A. Urakawa, A. V. Bavykina, T. A. Wezendonk, M. Makkee, J. Gascon, and F. Kapteijn, "Challenges in the greener production of formates/formic acid, methanol, and dme by heterogeneously catalyzed co2 hydrogenation processes," *Chemical Reviews*, vol. 117, no. 14, pp. 9804–9838, 2017. PMID: 28656757.

[44] M. S. Ahlquist, "Iridium catalyzed hydrogenation of co2 under basic conditions—mechanistic insight from theory," *Journal of Molecular Catalysis A: Chemical*, vol. 324, no. 1-2, pp. 3–8, 2010.

[45] I. Osadchuk, T. Tamm, and M. S. Ahlquist, "Theoretical investigation of a parallel catalytic cycle in co2 hydrogenation by (pnp) irh3," *Organometallics*, vol. 34, no. 20, pp. 4932–4940, 2015.

[46] X. Yang, "Hydrogenation of carbon dioxide catalyzed by pnp pincer iridium, iron, and cobalt complexes: a computational design of base metal catalysts," *ACS Catalysis*, vol. 1, no. 8, pp. 849–854, 2011.

[47] T. J. Schmeier, G. E. Dobereiner, R. H. Crabtree, and N. Hazari, "Secondary coordination sphere interactions facilitate the insertion step in an iridium (iii) co2 reduction catalyst," *Journal of the American Chemical Society*, vol. 133, no. 24, pp. 9274–9277, 2011.

[48] R. Tanaka, M. Yamashita, L. W. Chung, K. Morokuma, and K. Nozaki, "Mechanistic studies on the reversible hydrogenation of carbon dioxide catalyzed by an ir-pnp complex," *Organometallics*, vol. 30, no. 24, pp. 6742–6750, 2011.

[49] K. M. Waldie, K. R. Flajslik, E. McLoughlin, C. E. Chidsey, and R. M. Waymouth, "Electrocatalytic alcohol oxidation with ruthenium transfer hydrogenation catalysts," *Journal of the American Chemical Society*, vol. 139, no. 2, pp. 738–748, 2017.

[50] B. Mondal, F. Neese, and S. Ye, "Control in the rate-determining step provides a promising strategy to develop new catalysts for co2 hydrogenation: a local pair natural orbital coupled cluster theory study," *Inorganic chemistry*, vol. 54, no. 15, pp. 7192–7198, 2015.

[51] T. Ono, S. Qu, C. Gimbert-Surinach, M. A. Johnson, D. J. Marell, J. Benet-Buchholz, C. J. Cramer, and A. Llobet, "Hydrogenative carbon dioxide reduction catalyzed by mononuclear ruthenium polypyridyl complexes: discerning between electronic and steric effects," *ACS Catalysis*, vol. 7, no. 9, pp. 5932–5940, 2017.

[52] A. Urakawa, F. Jutz, G. Laurenczy, and A. Baiker, "Carbon dioxide hydrogenation catalyzed by a ruthenium dihydride: A dft and high-pressure

spectroscopic investigation," *Chemistry–A European Journal*, vol. 13, no. 14, pp. 3886–3899, 2007.

[53] D. J. Darensbourg, S. J. Kyran, A. D. Yeung, and A. A. Bengali, "Kinetic and thermodynamic investigations of co2 insertion reactions into ru–me and ru–h bonds–an experimental and computational study," *Eur. J. Inorg. Chem*, vol. 4024, p. 4031, 2013.

[54] J. Agarwal, R. P. Johnson, and G. Li, "Reduction of co2 on a tricarbonyl rhenium (i) complex: modeling a catalytic cycle," *The Journal of Physical Chemistry A*, vol. 115, no. 13, pp. 2877–2881, 2011.

[55] A. Urakawa, M. Iannuzzi, J. Hutter, and A. Baiker, "Towards a rational design of ruthenium co2 hydrogenation catalysts by ab initio metadynamics," *Chemistry-A European Journal*, vol. 13, no. 24, pp. 6828–6840, 2007.

[56] P. A. Dub and T. Ikariya, "Quantum chemical calculations with the inclusion of nonspecific and specific solvation: asymmetric transfer hydrogenation with bifunctional ruthenium catalysts," *Journal of the American Chemical Society*, vol. 135, no. 7, pp. 2604–2619, 2013.

[57] F. Hasanayn, L. M. Al-Assi, R. N. Moussawi, and B. S. Omar, "Mechanism of alcohol–water dehydrogenative coupling into carboxylic acid using milstein's catalyst: A detailed investigation of the outer-sphere pes in the reaction of aldehydes with an octahedral ruthenium hydroxide," *Inorganic chemistry*, vol. 55, no. 16, pp. 7886–7902, 2016.

[58] M. Brookhart, M. L. Green, and G. Parkin, "Agostic interactions in transition metal compounds," *Proceedings of the National Academy of Sciences of the United States of America*, vol. 104, no. 17, p. 6908, 2007.

[59] C. Foroutan-Nejad, S. Shahbazian, and R. Marek, "Toward a consistent interpretation of the qtaim: tortuous link between chemical bonds, interactions, and bond/line paths," *Chemistry–A European Journal*, vol. 20, no. 32, pp. 10140–10152, 2014.

[60] C. Outeiral, M. A. Vincent, Á. M. Pendás, and P. L. Popelier, "Revitalizing the concept of bond order through delocalization measures in real space," *Chemical science*, vol. 9, no. 25, pp. 5517–5529, 2018.

[61] Y. Zhao and D. G. Truhlar, "Density functional for spectroscopy: no long-range self-interaction error, good performance for rydberg and charge-transfer states, and better performance on average than b3lyp for ground states," *The Journal of Physical Chemistry A*, vol. 110, no. 49, pp. 13126–13130, 2006. PMID: 17149824.

[62] J. Tirado-Rives and W. L. Jorgensen, "Performance of b3lyp density functional methods for a large set of organic molecules," *Journal of Chemical Theory and Computation*, vol. 4, no. 2, pp. 297–306, 2008. PMID: 26620661.

[63] G.-B. Shen, K. Xia, X.-T. Li, J.-L. Li, Y.-H. Fu, L. Yuan, and X.-Q. Zhu, "Prediction of kinetic isotope effects for various hydride transfer reactions using a new kinetic model," *The Journal of Physical Chemistry A*, vol. 120, no. 11, pp. 1779–1799, 2016.

[64] J. E. Heimann, W. H. Bernskoetter, N. Hazari, and J. M. Mayer, "Acceleration of co 2 insertion into metal hydrides: ligand, lewis acid, and solvent effects on reaction kinetics," *Chemical science*, vol. 9, no. 32, pp. 6629–6638, 2018.

[65] D. H. Hong and L. J. Murray, "Carbon dioxide insertion into bridging iron hydrides: Kinetic and mechanistic studies," *European journal of inorganic chemistry*, vol. 2019, no. 15, p. 2146, 2019.

[66] D. H. Hong, R. B. Ferreira, V. J. Catalano, R. García-Serres, J. Shearer, and L. J. Murray, "Access to metal centers and fluxional hydride coordination integral for co2 insertion into [fe3 (μ-h) 3] 3+ clusters," *Inorganic Chemistry*, vol. 60, no. 10, pp. 7228–7239, 2021.

[67] D. Schnieders, B. T. H. Tsui, M. M. H. Sung, M. R. Bortolus, G. J. Schrobilgen, J. Neugebauer, and R. H. Morris, "Metal hydride vibrations: The trans effect of the hydride," *Inorganic Chemistry*, vol. 58, no. 18, pp. 12467–12479, 2019. PMID: 31456395.

[68] M. A. Lawrence, K.-A. Green, P. N. Nelson, and S. C. Lorraine, "Review: Pincer ligands—tunable, versatile and applicable," *Polyhedron*, vol. 143, pp. 11–27, 2018. Special issue on Pincer Ligands.

[69] H. Li, B. Zheng, and K.-W. Huang, "A new class of pn3-pincer ligands for metal–ligand cooperative catalysis," *Coordination Chemistry Reviews*, vol. 293-294, pp. 116–138, 2015. 41st International Conference on Coordination Chemistry, Singapore, July 2014.

[70] K. S. Sandhya, G. S. Remya, and C. H. Suresh, "Pincer ligand modifications to tune the activation barrier for h_2 elimination in water splitting milstein catalyst," *Inorganic Chemistry*, vol. 54, no. 23, pp. 11150–11156, 2015. PMID: 26575086.

[71] F. Bertini, M. Glatz, N. Gorgas, B. Stöger, M. Peruzzini, L. F. Veiros, K. Kirchner, and L. Gonsalvi, "Carbon dioxide hydrogenation catalysed by well-defined mn (i) pnp pincer hydride complexes," *Chemical science*, vol. 8, no. 7, pp. 5024–5029, 2017.

[72] S. C. Mandal, K. S. Rawat, and B. Pathak, "A computational study on ligand assisted vs. ligand participation mechanisms for co_2 hydrogenation: importance of bifunctional ligand based catalysts," *Phys. Chem. Chem. Phys.*, vol. 21, pp. 3932–3941, 2019.

[73] R. Noyori, M. Koizumi, D. Ishii, and T. Ohkuma, "Asymmetric hydrogenation via architectural and functional molecular engineering," *Pure and Applied Chemistry*, vol. 73, no. 2, pp. 227–232, 2001.

[74] F. Hasanayn and R. H. Morris, "Symmetry aspects of h2 splitting by five-coordinate d6 ruthenium amides, and calculations on acetophenone hydrogenation, ruthenium alkoxide formation, and subsequent hydrogenolysis in a model trans-ru(h)2(diamine)(diphosphine) system," *Inorganic Chemistry*, vol. 51, no. 20, pp. 10808–10818, 2012. PMID: 23031090.

[75] F. Hasanayn and A. Baroudi, "Direct h/or and or/or metathesis pathways in ester hydrogenation and transesterification by milstein's catalyst," *Organometallics*, vol. 32, no. 9, pp. 2493–2496, 2013.

[76] S. A. Morris and D. G. Gusev, "Rethinking the claisen–tishchenko reaction," *Angewandte Chemie International Edition*, vol. 56, no. 22, pp. 6228–6231, 2017.